University of Southern Queensland

NUMERICAL STUDY OF SOIL STABILITY ABOVE WATER MAINS

Thesis submitted by

Kiritharan Mahalingasivam

For the award of

Master of Engineering (Research)

Year 2022

ABSTRACT

Disasters caused by natural sinkholes have been a serious issue across the majority of the countries where the karst features formed due to the erosion of subsurface geological formations such as limestones and dolomite. Anthrophonic-driven sinkhole formation due to the water and sewage leakage, mining activities, underground infrastructure development started contributing to the increased number of sinkhole incidents.

Water leakage from the underground water pipelines causes several issues such as scarcity of drinking water, damaging the other utilities, and critically triggers roadside sinkholes. Road-related sinkholes incidents are intensively happening in many countries in the world as evidenced by the frequent news from the media. While there has been much research on tracing and predicting the sinkholes using the latest geophysics technologies, very limited research can be found on the actual stability analysis of the soil in the risk zones. Moreover, soil blowout stability analysis was rarely carried out in the past.

This thesis sets out to quantify the "collapse" and "blowout" stability performance of three idealised cavity shapes of horizontal, semicircular, and circular above the damaged pipe. Finite Element Limit Analysis (*FELA*) was used to obtain upper and lower bound solutions to the problem. The study provides useful engineering information in the form of design charts and tables for a wide range of design parameters, which would greatly assist in decision-making by practical engineers.

CERTIFICATION OF THESIS

This thesis is entirely the work of Kiritharan Mahalingasivam except wherever otherwise acknowledged. The work is original and has not previously been submitted for any other award, except where acknowledged.

Principal Supervisor: Associate Prof. Jim Shiau

Associate Supervisor: Dr. Habib Alehossein

Student and supervisors' signatures of endorsement are held at the University.

ACKNOWLEDGEMENTS

Firstly, and foremost I word like to thank Dr. Jim Shiau for his technical expertise, invaluable time, continuous engagement, intensive advice, encouragement throughout my research journey. Despite the difficult period of Covid-19, it is pleased to see the project outcomes of two journal papers. Without his incessant involvement and strong leadership, both the journal papers and the thesis would not have been possible.

Both Bishal Chudal and Suraparb Keawsawasvong deserve special thanks for their direct contribution to the two journal papers.

I would also like to thank the members of Associate Prof. Jim Shiau's research group: Mohammad Mirza Hassan, Fadhil Al-Asadi, Mathew Sams, Ji-Sung Lee, Fan Lin, and Xiang Yang for their indirect help during this journey. I am also thankful to my co-supervisor Dr. Habib Alehossein for his support whenever needed. Also, the Research Training Scheme (RTS) provided by the Australian Commonwealth Government through USQ is much appreciated.

Finally, I would like to thank my family for their much-needed encouragement and moral support. To my mother, my wife, and son, thank you provided with a lot of confidence which made the journey possible. I would not be able to stay in the course without love and support from my wife" Uma "and son "Chathu". I dedicate this thesis to my mum, my wife, and my son. Without any of the above, this study may not have been possible.

TABLE OF CONTENTS

LIST OF FIGURES

LIST OF TABLES

NOMENCLATURE

C	=	Cover depth of trapdoor
W	=	Width of horizontal/semi-circular/circular trapdoor
C/W	=	Trapdoor depth to diameter ratio
S_u	=	Undrained shear strength of the soil
$\gamma W/S_u$	=	Shear strength ratio
σ_s	=	Ground surface pressure
σ_t	=	Water pipe internal pressure
γ	=	Soil unit-weight

GLOSSARY

2*D*	=	Two-dimensional
3*D*	=	Three-dimensional
GPR	=	Ground penetration radar
UB	=	Upper bound
LB	=	Lower bound
LMM	=	Load multiplier method
N	=	Stability number
N_c	=	Critical stability number
OptumCE	=	2*D* finite element limit analysis software
CPU	=	Central processing unit
PR	=	Pressure ratio
FELA	=	Finite element limit Analysis
WSN	=	Wireless sensor network
SRI	=	Sinkhole risk index
PIV	=	Particle image velocimetry
DAQ	=	Data Acquisition System
IoT	=	Internet of Things
PSU	=	Pipe Safety Unit

CHAPTER 1 INTRODUCTION

1.1. BACKGROUND

The necessity for investigating the stability of sinkholes has been increased in recent decades because the devastation caused by the instability and collapse of sinkholes exponentially increased. A sinkhole is a ground depression that takes place without warning most of the time, often resulted in infrastructure damage and risk lives. The sinkhole is a term first introduced by Fairbridge (1968) to define subcircular surface depressions or collapse structures formed by the collapse of small subterranean karst cavities. Accurate prediction of the occurrence location and timing is rather difficult (Rosdi et al. (2017). Mechanical and/or chemical removal of material from the subsurface may generate large subsurface cavities (Al-Halbouni et al. 2018 &2019).

Kim et al. (2018) and Ali & Choi (2019) found that the main causes for the occurrence of anthropogenic sinkholes are leakage from the water and the sewer pipes in the major cities in many countries. Sewer pipes are crucial services and the number increased as the demand increased. Many existing sewer pipes exceeded the life span, and associated deterioration lead to leakage (Kan & Lee, 2015). Water leakage from a low-pressure source such as sewer pipes may erode the soil around the pipe and leave the soil media unstable with the opening created in the soil layer. In such a situation the possible failure scenario would be the collapse failure. Guarino et al. (2018) identified that the main triggering mechanism consists in saturation of the subsoil, due to water leaks coming from buried sewage and water pipelines. According to Bae et al. (2016) the sewer system failure was the main reason for the sinkhole in Seoul, South Korea and 81.4 % of the total sinkhole occurred between 2011 to 2014 due to leaks in sewer pipes. A survey with the special vehicle equipped with Ground Penetration Radar gears detected 105 cavities and 61 of those were in critical condition. The cavities discovered were around decrepit sewer pipes (Herald 2016).

Figure1.1. A sinkhole that opened in Sindorim-dong, Seoul (Herald, 2016)

In Iraq, the sinkhole numbers increased due to leakage and associated erosion in the past two decades. In Japan, more than seventeen thousand sinkholes occurred for the same reason between 2006 and 2009, (Yokota et al. 2012). In the United States, sudden-appearing caverns are prompting alarm because they are happening in places where they should not, and now seem to be proliferating nationwide. The usual cause found to be crumbling of water, drain, and sewer pipes, often neglected by cities with budget problems. Figure 1.1 represents sinkhole failure due to decrepit sewer pipe at Sindorim-dong, Seoul.

Significantly, leakage from high pressurised water main leads to upward pressure on the soil media above the pipeline (blowout) which ends up in a sinkhole. In such a situation water springs/or plenty of water at the site is evidenced. Recently, a burst of a water main created sinkhole in Newport, Sydney in Australia as in Figure 1.2 sent a spurt of water several metres up in the sky, and caused a sinkhole to open, which is purely a blowout case (NewsComAu, 2021).

Figure 1.2. A pipe burst in Sydney, Australia (NewsComAu, 2021)

On the other hand, leakage from the water main could lead to many issues such as scarcity of drinking water and polluting the ground water (Karoui et al. 2018). Even the developed countries such as United Kingdom, Australia have been suffering from scarcity of drinking due to leakage (Oren and Stroh 2012).

1.2. AIM AND OBJECTIVES

The objective of this research is to gain knowledge of pipe leakage-related ground stability and to develop a two-dimensional model which simulates the stability of soil above the damaged water main in a homogeneous soil medium. Stability has been assessed by computing the pressure ratio $\{PR, (\sigma_s - \sigma_t)/S_u\}$ variation with strength ratio ($SR, \gamma W/S_u$) and the depth ratio ($DR, C/W$). The investigation is carried out in two-dimensional plain strain conditions. In addition, three progressive types of trapdoor geometries have been used to analyse the problem as initiate from horizontal opening, transform into a semi-circular shape, and eventually into circular opening. Finite element limit analysis with load multiplier method used for studies with Tresca soil. The dimensionless ratios are used for the analysis.

The main aim of the project is to study the numerical model which represents the actual sewer/water pipe leakage-related openings. In the case of lower pressurised leakage such as sewer, leakage creates an opening and with gradual erosion finally fails due to the self-weight of the soil and surface pressure (surcharge pressure). This would be collapse case scenario. The pressurised leakage from the water main will push the soil media above the concerned pipe and in such a situation the blowout stability would be the case. Hence, the stability was investigated for the trapdoor openings for collapse and blowout cases.

Three progressive openings as horizontal, semi-circular, and circular are analysed. The pressure ratio approach derived from the Broms and Bennermark's stability number is used to investigate the solution to the problem. The pressure ratio is determined for a range of depth ratios and various strength ratios. This research is to explore the knowledge of undrained stability of the trapdoor problems and the surface failure extent from the pipe leakage created underground cavity.

The thesis objectives can be summarised as below:

- Numerical model is established in a realistic homogeneous soil medium,
- The model is analysed using *Optum G2* to compute the pressure ratio (*PR*),
- Design charts and graphs are produced to assist the practical use of stability numbers in design computations as illustrated in the examples,
- Results are validated by comparing with the published literature.

1.3. SCOPE OF THE WORK

The stability of the horizontal, semicircular, and circular trapdoors is studied by parametric investigation using dimensionless ratios that describe the soil parameters and different trapdoor geometries. Using the Tresca soil model, a two-dimensional finite element analysis is conducted by the load multiplier method in undrained homogeneous soil.

The problem can be defined by the following popular method, where it assumes the greenfield condition. The problem analysed with the pressure ratio (*PR*) approach derived by Davies et al. (1980) from popular Broms and Bennerrmark's (1967) principles, which accommodates the surcharge and supporting pressure. The results of these investigations are presented in terms of dimensionless design charts and tables for (*PR*). Moreover, this research investigated the extent of ground surface failure by examining the vertical velocity output and briefly discussed the effect of the arching phenomenon on the extent of failure. The comprehensive results of stability analysis and failure extent are presented in form of dimensionless design charts and equations.

1.4. THESIS OUTLINE

This thesis investigates the stability of trapdoor in three forms in homogeneous soil media using the parametric studies for various parameters with dimensionless ratios primarily focused on investigating the stability and surface failure extent of the sinkhole by undertaking parametric studies for various associated variables.

Chapter 2 – Literature Review

This Chapter presents the past studies in sinkhole stability and relevant findings. Also, summarises the application of sophisticated technology and the theory behind that in predicting the sinkhole sites.

Further, includes the case histories of waterpipe-related sinkholes incidents to illustrate the importance of the problem. Additionally, includes a theoretical background of stability analysis along with numerous citations on stability analysis.

Chapter 3 – Finite Element Limit Analysis (*FELA*)

This Chapter discusses the numerical software used in this analysis (*FELA*). Also, analyses about the software in detail including the tools and application. Further illustrates the upper bound and lower bound solutions along with the load multiplier method which has been used in this investigation. Further includes Shear Strength Reduction Method (SSRM).

Chapter 4 – Pipeline Burst – Related Collapse Stability

This Chapter is about the stability analysis of the horizontal, semi-circular, and circular trapdoors above the damaged sewer pipe in-plane strain condition under collapse cases with the homogeneous soil media and comparison amongst the geometries themself and with literature included. Also, five different depth ratios were used along with five range of strength ratios for collapse case investigation.

Chapter 5 – Pipeline Burst-Related Blowout Stability

This Chapter studies all three trapdoor geometries as in Chapter 4 for the blowout scenario. The analysis included various undrained shear strength ratios and layer thickness ratios along with five different depth ratios. All three geometries compared (*PR*) among themselves as well as with the post studies.

Chapter 6 – Conclusions

This Chapter summarises the outcome and discusses the key elements achieved in this research. Further, the future work and recommendations to improve results have been discussed. Followed by some general closing comments on the justification of the conducted research.

1.5. PUBLICATIONS

The following papers have been submitted or published during the research period. The candidate contributed to Validating, Formal analysis, Investigation, Data curation, Writing original draft of the publications.

- Shiau, J., Chudal, B., Mahalingasivam, K., and Keawsawasvong, S., 2021, 'Pipeline burst-related ground stability in blowout condition', *Transportation Geotechnics*, *29*, p.100587. https://doi.org/10.1016/j.trgeo.2021.100587

- Shiau, J., Mahalingasivam, K., Chudal, B., and Keawsawasvong, S., 2021, 'Pipeline Burst-Related Soil Stability in Collapse Condition', *Journal of Pipeline Systems* - Engineering and Practice. https://doi.org/10.1061/(ASCE)PS.1949-1204.0000657

CHAPTER 2 LITERATURE REVIEW

2.1. INTRODUCTION

Sinkhole tragedies in the non-karst environment have been significantly increased in the recent past decades particularly due to leakage from the water/sewerage pipes (Guo et al. 2013; Tohda and Hachiya 2005; Alsaydalani and Clayton 2014). The occurrence of anthropogenic sinkholes in the urban area often causes serious social losses.

The phenomenon often occurs due to damage to sewer pipes because of aging. An investigation by Kuwano et al. (2006) discovered that pipes older than 25 years have a greater chance of a breakdown. Burn et al. (1999) found that, over 54% of the pipes are older than 25 years and 24% are older than 50 years in Germany and pipes are in better condition in Australia as 47% of pipes that exceed 25 years of age and 13% older than 50 years. Hence, it is very crucial to better understand the problem so that losses could be minimised.

Rogers (1986) initially introduced the mechanism of the sewerage-induced sinkhole. The crack on the pipe causes the soil to infiltrate into the pipe when the water level reduces in the pipe and the soil above the pipe becomes looser which led to ground subsidence. Several researchers have been carried out investigation to study about the failure mechanism (Indiketiya et al. 2017; Renuka & Kuwano 2011). Comparable to the natural karst dissolution sinkholes, pipe leakage-driven subsidence has been instantaneous and catastrophic. To prevent the occurrence of such devastation, early detection of the actual location, remedial measures to prevent it from happening are crucial. The procedure includes the physical location of the trapdoor, stability calculation, and the failure extent of the sinkhole in the event of failure. Acquiring knowledge in ground conditions allows the respective authorities to take necessary steps to prevent such incidents and thereby save lives and minimise the economic impact.

The current study focuses on two categories. Firstly, the geophysical techniques could be used in identifying the physical location of the opening and followed by stability analysis of the trapdoor. Indiketiya et al. (2017) and Tang (2017) conducted experimental and numerical investigations on soil erosion and associated sinkhole creation and found that the general mode of sinkhole occurrence was induced due to soil erosion into the sewer system. i.e., during the heavy rain, the soil fluidised because of the water level rise together with the exfiltrate water from the sewer pipe. When the rain stops the groundwater level will go down, accompanied by dragging the loose soil particle into the sewer pipe through the crack in the pipe, creating a cavity in the soil, and eventually, a sinkhole will be created.

2.2. LOCATING SINKHOLES CREATED DUE TO PIPE LEAKAGE

The water supply and drainage pipelines run through the several different areas to provide services to the communities spread out in a town. Different regions have varied soil profiles, geomorphological and hydrological conditions which distinguish the soil characteristics from place to place. Hence, the leakage from the underground utilities impacts differently according to the subsurface soil strata. Leakage in the underground utility induces soil property variation and consequently leads to many other problems. Sinkhole creation due to the rapid deterioration of the underground service pipeline has been seen very often in the past couple of decades. The early warning system is the key to predict and prevent such events. Although, many techniques are available to identify and warn about the cavity formation most of them are in line with the natural formation of sinkholes associated with the karst dissolution. Concerning the warning system for the leakage-induced sinkholes, a ground-penetrating radar (*GPR*) test was selected because *GPR* is the most convenient and accurate tool. The *GPR* test can be carried out while driving on the road, so it is suitable for the urban area because it does not need traffic control and can quickly survey a large area.

Further, research is on the way of a sensor-based safety unit that detects leakage by analysing pipeline behaviour and leakage. The development of a system is in progress and the main aim is to make a sinkhole risk index (*SRI*) to prevent sinkholes creation due to leakage of underground sewer pipelines owing to human errors.

2.2.1. Cavity detection using Ground Penetrating Radar (*GPR*)

Seoul city of Korea is one the worst affected city from the road sinkhole due to water pipe leakage. They have developed *GPR* system to predict the road subsidence which fitted with the minibus as shown in Figure 2.1. The *GPR* test can be carried out while driving on the road.

Figure 2.1. The van fitted with a three-dimensional (3*D*)

GPR system in Seoul (Baek et al. 2018)

(a) *GPR*) Antenna

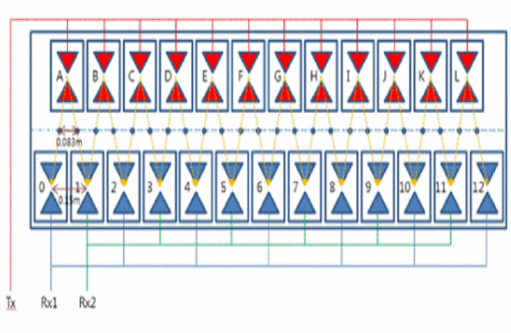

(b) *GPR* Antenna array

Figure 2.2. *GPR* components (Baek et al. 2018)

The (*GPR*) system consists of 16 channel 500 MHz antennas as in Figure 2.2 (a), a data acquisition system, 4 video cameras, *GPR* and Distance Measurement Equipment (*DME*) attached to a minibus. With the vehicle speed of 15 km/h, *GPR* system could collect data of roads width of 2.0 m and a depth of 1.5 m and every 10.0 cm in the longitudinal direction. The frequency of the data collection 10 cm longitudinal and 12.5 cm is 0.1 m transverse direction. The *GPR* antenna was installed at the rear of the vehicle and could move down during the survey.

The range of the *GPR* matched with need as road cavities found in Seoul were located at a depth of 0.3 m to 2.0 m as the depth of most utility pipes buried on roads in Seoul was 1.5 m to 2.0 m. Therefore, the penetration depth of *GPR* should be shallow enough to distinguish cavities from neighing materials (Water/sewer pipes are buried at 1-2meter depth in majority of the countries). This *GPR* system was upgraded in 2017. The New *GPR* system had 800 MHz 24 channels of *GPR* antennas which were combined with 12 transmitters and 13 receivers. So, the transverse interval was reduced from 12.5 cm to 7.5 cm and the longitudinal interval was reduced from 10.0 cm to 5.0 cm. In addition, Data Acquisition System (*DAQ*) system was enhanced so the survey speed could be 40 km/h which was doubled from the original *GPR* system.

2.2.2. Pipe leakage cavity detection by the Internet of Things (*IoT*) System

This system is an underground risk assessment system vicinity of the circumference of the pipes which facilitates sophisticated monitoring and forecasting of any unforeseen subsurface perils such as sudden road subsidence due to water leakage. As a part of developing a productive assessment technology, the Pipe Safety Unit (*PSU*) is in the process of development by Kwak et al. (2015) which detects the leakage together with pipe movement. *IoT* based subsurface risk assessment system surrounding water pipes is proposed which contains an early detection tool to find out the leakage along with correspondence services of analysed leakage and movement data collected by *PSU*. The present method is expected to be reliable and covers few kilometres of area. *IoT* system of risk assessment enables advanced monitoring and prediction of sudden roadside subsidence due to leakage.

2.2.3.1. Pipe Safety Unit (*PSU*) Development

Pipe Safety Unit (*PSU*) mainly have two units as the sensor unit and the communication unit. The sensor unit is made of stainless-steel material of the outer casing and the piezoelectric element, a gyroscope sensor, an accelerometer sensor, and a sensor controller which filters sound of leakage and positional displacement information. The sensor controller filters the ineffective leak sound. The system is under development which interprets risks by identifying changes in the position of leak location and channel. Figure 2.3 shows proposed case study and assessment algorithm which will be developed based on the field simulation of leakage tests for water supply pipelines. Possible subsidence area is evaluated to more than allowable leak and where the position variation has occurred as determined by the simulation. With this system, it is possible to monitor the problems of the water pipes and the administrator might proceed with the maintenance work.

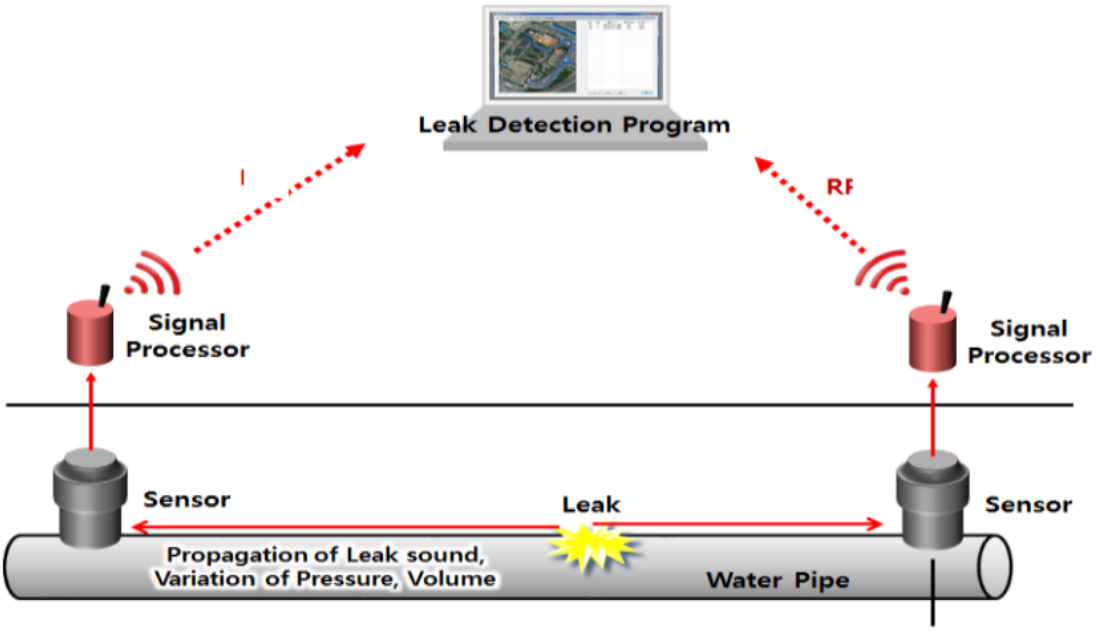

Figure 2.3. *PSU* management and analysis technology (Kwak et al. 2015)

The assessment algorithm will be developed based on the field simulation of leakage tests for water supply pipelines. Acceleration of sinkhole tragedy needs to be controlled to minimize the associated thread to the properties and life. Apart from the early detection technique, it is important to study more about the stability of soil medium above the damaged pipe assuming different trapdoor geometries as the number of sinkholes due to the leakage from the water/sewerage pipes have been increasing every year.

The increased number of incidents highlights the importance of understanding the problem better. The next section summarises the sinkholes created due to leakage of utilities across several countries which illustrates the importance of the problem.

2.3. CASE HISTORY

The utility leakage causes several problems such as endangering lives, damages to the infrastructure and scarcity of drinking water. This section summarizes the sinkhole cases due to utility leakages with the brief descriptions.

2.3.1 Sinkholes due to water/sewerage pipe damage in Australia.

Figure 2.4. shows the sinkhole of about six meters wide, which swallowed the road pavement and traffic light in Sunshine Blvd, Goldcoast, Australia. The burst of 20 centimetres diameter water main caused the sinkhole in December 2020. Road damaged due to the pipe burst and traffic build-up of up to 1 kilometre consequently.

Figure 2.4. Sinkhole at Gold Coast due to water main leakage (ABC News, 2020)

In Double Bay, Sydney, Australia, a road sinkhole opened in July 2020 due to a water main break as in Figure 2.5 and a vehicle has stuck in the road. Many families suffered from water cut on that day.

Figure 2.5. A truck got stuck in a road sinkhole (ABC News, 2020)

A car nosedived in a sinkhole as in Figure 2.6 and a water main burst caused the issue at Bennett Springs, Wester Australia in July 2020. Road and car are damaged due to the incident.

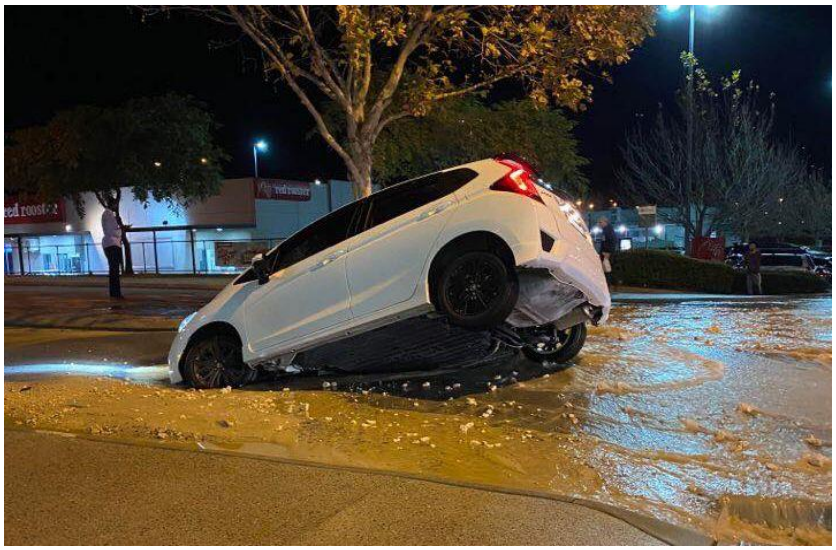

Figure 2.6. A car that “nosedived” into a road sinkhole (ABC News, 2020)

A bus has stucked in a sinkhole due to water main burst in September 2019 at Port Hacking Road in Caringbah, NSW, Australia as in Figure 2.7. Dozens of residents have been left without water across the area, traffic delayed for several hours, and road crumbled due to the sinkhole.

Figure 2.7. Bus stuck in sinkholes due to water main burst (9News, 2019)

A car suddenly slammed to a halt in a sinkhole in Gardenvale, Melbourne, Australia as in Figure 2.8 due to an underground water main burst in January 2019. The car and road are damaged.

Figure 2.8. A car has plunged into a sinkhole in Gardenvale (9 News, 2019)

Figure 2.9 shows a car that stuck in a sinkhole that was created because of a water main burst in South Australia in August 2017. Repair work on affected pipe interrupted water supply for residents in the local area.

Figure 2.9. A car became stranded in a sinkhole (NT News, 2017)

A Ute fell into a sinkhole in Wanneroo, Western Australia in June 2017. The sinkhole was caused by an underground water main burst, which weakened the road surface (Figure 2.10)

Figure 2.10. Ute was swallowed in sinkhole (Foster, 2017)

The whole section (two lanes) of a road was crumbled due to a sinkhole created because of a water main burst in Mona Vale, Sydney, Australia in February 2017. Figure 2.11 shows the details of damage and traffic in the road completely blocked.

Figure 2.11. Sinkhole damaged a road in Mona Vale (Hit Network, 2017)

A ruptured gas line was the cause for the sinkholes of backyard swimming pool size in Point Piper, NSW, Australia, as in Figure 2.12. The incident happened in February 2017 which resulted in traffic chaos and interrupted power supply.

Figure 2.12. Sinkhole created due to line rupture (Levy, 2017)

In November 2016 water the main burst created a sinkhole in Wickham, NSW, Australia, and a car nosedived as in Figure 2.13. Three cars were damaged and about 40 properties were without water for at least one day.

Figure 2.13. Sinkhole swallowed car at suburban roadway (ABC News, 2016)

A huge deluge triggered as in Figure 2.14 due to a water main burst along Carlton North, Victoria, Australia in January 2016. The deluge extracted rocks from the torrent and sinkhole created at the scene. A car was damaged due to the water pour and flood homes.

Figure 2.14. Water main burst created a sinkhole (NewsComAu, 2016)

Three lanes of a busy road at Caulfield, Australia damaged due to a sinkhole caused by a century-old water main burst as in Figure 2.15. Traffic flow severely affected and road damaged.

Figure 2.15. Massive sinkhole appeared in Glen Eira Road (Calligeros, 2015)

Burst of 350 mm diameter cast iron water main flooded six homes and caused a sinkhole that swallowed two cars in Port Melbourne, Australia in December 2014 (Figure 2.16).

Figure 2.16. Sinkhole opened due to water main burst (ABC News, 2014)

Road damage and traffic chaos were caused due to a 10m wide sinkhole created because of a defective pipe burst in Gold Coast, Australia in July 2014. Figure 2.17 below illustrates the damage. Water supply, telecommunication, and power supply were disturbed.

Figure 2.17. Sinkhole at Gold Coast Highway (Goldcoastbulletin, 2014)

An Ambulance stucked in a sinkhole caused by water main damage (Figure 2.18) at Northern Beaches, Sydney, Australia in May 2014. A section corroded cast iron pipe was the cause for the issue. Road and vehicle were damaged.

Figure 2.18. Corroded water main burst caused a sinkhole (Sutton, 2014)

The sinkhole of a meter wide and two meters deep created in June 2020, at Collins Street, Melbourne, Australia (Figure 2.19). The cause of the sinkhole was a crack in the barrel drain running down the street. Road damaged and traffic congested.

Figure 2.19. One-meter-wide sinkhole opened in Collin Street (Mimic News, 2020)

2.3.2. Sinkholes due to water pipe damage outside Australia.

Figure 2.20 represents a sinkhole created due to an 8-inch concrete water main burst at Z streets, San Diego, California in January 2020. There were fifty-five customers without water, traffic blocked due to road damage because of the sinkhole.

Figure 2.20. Sinkhole at a road in San Diego (McKinnon Broadcasting, 2020)

As in Figure 2.21, a car trapped in a sinkhole opened due to a water pipe burst in Norfolk, Virginia in December 2019. A car and access road were damaged due to the incident.

Figure 2.21. Sinkhole opened on a street in Norfolk (13newsnow.com, 2019)

Figure 2.22 shows a waterspout because of a water main break. Water flow eventually created a sinkhole at Green Valley Parkway, Henderson in December 2018. Two lanes for southbound traffic and one lane for northbound traffic were affected.

Figure 2.22. Water main break has forced to close the road (Seeman, 2018)

A car was completely damaged due to a sinkhole created by a water pipe burst in North York, Ontario, Canada in October 2018 (Figure 2.23). Water supply affected and road damaged because water main break.

Figure 2.23. Car was swallowed by a sinkhole (toronto.citynews.ca, 2018)

A sinkhole of at least 20 feet wide opened at 82nd Street, New York in November 2017 (Figure 2.24). The cracked water main caused the pavement to suddenly buckle. Many families were affected by water supply issues and traffic disturbed due to the incident.

Figure 2.24. Sinkhole opened in the middle of a road (Business Insider, 2017)

In August 2015, a sinkhole measured 20 feet wide, and 20 feet deep has opened due to a water leak from a 48-inch cast-iron water main at the intersection of Brooklyn, New York (Figure 2.25). The sinkhole disrupted the traffic flow, and the water supply was cut off for several customers.

Figure 2.25. Sinkhole disrupts water supply (Berger, 2015)

A sinkhole has swallowed a parked car in St Louis, Missouri City, Texas, USA in June 2017. The sinkhole is about six meters deep and two meters wide (Figure 2.26) and it was caused by a water main break.

Figure 2.26. The gaping sinkhole ate a car (Morrison, 2017)

Figure 2.27 shows a car that plunged into a sinkhole created due to a water main leak in May 2017 at Olde Highway 80, California. The car and road were damaged and one side road blocked.

Figure 2.27. Car fallen into the sinkhole formed due to water pipe break (KGTV, 2017)

A huge sinkhole of 30-meter long, 20-meter wide, and nine-meter-deep opened because of water pipe break on a street in, the central province of Henan, China, in August 2016. It's swallowed a section of the road and at least three people (Figure 2.28). Two people rescued and one is missed.

Figure 2.28. Sinkhole opened on a street in China (ABC News, 2016)

A pipe burst caused a sinkhole in Nottinghamshire, UK in February 2016 (Figure 2.29). A car was completely damaged as it submerged in water and 20000 homes were affected by flooding because of the burst pipe.

Figure 2.29. Sinkhole 'sucked' car (HuffPost UK, 2016)

A sinkhole of 10 feet deep swallowed a car in Toledo, Ohio,USA (Figure 2.30). The crater was caused by a broken water line in July 2013. Car completely damaged, traffic blocked for hours.

Figure 2.30. Sinkhole has swallowed the car in Toledo (Taylor,2013)

A fire engine plunged into a sinkhole due to a 6-inch cast-iron water pipe break in the Valley Village neighbourhood of Los Angeles in September 2009. Figure 2.31 shows the incident, the vehicle was completely damaged, and traffic blocked due to road damage.

Figure 2.31. Fire truck stuck in a sinkhole (Otago Daily Times Online News, 2009)

2.3.3. Sinkholes due to sewer/drainage line damage outside Australia

A 30-inch sewer pipe break created a sinkhole of 20 feet wide, 12 feet deep which nearly swallowed a car in Brooklyn, New York in August 2019. The car was partially damaged, and the road crumpled (Figure 2.32).

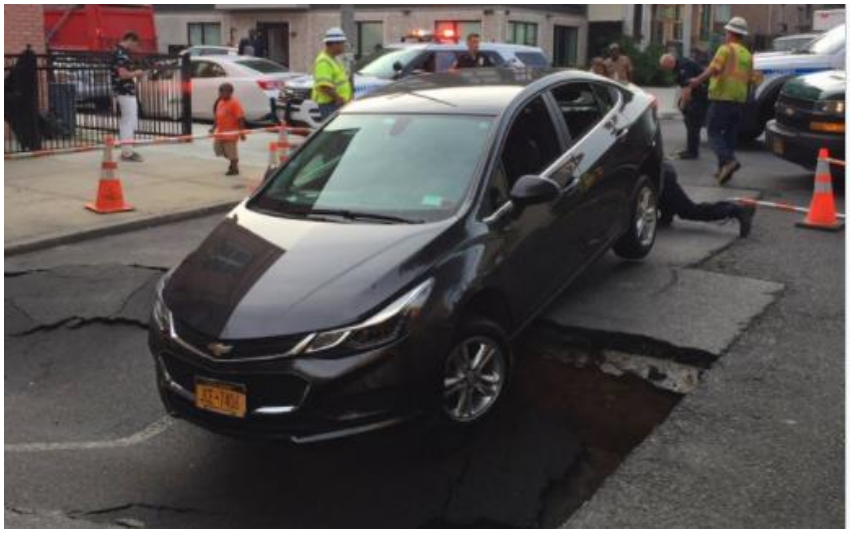

Figure 2.32. Sewer pipe break created a sinkhole in New York (Anon, 2019)

A leak in the drainage pipe caused a six feet deep sinkhole in Chennai, India in January 2019 (Figure 2.33). Traffic congestion increased due to slower vehicular movement.

Figure 2.33. Sinkhole opened due to a leak in drainage pipe (The News Minute, 2019)

Figure 2.34 shows a sinkhole of 5 meters deep, and 7 meters diameter opened at Mexican highway, Mexico, the US in July 2017. Blockage of drainage leads to the devastation. Two dead due to the tragedy, road damaged, and traffic blocked for 8 hours because of the issue.

Figure 2.34. Sinkhole created due to a drainage leak (ABC News, 2017)

Figure 2.35 shows a sinkhole that swallows a big rig in San Francisco in May 2017. A sewer main break caused the sinkhole formation of 3 m by 6 m and 2.5 m deep which damaged the vehicle and road.

Figure 2.35. The parked truck swallowed into sinkhole (Press, 2017)

Michigan sinkhole at Fraser in U.S. opened in January 2017 (Figure 2.36). The reason for the sinkhole was found to be a broken sewer. The repair cost is estimated as more than $78 million. Twenty-four houses affected with water supply and road damaged due to the crater.

Figure 2.36. Sinkhole the size of a football field lands country (Yahoo News, 2017)

A truck of 55,000-pound swallowed in a sinkhole (Figure 2.37) due to a damaged storm drain at Oakwood, Georgia in January 2017.

Figure 2.37. Heavy vehicle was swallowed in a sinkhole (Szathmary, 2017)

Figure 2.38 represents a sinkhole opened due to a drainage pipe burst on a road in Oakland, California,USA in January 2017. The size of the sinkhole measured 8 feet wide, 10 feet long, and 10 feet deep. Road damaged due to the sinkhole and traffic flow disturbed.

Figure 2.38. Broken drainage that caused the sinkhole (Detman, 2017)

A sewer line rupture created a sinkhole that killed one person and swallowed two cars (Figure 2.39). The incident happened in San Antonio in December 2016. A section of the road was washed away, and two cars were completely damaged due to the crater.

Figure 2.39. Sinkhole in Texas swallows two cars (Paulam, 2016)

Drainage/water supply pipe damage caused sinkholes in section of Mancunian Way, Manchester in August 2015 (Figure 2.40). The second incident happened in two months. Road damaged, traffic congestion builds up because of the 40ft crater.

Figure 2.40. Sinkhole opened a second time in two months (The Guardian, 2015)

A sewer main collapse created a sinkhole at Bronx, New York in April 2010 (Figure 2.41). The sinkhole size was 25-feet wide; 20-feet deep has left 200 people out of the water supply and street closures affected the traffic flow.

Figure 2.41. Sinkhole cutoff water for 200 people (staff/zoe-schlanger, 2010)

As in Figure 2.42, a huge sinkhole was caused because of a collapse in the sewage system in the neighbourhood of San Antonio, north of Guatemala City, in February 2007. Three people were killed due to the collapse, twelve homes were swallowed up.

Figure 2.42. The sinkhole was opened due to a sewerage break (Avax News, 2007)

2.4. ANALYSIS OF SINKHOLE

Terzaghi (1936) initiated the stability analysis of trapdoor by using experimental investigation of stresses on the sand to define the active and passive trapdoor failure. Terminology used for the active mode as overburden/surcharge and passive mode as an uplifting force which stimulate cavity failure. Two pressures that acting on the trapdoor are the overburden pressure (γH) and the surcharge stress (σ_s). It is assumed that the surcharge pressure is inactive which is defined as a greenfield condition ($\sigma_s = 0$).

The laboratory investigation of the stability of soil for the underground cavity is introduced by Broms and Bennermark (1967). The stability number equation is defined in equation 2.1.

$$N = \frac{\sigma_s - \sigma_t + \gamma H}{S_u} \tag{2.1}$$

Where σ_s, σ_t, S_u and γ are is soil surcharge pressure, supporting pressure, undrained shear strength and unit weight of the soil, respectively. Through laboratory experiments and field data collection, they studied the plastic flow of undrained clay in vertical openings as shown in Figure 2.43.

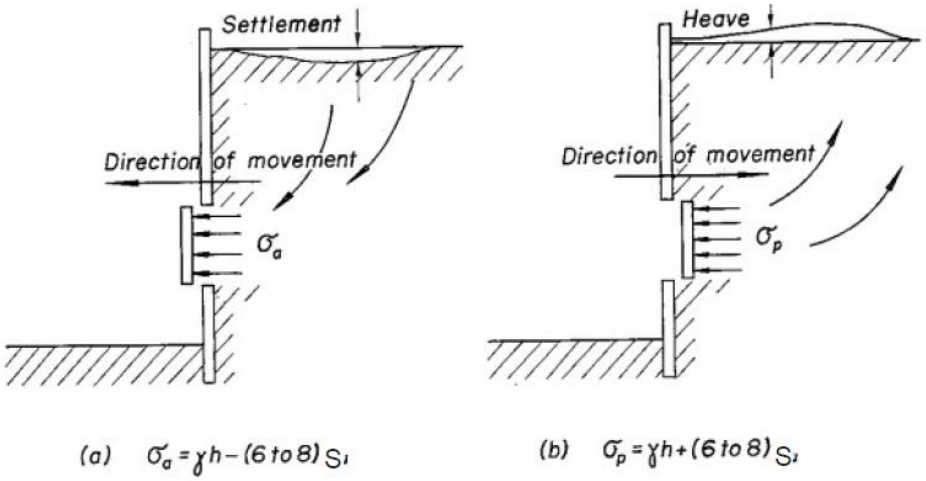

Figure 2.43. Vertical wall stability model of Broms and Bennermark (1967)

The stability of the vertical opening in the retaining wall was investigated by Brom and Bennermark (1967) and found that failure occurs when total overburden pressure ($\sigma_s+\gamma H$) is six to eight times greater than the undrained shear strength of the soil. The value of six to eight would depend on the shape of the opening and the roughness of the wall.

The stability number (N) is a function of the surface surcharge pressure (σ_s), the overburden pressure (γH), the supporting pressure (σ_t), and the undrained shear strength (S_u). The (σ_t/S_u) component in the equation indicates the supporting pressure from the opening. ($\sigma_s+\gamma H)/S_u$ component indicates the overburden pressure. The passive failure trapdoor problem is similar to the pull-out capacity problem of a vertical plate anchor in soils (Merifield et al. 2001 and 2006; Sahoo and Khuntia 2018). The example for the active failure mode is the underground roof of the tunnel and the mining work (Suchowerska et al. 2012), underground pipe stability without the ground support (Costa et al. 2009; Keawsawasvong & Ukritchon 2017).

Craig (1990) has performed in a large centrifuge to investigate the conditions for critical stability of a circular cavity formed by removal of underlying support strata beneath a soft to very soft cohesive overburden. Craig tested the failure by increasing the overburden weight by the centrifuge speed and the sand extracted from a void beneath the layers. Abdulla and Goodings (1996) examined the stability of cemented layer above the cylindrical void with and without overburden pressure. The Broms and Bennermark's stability number has been continued by (Jacobsz 2016). Also, it has been used by our research group (Shiau & Al-Asadi 2018).

Atkinson and Potts (1977) used the bound theory and experimental method to study the stability of shallow circular tunnels in cohesionless soil under plane strain conditions. The centrifugal experimental investigation consisted of small-scale models. They have concluded that the accuracy is high with *FELA* solution of lower and upper bound and coincides with experimental centrifugal solutions. A similar analysis was later followed and expanded by other researchers, such as Mair (1979), Davis et al. (1980), Muhlhaus (1985), and Leca et al. (1990) to investigate various types of underground openings.

Davis et al. (1980) used the limit analysis theorem to determine the upper bound and lower bound solution of the problem. The approach was different from the original Brom and Bennermark (1967) approach, the stability number in this present form is called as pressure ratio as in the equation below in which the parameters have been presented independently and the stability pressure ratio (*PR*) has become the function of the strength ($\gamma W/S_u$) and depth ratio$_s$ (*C/W*), as indicated below.

$$PR = \frac{\sigma_s - \sigma_t}{S_u} = f\left(\frac{C}{W}, \frac{\gamma W}{S_u}\right) \tag{2.2}$$

Where (S_u) undrained shear strength, (γ) unit weight of soil, meantime, (W) is the width of the opening, and (C) is cover to the crest of opening. When ϕ_u =0, the undrained stability solution is independent of loading directions in the homogeneous soils. Davis's pressure ratio approach did not appear to reduce the complexity of presenting the results. The strength ratio component ($\gamma W/S_u$) has been considered in Broms and Bennermarks' stability number equation, which is more effective and efficient in this aspect (Shiau & Al-Asadi 2018).

Noticeably, ($\gamma W/S_u$) has little effect on the final critical stability number (N_c) solutions when its value is small, in another word, either the tunnel diameter W is very large (C/W very small) or S_u is very small, it will have a considerable effect on the stability results. In this case, the soil pressure distribution is highly nonlinear. Numerically speaking, it is an unstable case, and one may not get a solution for such an extreme case. If we do get a solution, it may become inaccurate due to numerical non-convergence.

This is also evidenced from the linear relationship between the pressure ratio $\{(\sigma_s - \sigma_t)/S_u)\}$ and the strength ratio ($\gamma W/S_u$) in the past results (Augarde et al. 2003; Wilson et al. 2011; Ukritchon & Keawsawasvong 2017; Zhang et al. 2018). Based on an assumed collapse mechanism Osman et al. (2006) have developed an upper bounds solution for obtaining the stability of a circular tunnel in clay, that is, within the boundary of the deformation mechanism, the soil was assumed to deform compatibly following a Gaussian distribution, and outside this mechanism, the soil was assumed to be rigid. For two-dimensional (2D) and three-dimensional (3D) stability analyses of circular tunnels in a purely cohesive soil, Klar et al. (2007) suggested a new kinematic approach in limit analysis theory based on an admissible continuous velocity field. Osman (2010) proposed a new methodology for calculating an upper bound for twin tunnels based on the superposition of the plastic deformation mechanisms of each tunnel.

A new kinematic approach in limit analysis theory for circular tunnels in a purely cohesive soil based on an admissible continuous velocity field in two-dimensional (2*D*) and three-dimensional (3*D*) stability analyses was suggested by (Klar et al. 2007). Following this analysis, Osman (2010) carried out an undrained stability number of twin tunnels, and a methodology for calculating an upper bound for twin tunnels based on the superposition of the plastic deformation mechanisms of each tunnel was proposed.

In the past, mostly deep-seated cavities such as tunnels were investigated by numerous researchers. Flat planar trapdoor stability under active plain strain conditions were investigated by several researchers (Koutsabeloulis & Griffiths 1989; Sloan et al. 1990; Martin 2009; Wang et al. 2017; Keawsawasvong & Ukritchon 2017, 2021; Shiau and Hassan 2020 & 2021 and Keawsawasvong & Likitlersuang 2020).

A circular cavity or tunnel in plain strain condition was studied by Drumm et al. (2009), Wilson et al. (2011), and Yamamoto et al. (2011) to derive the active stability solutions. The problems of flat rectangular and circular trapdoors under three-dimensional conditions were considered by (Ukritchon et al. 2019 and Shiau et al. 2021). (Augarde et al. 2003; Keawsawasvong & Ukritchon 2019 and Keawsawasvong 2021) were also investigated the active collapse of spherical cavities. Out of the above-mentioned studies, only few studies considered the passive failure of trapdoors (Koutsabeloulis & Griffiths 1989; Wang et al. 2017 and Shiau et al. 2021). Very recently, Shiau and Al-Asadi (2020a-d, and 2021) have also studied both the collapse and the blowout problem for two- and three-dimensional tunnels using the latest nonlinear programming technique of finite element limit analysis. Compared to deeper cavity investigations, very few past studies are related to the shallow depth cavities stability due to the water main leakage.

A case study was conducted by Hadjmeliani (2015) on sinkhole formation due to the degradation of a sewage pipe. The study was carried out on the large hole that occurred on the main road of Tripoli. The failure analysis was a collapse in the form of a large hole was observed on one of the main roads of Tripoli, Libya. The investigation results revealed that the pipe interior surface suffering from severe degradation. The original wall thickness was reduced catastrophically. Damages in pipe wall allowed fluid leaks, cavities in soil, and collapse of pavement layers. The condition underneath the road resulted in this big sinkhole.

Soil erosion around the cracked sewer pipe and consequent sinkhole formation was studied by Guo et al. (2013) and found that erosion triggers because of the groundwater infiltration into the sewer. Additionally, four factors (crack size, soil grain size, water head, and soil layer thickness) were investigated to determine whether they have any influence on the erosion process. It was found that soil height and the water head influence geometry of the erosion opening. Also, the relationship was established for computing soil-discharge rate, water-discharge rate, and void diameter.

Indiketiya et al. (2017) investigated erosion-induced ground settlement and the susceptibility of pipe bedding materials to internal erosion. The corresponding ground displacement is tracked by image correlation based on particle image velocimetry (*PIV*). The results indicate that particles less than 0.3 mm are highly vulnerable to erosion through 5 mm openings of embedment material with a maximum particle size of 4.75 mm. The proposed method is beneficial, as it allows measurement of the deformation at any time and any location throughout the test and facilitates checking the resistance to erosion of pipe embedment materials. Kim et al. (2017) studied the ground failure mechanism caused by water and sewer pipe breakdown by model experiment to verify characteristics of ground subsidence.

Lower relative density and lower seepage pressure resulted in small-scale ground subsidence, but when the conditions are opposite, large-scale ground subsidence occurred and expands to ground level over time.

The effect of the leak size of defective sewer pipes on soil erosion was studied by (Ghulam et al. 2018). The results indicated that leak width and the soil particle have a high level of influence in the loss of soil particles into the pipe. i.e. the amount of soil loss of soil particles is inversely proportional to the ratio of soil particle to leak width. A logistic regression model to sewer damage-induced sinkholes was developed by Kim et al. (2018) to evaluate the susceptibility of sinkholes due to the leakage of the sewer line. The model was established by analysing the sinkhole cases and the sewer pipe network in Seoul, South Korea. Nine independent variables were incorporated in the final model and out of that the length, age, and equivalent radius of sewers showed a positive relationship with sinkhole probability.

Karoui et al. (2018) conducted series of tests to investigate ground subsidence mechanisms spawned by sewer pipe leakage according to different groundwater flow modes and found that the process of ground subsidence occurrence is cavity formation around the groundwater leakage point, either by ground loosening or by external soil erosion. Mechanisms are repeated until the complete collapse of the soil specimen. Cyclic leakage leads to a faster collapse than a continuous leakage system and a succession of fast water supply and drainage cycles leads to a faster collapse than slow water supply and drainage cycles.

The viability of using Wireless Sensor Networking (*WSN*) for monitoring underground pipelines leakages and sinkholes was evaluated by (Ali and Choi 2019). Various approaches as patent analysis, web-of-science analysis, and *WSN* based pipeline leakage and sinkhole monitoring have been discussed based on different objectives and their applicability.

The study found that the research on using the *WSN* technique in the detection of a sinkhole is in an early stage and demands further investigation and research contributions. Additionally, the authors have suggested prospects for future research by comparing, analysing, and classifying the reviewed methods.

Very few studies can be found concerning soil blowout due to water main bursts. Especially, no researchers have considered the changes in cavity shapes. In terms of collapse analysis related to the low pressurised utilities such as sewer pipes, no investigation has been carried out with three progressive openings. This thesis utilises the recent robust finite element limit analysis (*FELA*) technique and adaptive mesh capability to study soil-related blowout and collapse stability due to defective pipelines. Three internal cavity shapes are studied for a wide range of depth ratios and soil strength ratios. Design charts are presented, allowing accurate assessment of blowout and collapse stability.

CHAPTER 3 FINITE ELEMENT LIMIT ANALYSIS

3.1. INTRODUCTION

Stability analysis is used to predict the maximum load a geostructure can carry without failure (Sloan 2013). Finite Element Limit Analysis (*FELA*) is one of the four widely used stability analyses namely limit equilibrium, limit analysis, slip-line methods. The precious parameters studied using the finite element software *Optum CE* are strength and deformation. Although the common solution technique is the same, it differs in some features. The program has features that are common to many other finite element earth technology programs but differs in several ways. *Optum CE* packages give the exact solutions directly with rigorous calculations for the upper and lower bounds, rather than in a traditional step-by-step elastomeric plastic process. A set of fixed soil and structural parameters are used to calculate the maximum load and the bearing capacity. Conversely, it can fix a set of load values and determine the commutation of the upper and lower limits (*Optum CE,* 2020).

3.2. FINITE ELEMENT LIMIT ANALYSIS (*FELA*)

The finite element limit analysis uses discrete formation by utilising the elements. Theoretically, the finite element limit analysis approach is very different from the other conventional approaches. The finite element limit analysis (*FELA*) presents the solution in terms of the lower bound and upper bound. In this approach, the upper bound solution outlines the kinematically admissible velocity field, which will provide an unsafe solution, while the lower bound represents the statically admissible stress field of stability number.

Initially, this method was followed by Drucker et al. (1952) and was developed into linear and nonlinear programs (Sloan 1988, 1989; Lyamin et al. 2002a, 2002b and Krabbenhoft et al. 2003). The complete development and description of *FELA* can be found in (Sloan 2013). The basic theorem of the numerical stability solution is the finite element formulation of the plastic limit boundaries which are upper and lower bounds. The upper and lower bounds theorems in the classical plasticity theory are a very useful tool for estimating the stability of the problems. The material model assumed to be perfectly plastic and obeys the associate flow rule.

3.2.1. Development of the lower bound theorem

The lower bound theorem is so-called a safe theorem. It employs the statically admissible stress field, which is to find the stress in equilibrium with the applied loads and satisfy the yield condition. Lysmer (1970) was an early pioneer in applying finite elements and optimisation theory to compute rigorous lower bounds for plane-strain geotechnical problems. He used internal polyhedral approximation to linearise the yield surface which replaced each non-linear yield inequality. Even though the development of Lysmer's development was an important milestone, its limitation prevented it from use.

Anderheggen & Knöpfel (1972); Pastor (1978) and Bottero et al. (1980) proposed various discrete methods for two-dimensional lower-bound limit analysis that were all based on linear triangles and linear programming. These procedures introduced several key improvements, including the use of Cartesian stresses as problem variables to simplify the formulation, and the development of special extension elements for generating complete solutions in semi-infinite media. Followed by Pastor & Turgeman (1982) proposed a lower-bound technique for modelling the important case of axisymmetric loading.

Although potentially powerful, these early methods were limited by the computational performance of the linear programming codes at the time and could solve only relatively small problems. To resolve this problem, Sloan (1988a, 1988b) proposed a fast linear programming formulation that can solve small to medium scale two-dimensional problems on a standard desktop machine.

Also, successfully used to resolve two-dimensional problems such as tunnels (Sloan & Assadi 1991, 1992), slopes (Yu et al. 1998), and foundations (Ukritchon et al., 1998). As the lower-bound methods based on linear programming are provided an effective solution for the two-dimensional problem of moderate size and huge numbers of inequalities arise when yield criterion is linearised for the three-dimensional problem. The above issues can be avoided by adopting non-linear programming algorithms. Formulation of non-linear programming is described by Belytschko and Hodge (1970) even though slow for the large-scale problem. Using the extended penalty method (Kavlie & Moe 1971) to convert constrained optimisation problem into unconstrained problem. Basudhar et al.(1979) computed the best lower bound solution also using a variant of the sequential unconstrained minimisation technique (Powell 1964). To obtain an admissible stress field for geotechnical problems, coupled solution of gradient algorithm by Fletcher and Reeves (1964) used by Aria and Tagyo (1985) in conjunction with constant-stress elements and the sequential unconstrained minimisation technique. Lyamin (1999) and Lyamin & Sloan (2002b) dramatically improved the practical utility of the discrete lower-bound method by employing linear stress elements, imposing the non-linear yield conditions in their native form, and solving the resulting non-linear optimisation problem using a variant of an algorithm developed for mixed limit analysis formulations (Zouain et al., 1993). The solution method used by Lyamin and Sloan (2002b) exploits the underlying structure of the optimization problem and its iteration as independent of the refinement grid.

As such this technique can be used to resolve a large number of meshes in the two-dimensional investigation and the three-dimensional problem with a large number of unknowns. To solve the structural engineering problems, Krabbenhoft and Damkilde (2003) introduced separate non-linear programming.

Tresca and Mohr-Coulomb criteria create special difficulties in the finite-element limit analysis because of the presence of singularities on the yield surfaces where the gradient in respect of stress becomes undefined. Lyamin and Sloan (2002b) solved this issue by local smoothing of the yield surface vertices, locally by a modification to the search direction preserve practicability during the optimization iterations. Another method to resolve the lower-bound analysis problems is second-order cone programming (Ciria 2004; Makrodimopoulos & Martin 2006; Bhattacharya et al. 2020) and the method does not require differentiability of the yield surface in the optimization process. The method could be applied to various two-dimension problems including Tresca and Mohr-Coulomb models. Also, evident to be vigorous and efficient even for the large geotechnical problems (Krabbenhoft et al. 2007). Cone programming can be used for Von Mises and Drucker-Prager yields criteria of three-dimensional cases but cannot be used for Tresca or Mohr-Coulomb models.

In addition, Krabbenhoft et al. (2008) developed a different cone-based solution algorithm that is known as semi-definite programming that can be used for Tresca and Mohr-Coulomb models. This approach does not require the smoothing of any yield surface vertices. Also proved to be vigorous and effective for large-scale applications. concisely, the second-order cone method and the semidefinite method are the solution methods for the Tresca and Mohr-Coulomb model of two and three-dimensional conditions, respectively.

3.2.2. Development of the upper bound theorem

The upper bound theorem of the classical plasticity material employs the kinematically admissible velocity field which can be satisfied to the external loads; therefore, it enables a strict upper bound on the limit load to be reduced. The upper bound theorem has been used frequently to investigate the undrained stability problems with the Tresca yield condition soil. In this condition, the power is assumed to be depleted at the interfaces between the adjacent elements, and the geometry is modified to yield the minimum depleted power.

Anderheggen & Knöpfel (1972 and Maier et al. (1972) proposed the early distinct in formulations of the upper-bound theorem, based on finite elements and linear programming. Although structural applications were the general practice with upper-bound theorem, the subsequent plane-strain procedures by Bottero et al. (1980), which focused on geotechnical applications with Tresca and Mohr-Coulomb yield criteria, permit a limited number of velocity discontinuities to occur between elements, but require the direction of shearing to be specified a priori. Pastor and Turgeman (1982) expanded the upper-bound formulation of Bottero et al. (1980) to handle axisymmetric geometries in addition to the early practices that centered on plane problems, although only for Von Mises and Tresca materials.

Since more time is required for the *CPU* to solve the related linear programming problems they were not widely applied in practice although the upper-bound methods succeed to all the key advantages of the finite-element technique with two-dimensional problems. To rectify this drawback, Sloan (1989) introduced an upper-bound method centered on the steepest-edge active set solution scheme (Sloan 1988b), which had proved as successful for lower-bound limit analysis. The procedure proved to be inefficient for large-scale examples involving thousands of elements.

A good guess of the likely collapse mechanism in advance required to specify both the location and the direction of shearing for each discontinuity in an upper-bound analysis is a significant drawback. Sloan and Kleeman (1995), addressed the issue by generalising the upper-bound formulation of Sloan (1989) to include velocity discontinuities at all edges shared by adjacent triangles. Hodge and Belytschko (1968) were introduced the plate formulation described by one of the first attempts to develop a finite-element upper-bound method based on non-linear programming. Their analysis used classical theory to specify the deformation field solely by the velocity normal to the original middle surface of the plate.

Subsequently, numerous other non-linear programming formulations were proposed for computing upper bounds on the load capacity of plates, shells, and structures (Biron & Charleux 1972; Nguyen et al. 1978). Huh and Yang (1991) developed a general upper-bound procedure for plane stress problems using triangular elements with a linear velocity field. Capsoni and Corradi (1997) proposed another separate upper-bound approach in an attempt at further development, where the straining modes are modelled independently of rigid-body motions. By assuming the material is viscous-plastic and uses two parameters to characterise its creep behaviour, Jiang (1994) proposed an upper-bound formulation in another separate non-linear approach, based on a normalised model of limit analysis. Jiang (1994) used the augmented Lagrangian method in conjunction with the algorithm of Uzawa (Fortin & Glowinski, 1983) to solve the resulting non-linear optimisation problem. In another publication, it was established that the same non-linear programming scheme could be utilised to perform upper-bound limit analysis precisely by (Jiang 1995). But the application with three-dimensional geometries and discontinuities in the velocity field has not been extended although worked well with two-dimensional (2*D*) models.

An iterative method for performing three-dimensional upper-bound limit analysis was developed by Liu et al. (1995) at the same time. This method handled the rigid zone separately from the plastic zones throughout the iteration process and conveniently avoided the numerical difficulties that stem from a non-differentiable objective function. Lyamin and Sloan (2002a) also developed an upper-bound finite-element method that was also based on non-linear programming. This procedure assumes that the velocities vary linearly over each element and that each element is associated with a constant stress field and a single plastic multiplier rate.

The upper-bound formulation of Lyamin and Sloan (2002a) was modified by Krabbenhoft et al. (2005) by proposing an alternative stress-based method that uses patches of continuum elements to incorporate velocity discontinuities in two and three dimensions.

3.3. NUMERICAL MODELLING IN OPTUM CE

Software packages are used to solve most of the geotechnical problems. The present analysis (*OptumG2*) is used as finite element software designed to solve boundary geotechnical problems. Many features in the software are used to detail the road sinkhole analysis, repetitive procedures adopted with different sizes and types of geometry.

The basic sketches for the software milieu are presented in Figure 3.1. The two-dimensional design grid is cantered in the overview, and the Stage Manager to the right, while the four tabs; Geometry, Materials, Features, and Results are presented above the grid. The geometry of the problem is defined initially using the functions such as Point, Line, Arc, Circle, and Rectangle by clicking on the relevant icon in the top bar and clicking the cursor in the required grid point. The function icons are shown top bar (Figure 3.1).

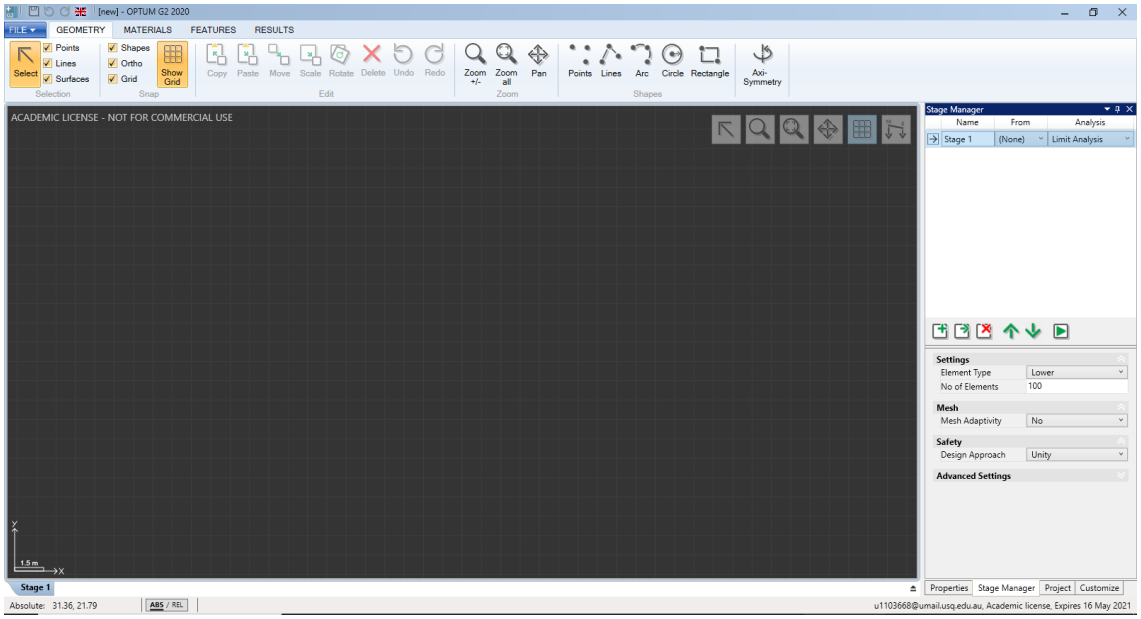

Figure 3.1. Software background view (*Optum G2*, 2020)

The tap menu also includes the editing tools such as cut, paste, move, delete, rotate, undo and redo. When the model has been created on the grid, the material should be defined using the material toolbar as shown in Figure 3.2. A range of materials is available in the software for use in the model to match the actual field requirement. Various varieties of material are inbuilt with *Optum*G2 namely Mohr-Coulomb and Tresca. Additionally, custom material also could be defined as per the user's requirement.

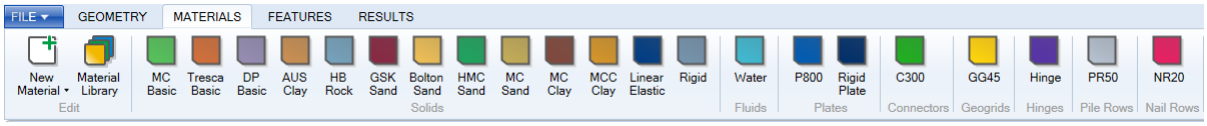

Figure 3.2. Material archive (*Optum G2*, 2020)

An example of the semi-circular trapdoor is presented in Figure 3.3 with allocated Tresca soil and the left-hand side 'properties' bar showing the soil properties. The material could be altered to match up with the actual need. Also, there are taps available to change the properties such as General, Material, Stiffness, Strength, Flow rule, Tension Cut-Off, Unit weights, and Initial Conditions.

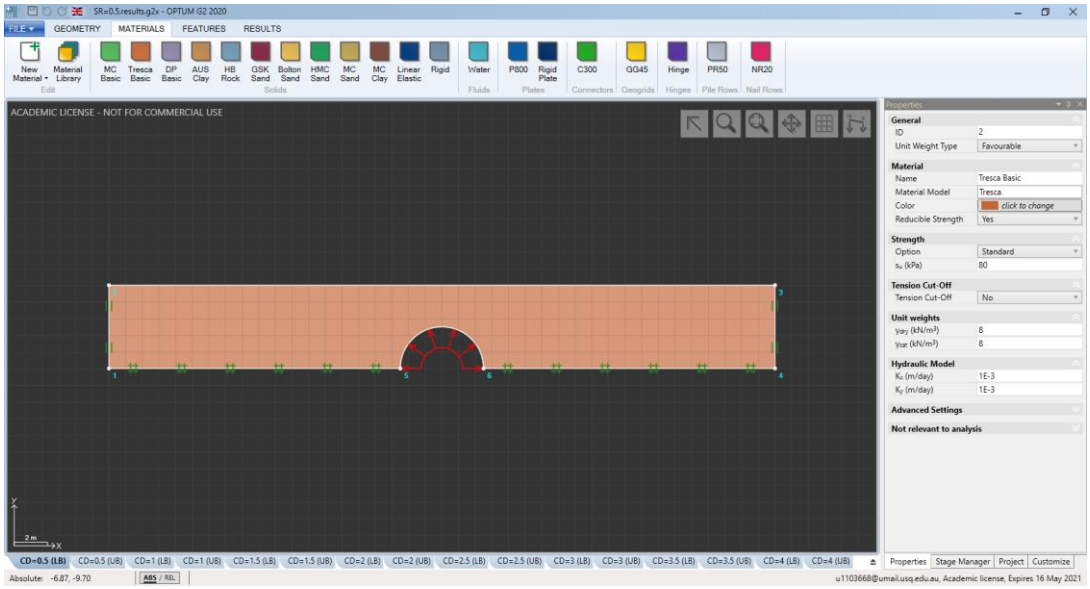

Figure 3.3. Geometry illustration and material properties for Mohr-Coulomb soil (*Optum G2*, 2020)

Boundary support condition varies for each side of the model according to the need. *Optum CE* (2020) featured with three support conditions are the Full, Normal, and Tangential supports. Physical application is processed by selecting the relevant boundary and applying the support icon. Full restrain resits the movement in all directions whilst the Normal and Tangential supports restrain movement in the perpendicular and parallel directions of the lines or surfaces, respectively (Figure 3.4).

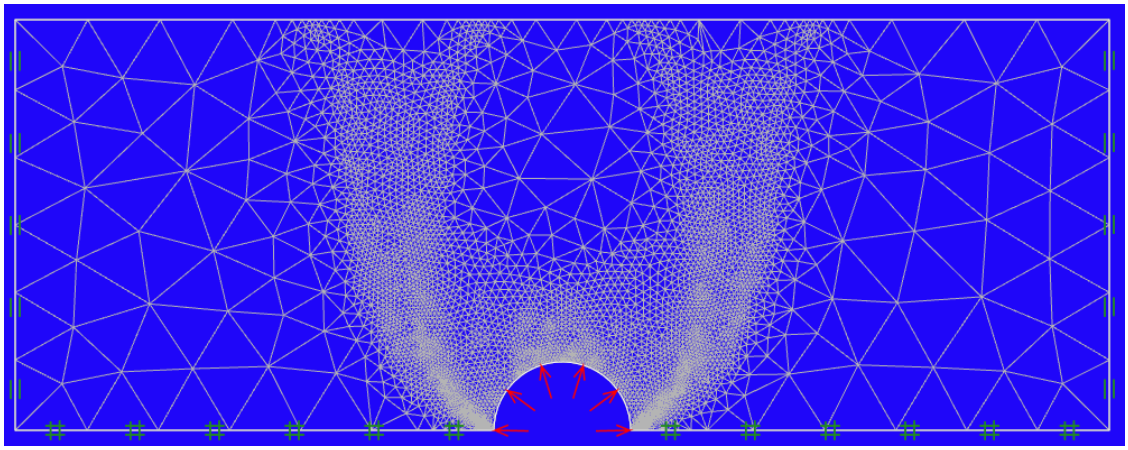

Figure 3.4. Standard boundary condition for the domain (*Optum G2*, 2020)

There are few more features with the *Optum CE* that could be used for a range of geotechnical problems. They are Connector, Fixed End Anchor, Plate, Geogrid, Shear Joint, Mesh Size, and Mesh Fan. These features are mostly used for specialised analyses of geotechnical and structural problems. Loading conditions could be chosen to suit the problem. Two loading conditions available for use are Fixed loads and Multiplier loads specified green and red colours, respectively. Multiplier load initially starts with the value of 1kN/m^2. According to the requirement the load type could be selected as concentrated, distributed or body loaded and the application spot such as nodes, lines, surfaces, and solids as presented in Figure 3.5. Depending on the analysis type, the load type will be decided. For instance, when computing the maximum allowable pressure in pipe burst related analysis, the uniform distributed Multiplier load should be applied at the trapdoor to simulate the actual case as shown in Figure 3.5.

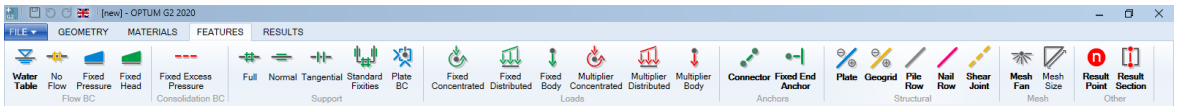

Figure 3.5. Loading features toolbar (*Optum G2*, 2020)

The tap namely the Stage Manager located at the bottom right-side is to choose the analysis type. Analysis type together with the initial conditions activated for each analysis. The options in the Analysis tab are Mesh, Seepage, Initial Stress, Limit Analysis, Elastoplastic, and Feasibility. In the case of Limit Analysis, the multiplier loads (which also known as collapse multiplier) are magnified up until the model reaches the failure stage. Further to the collapse multiplier for a set of external loads, it is also possible to compute the gravity amplified factor at the state of failure. This feature is useful in slope stability computations. The element type in *Optum CE* can be Lower, Upper, 6-node Gauss, 15-node Gauss, or something else. The present study is a Limit analysis that calculated both lower and upper bound for load multiplier in two- dimensional (2*D*).

The number element tab is to establishes the total number of elements used in the model geometry which determines the accuracy of the analysis. The mesh adaptivity is to refine the failure mechanism. The number of elements at the initial mesh is Start Elements meantime the Adaptivity Control tab is the control variable adopted. Recommended iteration to adopt is either three or four iterations for better accuracy. A full illustration of Stage Manager is presented in Figure 3.6.

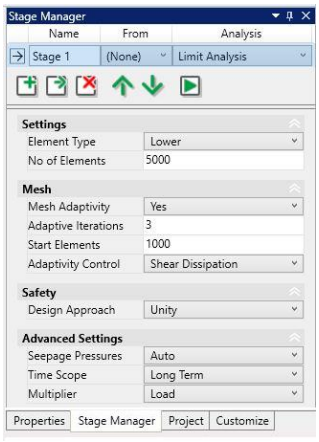

Figure 3.6. Stage Manager for Limit Analysis (*Optum G2*, 2020)

Figure 3.7. represents the pipe burst-related stability problem in two-dimensional (2*D*) space. The model is analysed using Limit analysis with Load Multiplier and presented in the form of shear dissipation contour with mesh overlay. The plasticity of the model is indicated by the shear dissipation quantity, and which is shear stress times shear strain at failure. Hence, the contour animation indicates the failure mechanism of blowout failure.

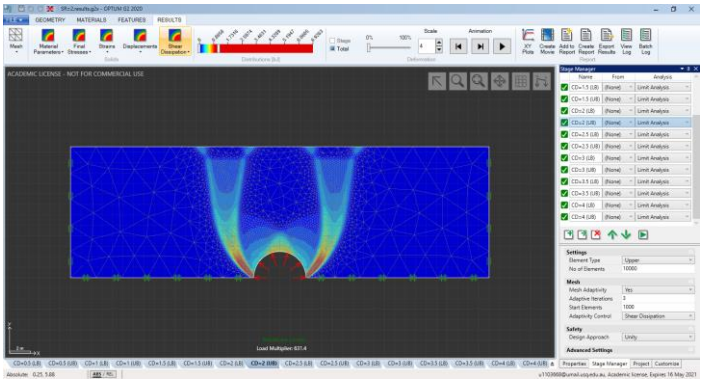

Figure 3.7. Shear dissipation of the pipe blowout case (*Optum G2*, 2020)

3.4. SHEAR STRENGTH REDUCTION METHOD (SSRM)

With the development of computer technology over the past decades, numerical modelling has become an essential tool in geotechnical engineering. Stability analysis can be performed by the calculation of factors of safety in FLAC using the shear strength reduction method (SSRM). The SSRM is commonly applied through the factor of safety calculation by gradually reducing the shear strength of the testing material to estimate the point where the system reaches a state of limiting equilibrium. This method is popular in the stability analysis of slopes, retaining walls and tunnels; however, it has rarely been used in stability analysis of sinkholes. The shear strength reduction method (SSRM) with the aid of the built-in program language, FISH, to analyse the stability problem. This method was utilised as early as 1975 by Zeinkiewicz et al. (1975), followed by Naylor (1982), Matsui and San (1992), Ugai and Leshchinsky (1995), Griffiths and Lane (1999), Michalowski (2002), Zheng et al. (2005) and numerous researchers. The SSRM is coded in the finite difference software FLAC as well as many other computational tools, such as Plaxis (2011) and Optum G2 (Optum CE 2020). In the method of shear strength reduction, a factor of safety is defined as the ratio of the actual undrained shear strength and the critical undrained shear strength, as shown in equation (3.1).

$$FoS = \frac{S_u}{S_c} \tag{3.1}$$

Where (S_u) is the actual undrained shear strength of the soil and (S_c) is a critical shear strength at collapse. In practice, the factor of safety above one demonstrates a stable condition. In this study, the soil body is defined as a homogeneous, undrained clay, following the Tresca material. The shear strength reduction method (SSRM) is usually applied to the conventional model of Mohr-Columb material.

CHAPTER 4 PIPELINE BURST-RELATED COLLAPSE STABILITY

4.1. INTRODUCTION

Underground water main leakage is one of the main causes for the instability of the soils and sinkholes. Infrastructure and road surface damages, traffic interruption, and in some cases a loss of life are the major problems facing many authorities nowadays. In the event of a water main burst, the pressure would be upward and hence the soil layer should be analysed for blowout stability. Conversely, leakage from low-pressure utilities such as sewer pipes would erode the soil media around and leave it unstable with the internal opening created. In such a situation, the possible failure scenario would be for collapse stability.

This study sets out to quantify the "collapse" stability performance of three idealised cavity shapes above the damaged pipe. Advance numerical limit analysis was used to obtain upper and lower bound solutions to the problem. The study provides useful engineering information in the form of design charts and tables for a wide range of design parameters, which would greatly assist in decision-making by practical engineers.

4.2. PROBLEM SCOPE AND *FELA* MODELLING

The problem definition of a horizontal trapdoor is shown in Figure 4.1 with a typical adaptive *FELA* mesh. Similarly, the semi-circular and circular trapdoor problems are shown in Figures 4.2 and 4.3, respectively. All three trapdoors have a cover (C) and a width (W). The face of the trapdoor (cavity opening) is subjected to normal pressure (σ_t, positive as compression), while the ground surface is subjected to a surface pressure (σ_s, positive as compression). The soil is considered as a rigid-perfectly plastic Tresca material, soil unit weight is (γ) and (S_u) represents the undrained shear strength of the soil.

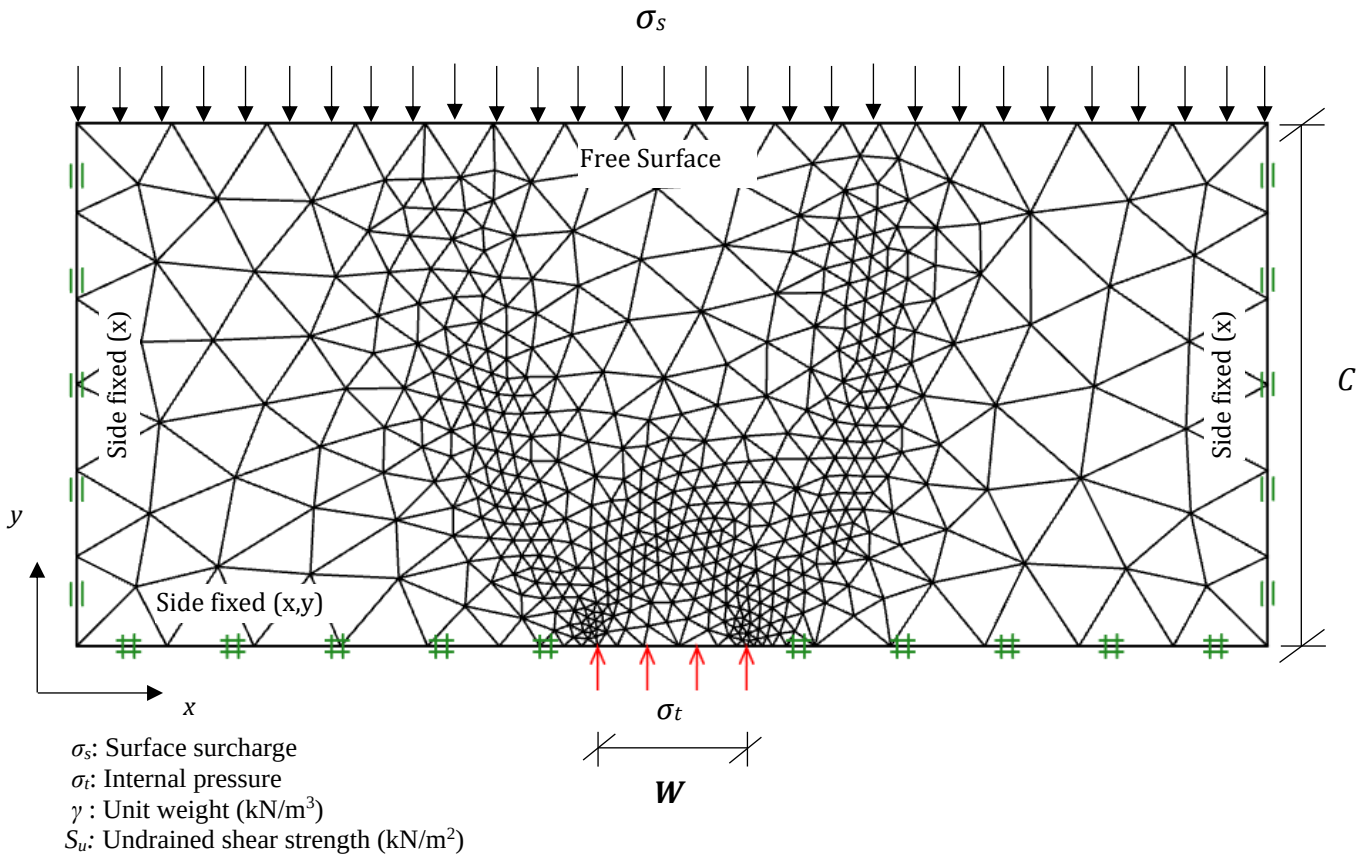

Figure 4.1. Problem definition (horizontal opening)

The domain size for the horizontal trapdoor, as in Figure 4.1, is chosen in such a way that all sides do not have any effect on the overall development of the velocity field. Note that both vertical sides are restrained in the *x*-direction and the bottom of the domain fixed in both *x* and *y*-direction. The nodes on the ground surface are free to move in all directions. The same boundary conditions apply to semi-circular and circular trapdoors (Figures 4.2 and 4.3). In this study, numerical solutions are obtained using the two numerical techniques of upper and lower bound theorems with finite element limit analysis (*FELA*). The kinematically admissible velocity field can be achieved by solving the upper bound optimisation problem, while the solution to the lower bound optimisation problem requires a statically admissible stress field. With the latest advances, the automatically adaptive mesh refinement is utilised in both *UB* and *LB* simulations to define the upper and lower limit loads (*Optum CE*, 2020). More details of the finite element formulations of upper and lower bound theorems can be found in (Sloan 2013).

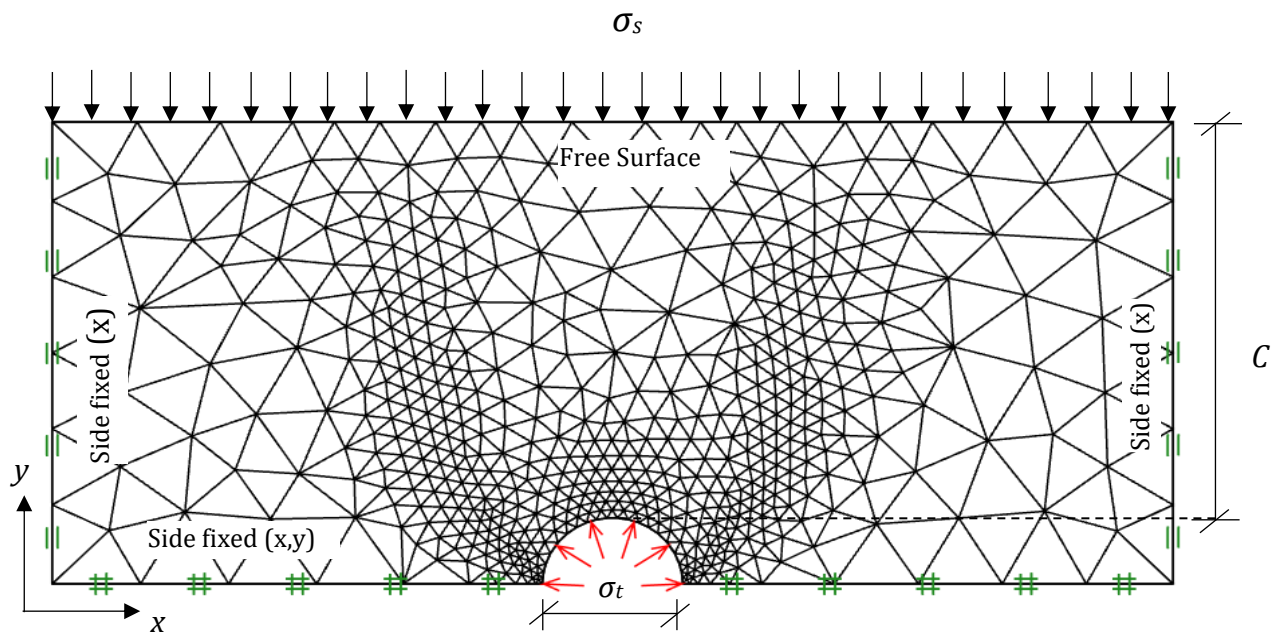

σ_s: Surface surcharge
σ_t: Internal pressure
γ : Unit weight (kN/m^3)
S_u: Undrained shear strength (kN/m^2)

Figure 4.2. Problem definition (semi-circular opening)

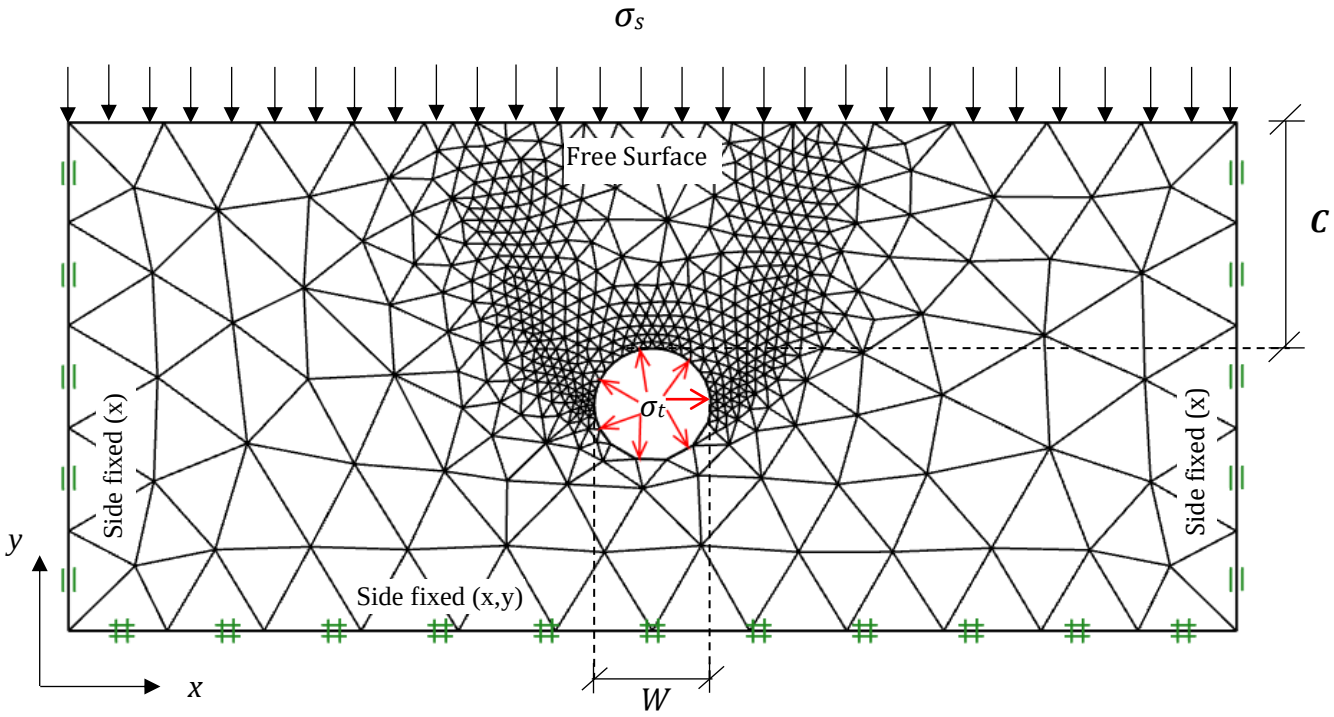

σ_s: Surface pressure
σ_t: Internal pressure
γ: Unit weight (kN/m^3)
S_u:Undrained shear strength (kN/m^2)

Figure 4.3. Problem definition (circular opening)

The stability number (N) was originally stated in Broms and Bennermark (1967) as a combination of the surcharge pressure(σ_s), overburden pressure (γH), and the supporting pressure (σ_t). To make it a dimensional ratio, the three combinations were divided by the undrained shear strength (S_u). The relationship is shown in equation (4.1).

$$N = \frac{\sigma_s + \gamma H - \sigma_t}{S_u} = f\left(\frac{H}{W}\right) \tag{4.1}$$

For the horizontal trapdoor problem, the stability number is a function of the depth ratio (H/W) only. H is the cover depth of soils. This approach was used by many researchers to formulate stability solutions. Shiau and Al-Asadi (2020d) studied the interaction effects between twin tunnels using the stability number. The same principle was used to analyse the three-dimensional (3D) face stability of the twin circular tunnel (Shiau and Al-Asadi 2020e). Based on the definition of the above-mentioned stability number, Davis et al. (1980) proposed an alternative way to express soil stability by using a pressure ratio that is defined as { $PR = (\sigma_s - \sigma_t)/S_u$ }.

$$PR = \frac{\sigma_s - \sigma_t}{S_u} = f\left(\frac{C}{W}, \frac{\gamma W}{S_u}\right) \tag{4.2}$$

The pressure ratio (PR), shown in equation (4.2), is a function of the shear strength ratio (SR, $\gamma W/S_u$) and the depth ratio (DR, C/W). In this Chapter, various depth ratios (C/W = 0.5-4) and shear strength ratio (SR = 0-2) are chosen to establish the lower and upper bound limits of the pressure ratio (PR). The value of the pressure ratio (PR) was computed by substituting the obtained critical “supporting” pressure (σ_t) and the relevant "designed” parameters (C, W, σ_s, γ, and S_u) into equation 4.2. This whole process applies to the proposed three idealised cavity shapes, which are all investigated under the active collapse scenario.

4.3. RESULTS AND DISCUSSION

4.3.1. Stability results - pressure ratio

Figures 4.4 - 4.9 show the relationship between the pressure ratio {*PR*, $(\sigma_s - \sigma_t)/S_u$} and the depth ratio (*DR*, *C*/*W* = 0.5 - 4.0) for the various strength ratios (*SR*, $\gamma W/S_u$ = 0 - 2) of the three idealised cavity shapes. The data used to plot the Figures are summarized in Tables 4.1- 4.3.

For the horizontal trapdoor in Figure 4.4, the results show that *PR* may either increase or decrease with the increasing depth ratio (*C*/*W*). According to the definition of *PR* = $(\sigma_s - \sigma_t)/S_u\}$, an increase in *PR* indicates that a larger surcharge pressure σ_s is required to fail the system. Conversely, a decrease in *PR* suggests the need for a larger supporting σ_t to prevent failures (a weaker system). Also, note that some of the results are negatives such as for $\gamma W/S_u$= 2 in the Figure4.4.

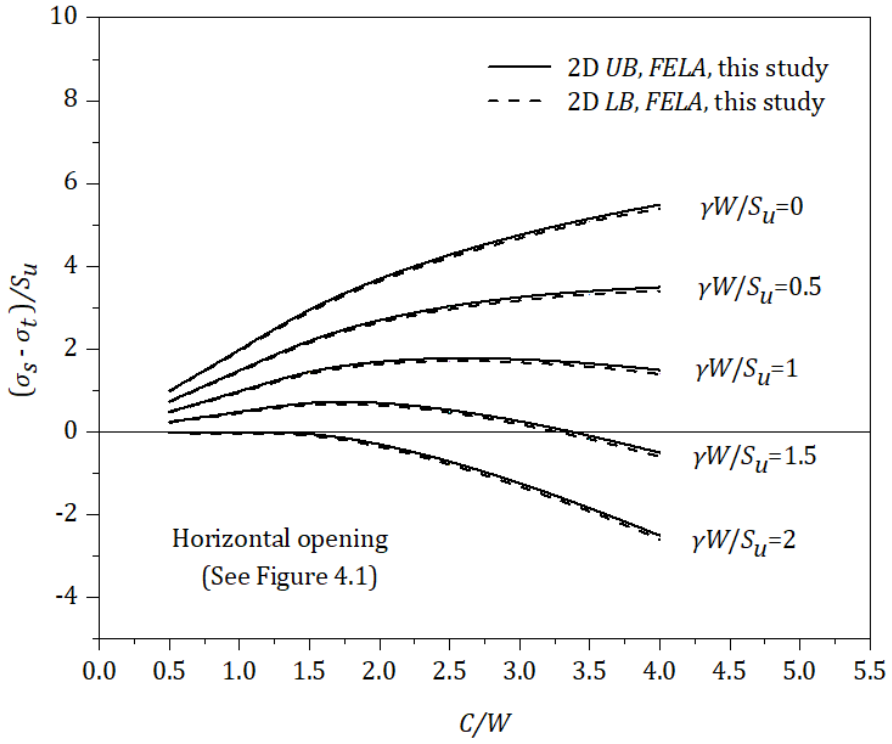

Figure 4.4. $(\sigma_s - \sigma_t)/S_u$ vs (*C*/*W*) for various ($\gamma W/S_u$) (horizontal opening)

For such a "heavy" system, σ_t must be greater than σ_s to maintain stability, and therefore a negative *PR* value is presented. In general, upper bound *PR* values (*UB*) are found to be greater than lower bound values (*LB*) and the true solutions are always bracketed in between within a percentage.

Figure 4.5 presents a design contour chart for the horizontal trapdoor. One needs to input the "designed" depth ratio (*DR, C/W*) and strength ratio (*SR,* $\gamma W/S_u$) to obtain a pressure ratio (*PR*), from which a limiting pressure (σ_s or σ_t) can be determined. Table4.1 shows the values used to plot the Figure 4.5.

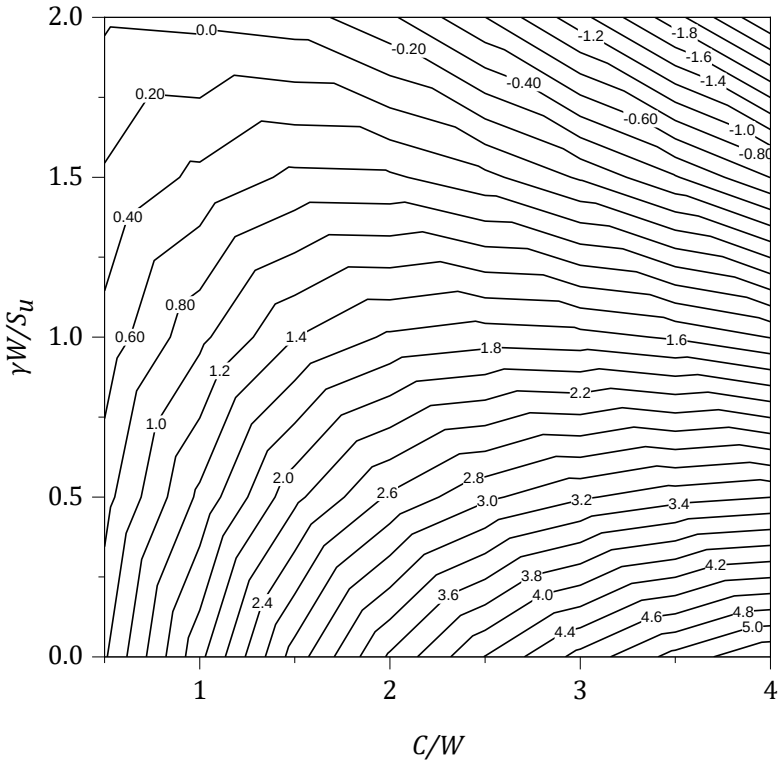

Figure 4.5. Collapse design chart for obtain *PR* (horizontal opening)

Likewise, the same trends are noticed for the semi-circular opening, but with different *PR* values as presented in Figures 4.6 and 4.7 as well as Table 4.2. Whereas for the circular opening, the results are presented in Figures 4.8, 4.9, and Table 4.3.

Table 4.1. Pressure ratio (*PR*) for horizontal opening

C/W	$\gamma W/S_u$									
	0		0.5		1.0		1.5		2	
	LB	*UB*	*LB*	*UB*	*LB*	*UB*	*LB*	*UB*	*LB*	*UB*
0.50	0.97	0.99	0.72	0.74	0.47	0.49	0.22	0.24	-0.03	-0.01
1.0	1.95	1.98	1.45	1.48	0.95	0.98	0.45	0.48	-0.05	-0.02
1.5	2.89	2.94	2.15	2.19	1.40	1.44	0.65	0.69	-0.10	-0.06
2.0	3.63	3.69	2.63	2.69	1.63	1.69	0.63	0.69	-0.36	-0.31
2.5	4.21	4.28	2.96	3.03	1.71	1.77	0.46	0.52	-0.80	-0.73
3.0	4.67	4.75	3.17	3.25	1.67	1.75	0.17	0.25	-1.33	-1.25
3.5	5.07	5.15	3.32	3.40	1.57	1.65	-0.18	-0.10	-1.93	-1.85
4.0	5.39	5.49	3.40	3.49	1.39	1.49	-0.60	-0.51	-2.60	-2.51

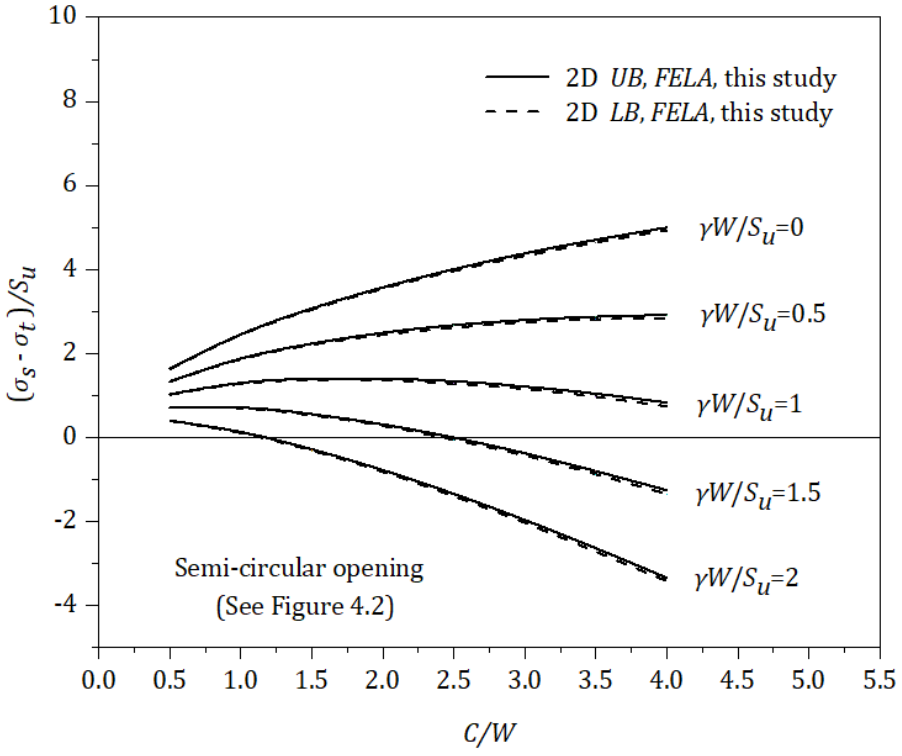

Figure 4.6. (σ_s - σ_t)/S_u vs (*C/W*) for various ($\gamma W/S_u$) (semi-circular opening)

The results obtained in Figures 4.4 - 4.9 and Table 4.1- 4.3 were generally consistent with field observation, and they can be used to estimate the critical pressures σ_t to cause a collapse failure.

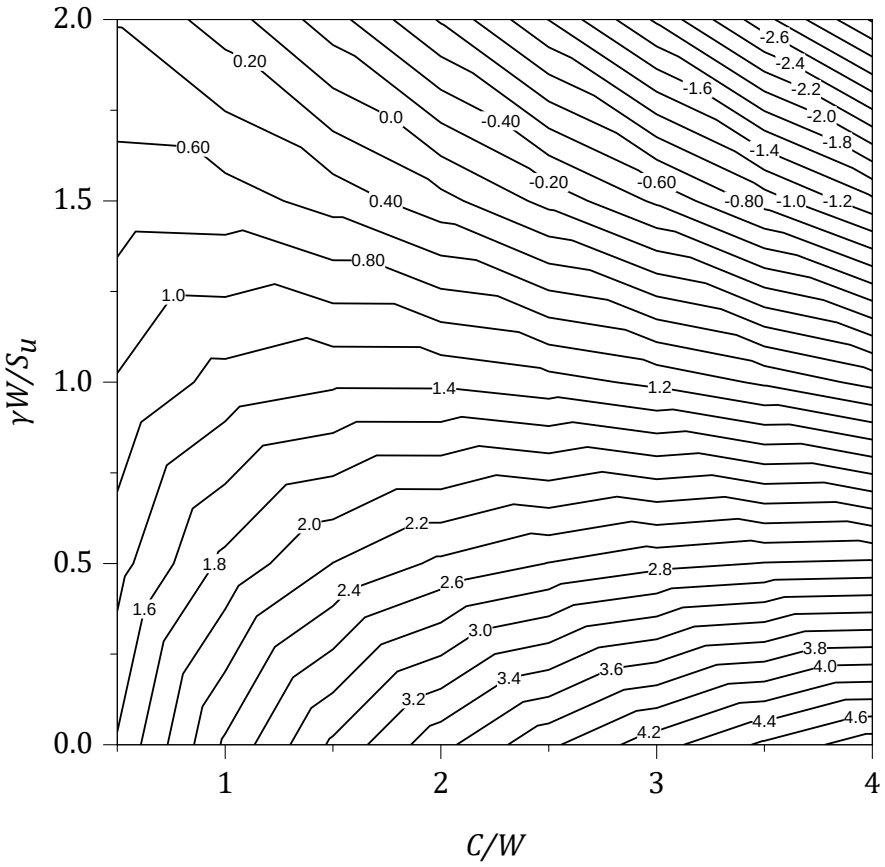

Figure 4.7. Collapse design chart to obtain *PR* (semi-circular opening)

Table 4.2. Pressure ratio (*PR*) for semi-circular opening

C/W	$\gamma W/S_u$									
	0		0.5		1.0		1.5		2	
	LB	*UB*	*LB*	*UB*	*LB*	*UB*	*LB*	*UB*	*LB*	*UB*
0.50	1.62	1.63	1.32	1.33	1.02	1.02	0.70	0.71	0.39	0.40
1.0	2.44	2.45	1.85	1.87	1.28	1.29	0.69	0.71	0.10	0.12
1.5	3.04	3.06	2.20	2.23	1.37	1.39	0.52	0.55	-0.32	-0.29
2.0	3.54	3.57	2.44	2.49	1.36	1.40	0.27	0.31	-0.82	-0.78
2.5	3.96	4.00	2.61	2.67	1.28	1.33	-0.06	-0.01	-1.41	-1.35
3.0	4.32	4.38	2.74	2.79	1.15	1.21	-0.44	-0.38	-2.04	-1.97
3.5	4.64	4.71	2.81	2.87	0.96	1.03	-0.88	-0.80	-2.73	-2.65
4.0	4.93	5.00	2.84	2.91	0.73	0.82	-1.35	-1.26	-3.43	-3.36

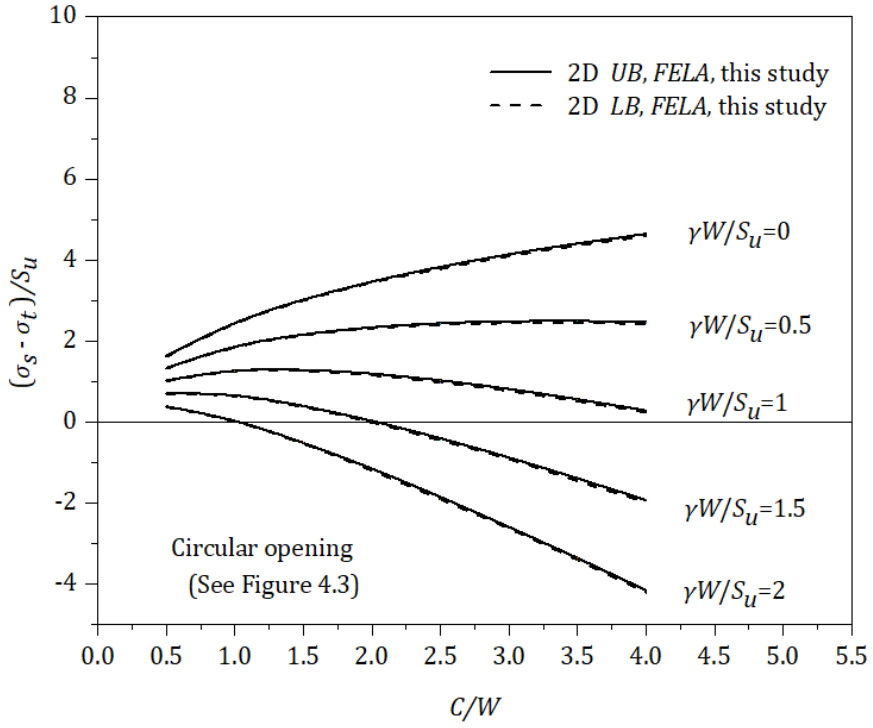

Figure 4.8. $(\sigma_s - \sigma_t)/S_u$ vs (C/W) for various $(\gamma W/S_u)$ (circular opening)

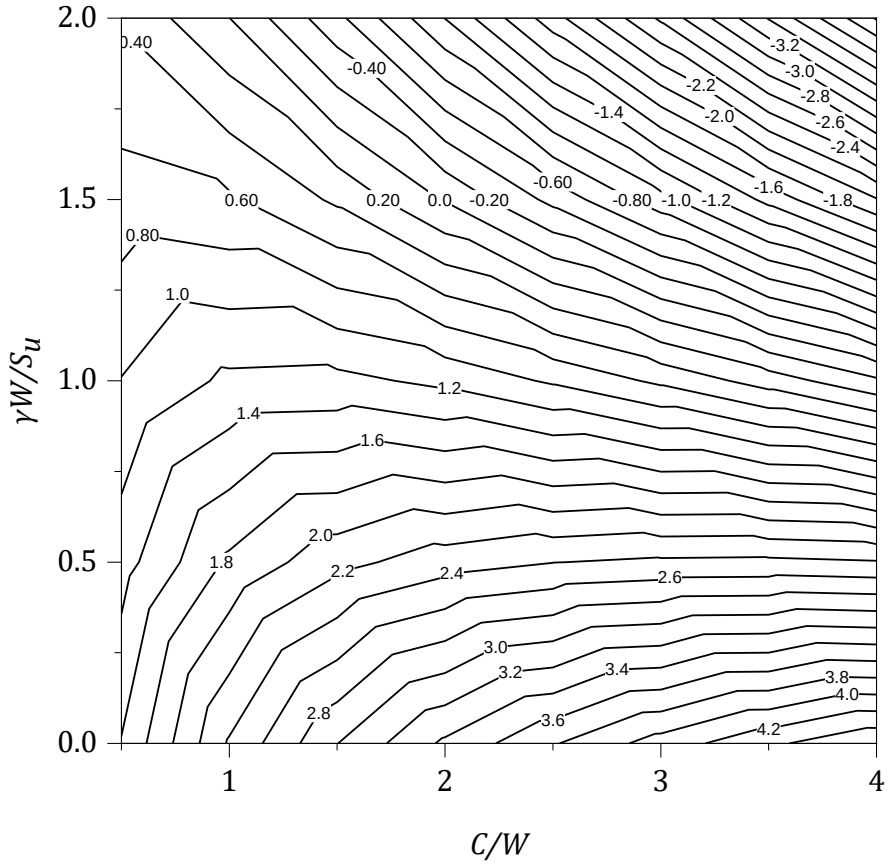

Figure 4.9. Collapse design chart to obtain *PR* (circular opening)

Table 4.3. Pressure ratio (*PR*) for the circular opening

C/W	$\gamma W/S_u$									
	0		0.5		1.0		1.5		2	
	LB	*UB*	*LB*	*UB*	*LB*	*UB*	*LB*	*UB*	*LB*	*UB*
0.5	1.61	1.63	1.32	1.33	1.01	1.02	0.69	0.71	0.37	0.38
1.0	2.42	2.44	1.84	1.86	1.24	1.26	0.63	0.65	0.00	0.02
1.5	3.00	3.02	2.14	2.16	1.26	1.28	0.36	0.39	-0.55	-0.52
2.0	3.44	3.46	2.31	2.33	1.15	1.19	-0.02	0.02	-1.20	-1.16
2.5	3.78	3.83	2.40	2.44	0.97	1.02	-0.46	-0.41	-1.92	-1.86
3.0	4.09	4.14	2.44	2.48	0.76	0.81	-0.92	-0.88	-2.64	-2.60
3.5	4.36	4.41	2.45	2.49	0.51	0.56	-1.46	-1.40	-3.41	-3.37
4.0	4.59	4.64	2.42	2.47	0.23	0.28	-1.99	-1.93	-4.22	-4.16

4.3.2. Failure extent and soil arching

Contour plots of the absolute velocity for depth ratios (*C/W* = 1 to 4) are shown in Figures 4.10- 4.12 for the three idealised cavity shapes, respectively. The plots are for $SR = \gamma W/S_u$ = 2.0. For the horizontal trapdoor demonstrated in Figure 4.10, a near-vertical slippage was shown for the shallow case (*C/W*=1). It was found that as the depth ratio *C/W* increases, the ground failure extent increases, and the slip surfaces have a higher curvature. Similar to the classic bearing capacity problem, there exists a triangular wedge located immediately above the trapdoor, showing the elastic zone with uniform velocity. This is shown in Figure 4.10 for *C/W*=1-4. For the semi-circular and circular openings, the contour plots of the velocity field are shown in Figures 4.11 and 4.12, respectively.

The overall collapse failure patterns are generally consistent with the horizontal opening. However, unlike the horizontal trapdoor, the elastic triangular pattern does not appear in these two “curved” openings. Further, a deep-seated failure mechanism is demonstrated throughout the deep cases in the circular opening (Figure 4.12).

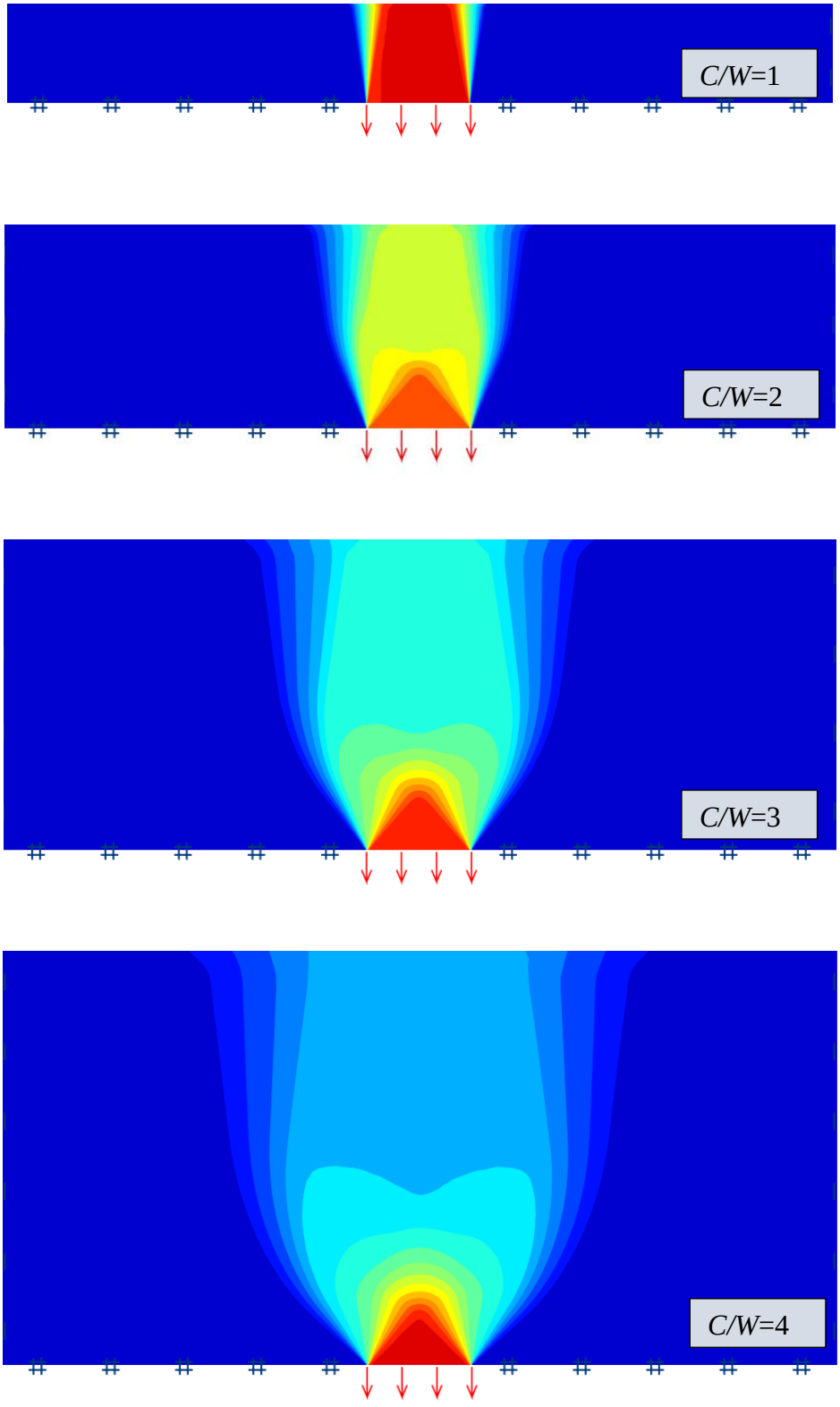

Figure 4.10. Absolute velocity (|u|) contour plot horizontal opening (*C/W* =1-4, *SR*=2)

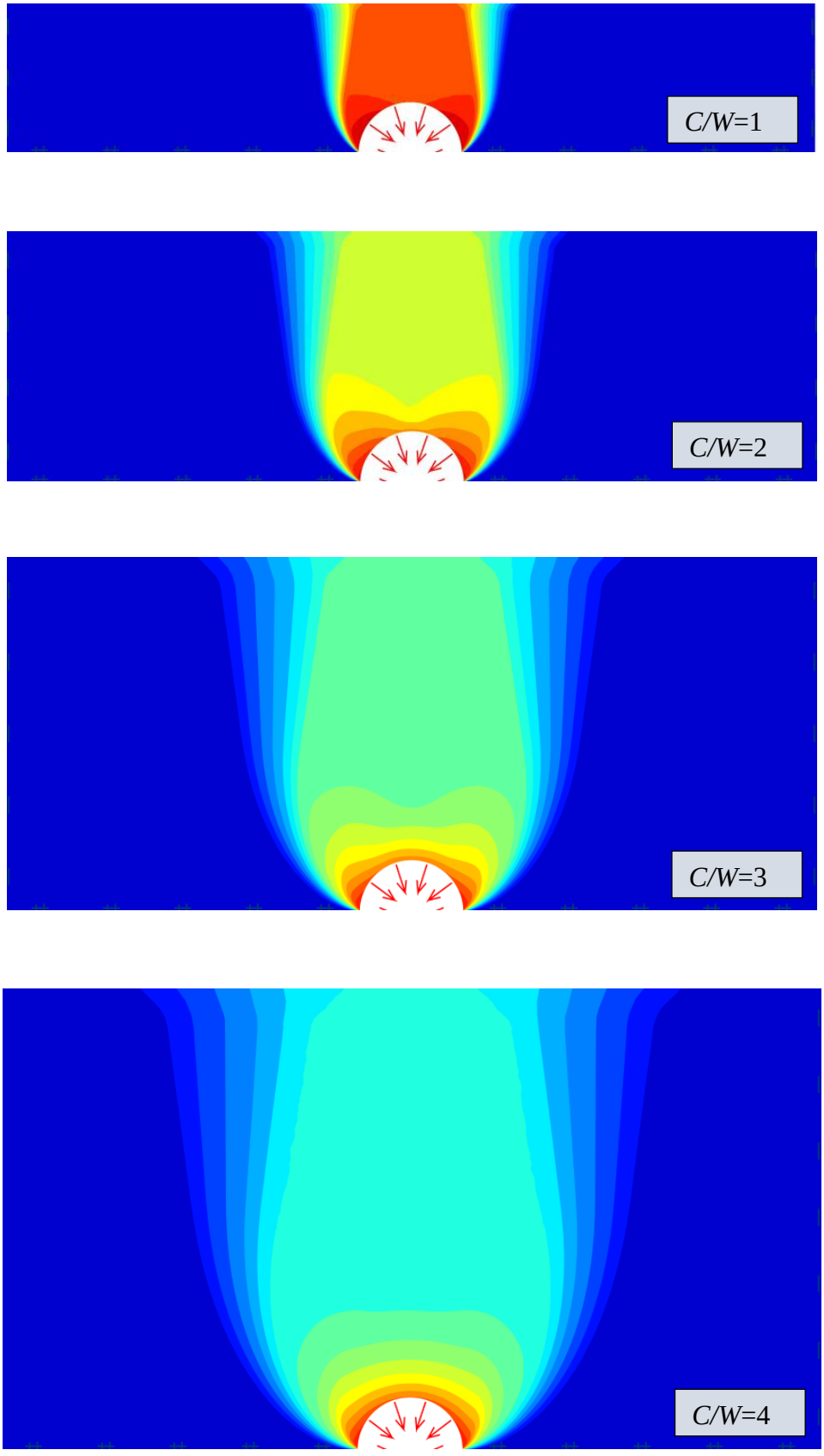

Figure 4.11. Absolute velocity (|u|) contour plot semi-circular opening (*C/W* =1-4, *SR*=2)

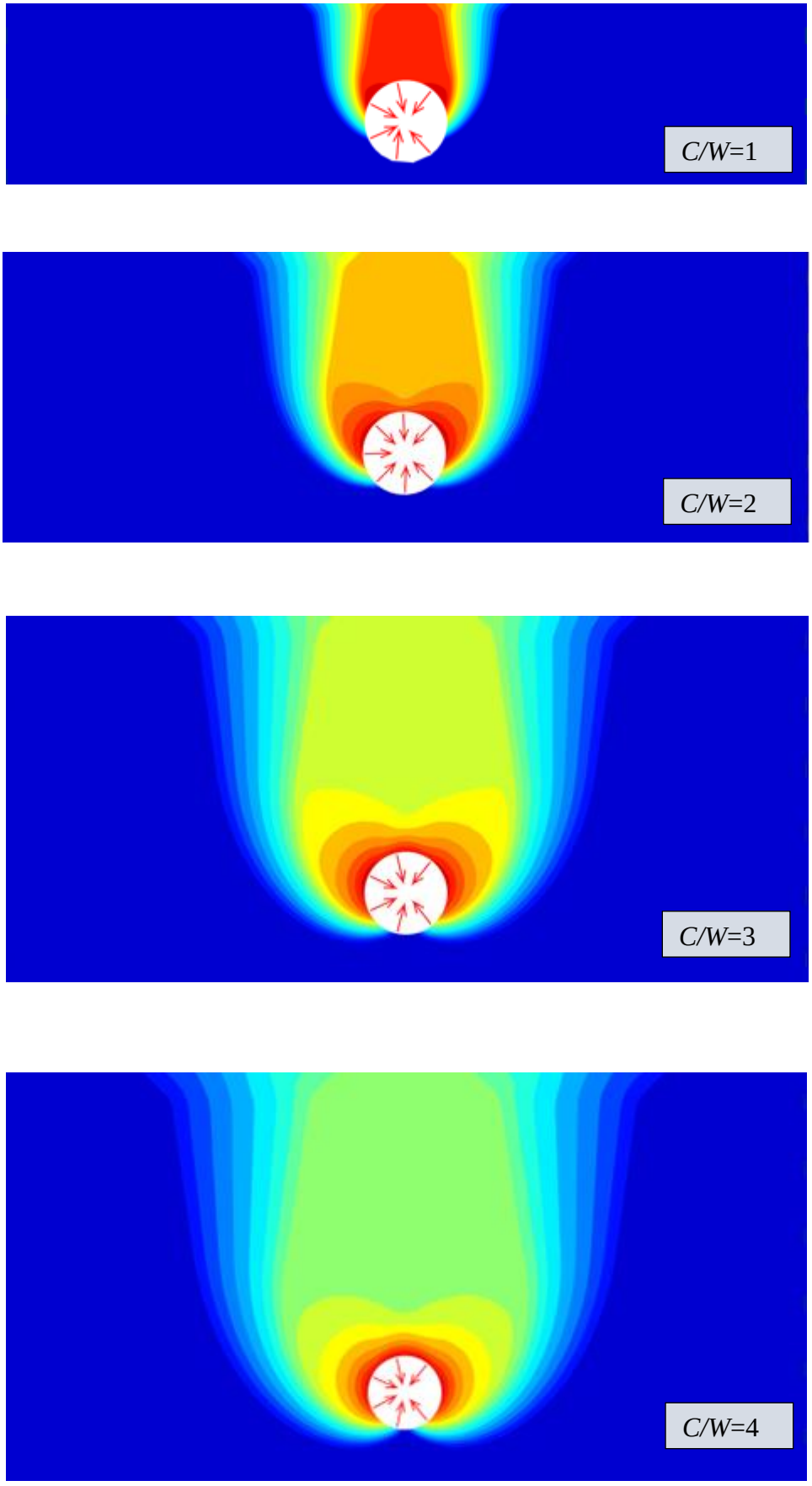

Figure 4.12. Absolute velocity (|u|) contour plot circular opening (*C/W* =1-4, *SR*=2)

4.3.3. Comparison of three cavity shapes

A comparison of stability results amongst the three different cavity geometries is presented in Figure 4.13. The plot shows the relationship between *PR* $\{(\sigma_s - \sigma_t)/S_u\}$ and *DR* (*C/W*) for the various *SR* ($\gamma W/S_u$) of the three idealised cavity shapes. Three interception points were found from the nine curves (three cavity shapes), and they are at approximately $C/W = 1.75$ ($SR = 0$), $C/W = 1.35$ ($SR = 1$) and $C/W = 1.15$ ($SR = 2$), respectively. The use of only one cavity shape cannot fully represent the whole problem involving the process of soil erosion.

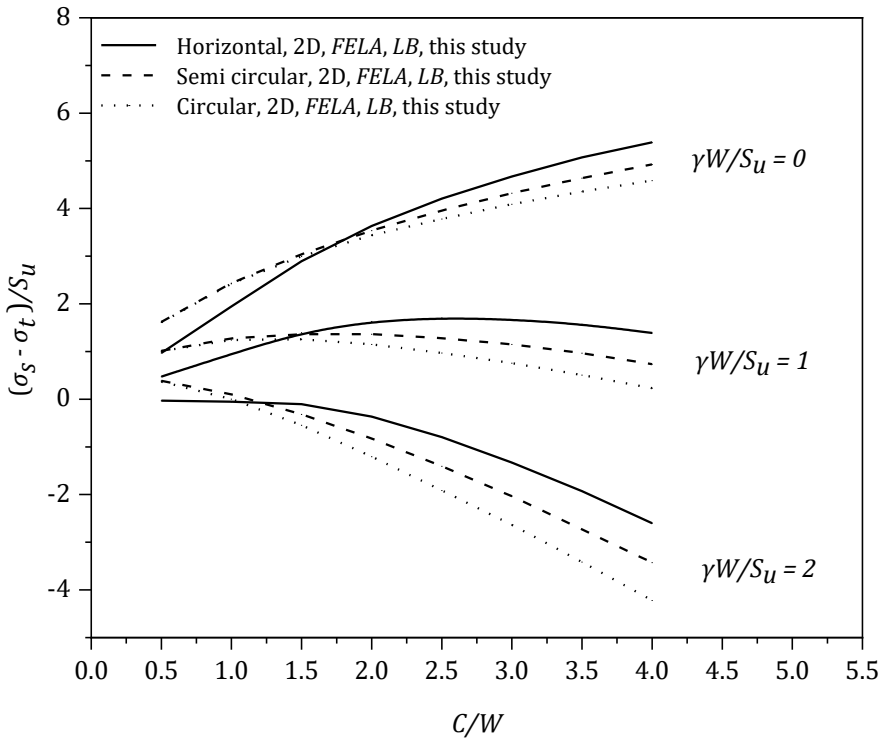

Figure 4.13. Comparison of three cavity shapes

For $C/W < 1.75$ ($SR = \gamma W/S_u = 0$), the results show that both the semi-circular and the circular trapdoors have the same *PR* values, which are greater than the horizontal trapdoor. This finding is for small depth ratios (*DR*), which are to the left-hand side of the respective interception point.

The findings were generally consistent with the velocity plots shown in Figures 4.14 and 4.15 for the shallow cases. Although the plots are not in scale, both the semi-circular and the circular cases have similar failure mechanisms and hence their *PR* values are the same. Those mechanisms are different from the horizontal trapdoor whereas a more chimney type of vertical slip is observed.

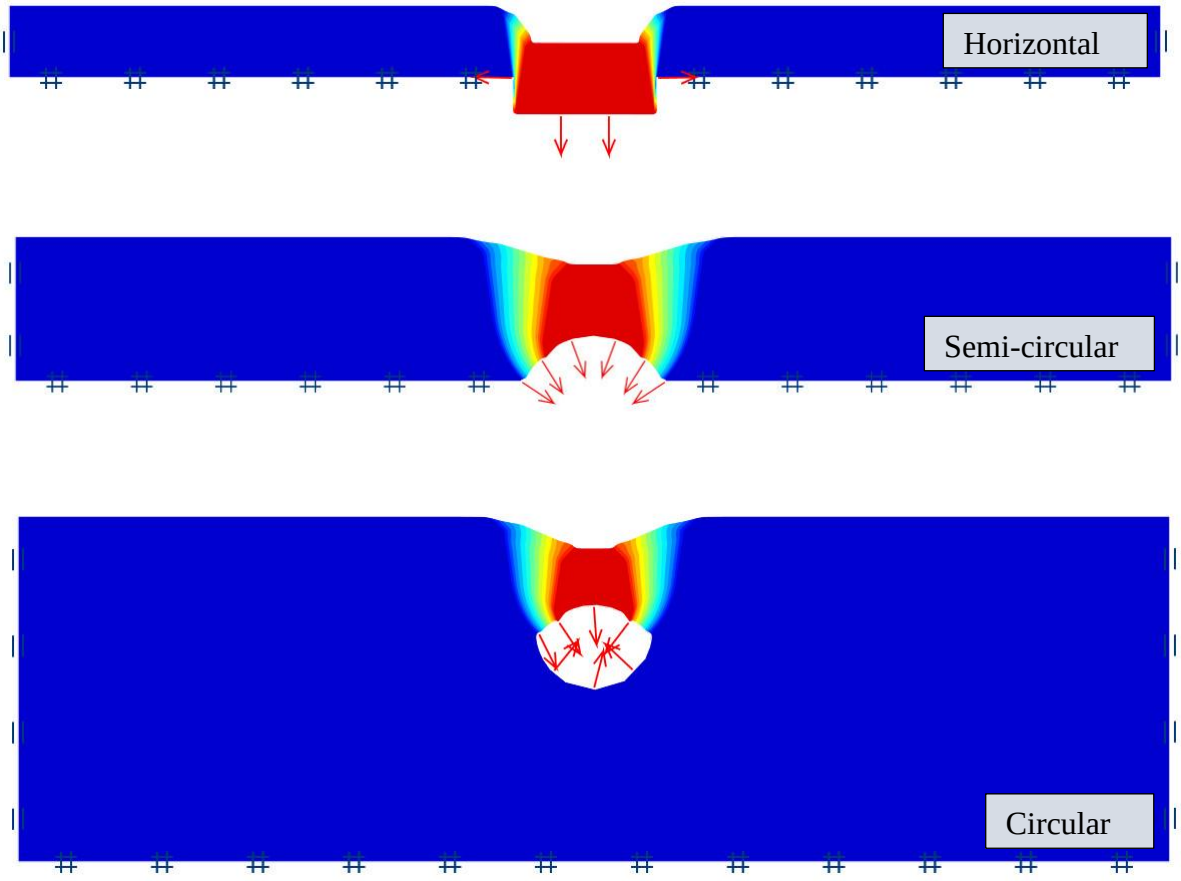

Figure 4.14. Absolute velocity (|u|) plots of three cavity shapes (*SR*=1, *C/W*=0.5)

In contrast to the shallow depth ratios, for the large depth ratios such as *C/W* > 1.75, the horizontal trapdoor yields the largest *PR* values amongst the three cavity shapes whereas the circular trapdoor gives the smallest *PR* values. It seems that our deep cases can be explained by the velocity plots shown in Figures 4.16 and 4.17.

The horizontal trapdoor provides greater constraints to soil movements than the other "curved" trapdoors, thus giving the least ground surface failure extent. It can therefore be concluded that the horizontal trapdoor provides the largest value of *PR* amongst the three cavity shapes.

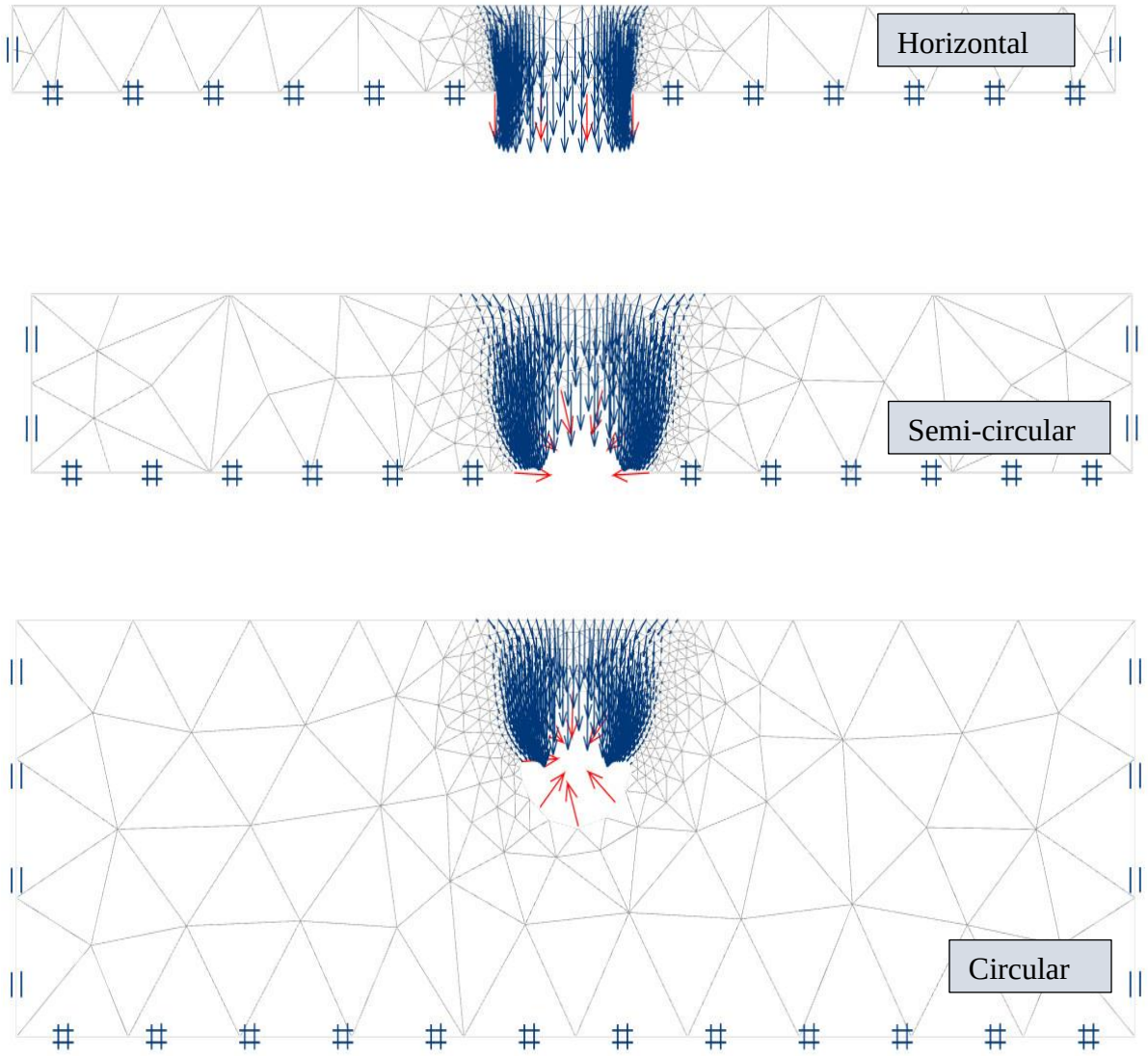

Figure 4.15. Velocity vector (v) plots of three cavity shapes (*SR*=1, *C/W*=0.5)

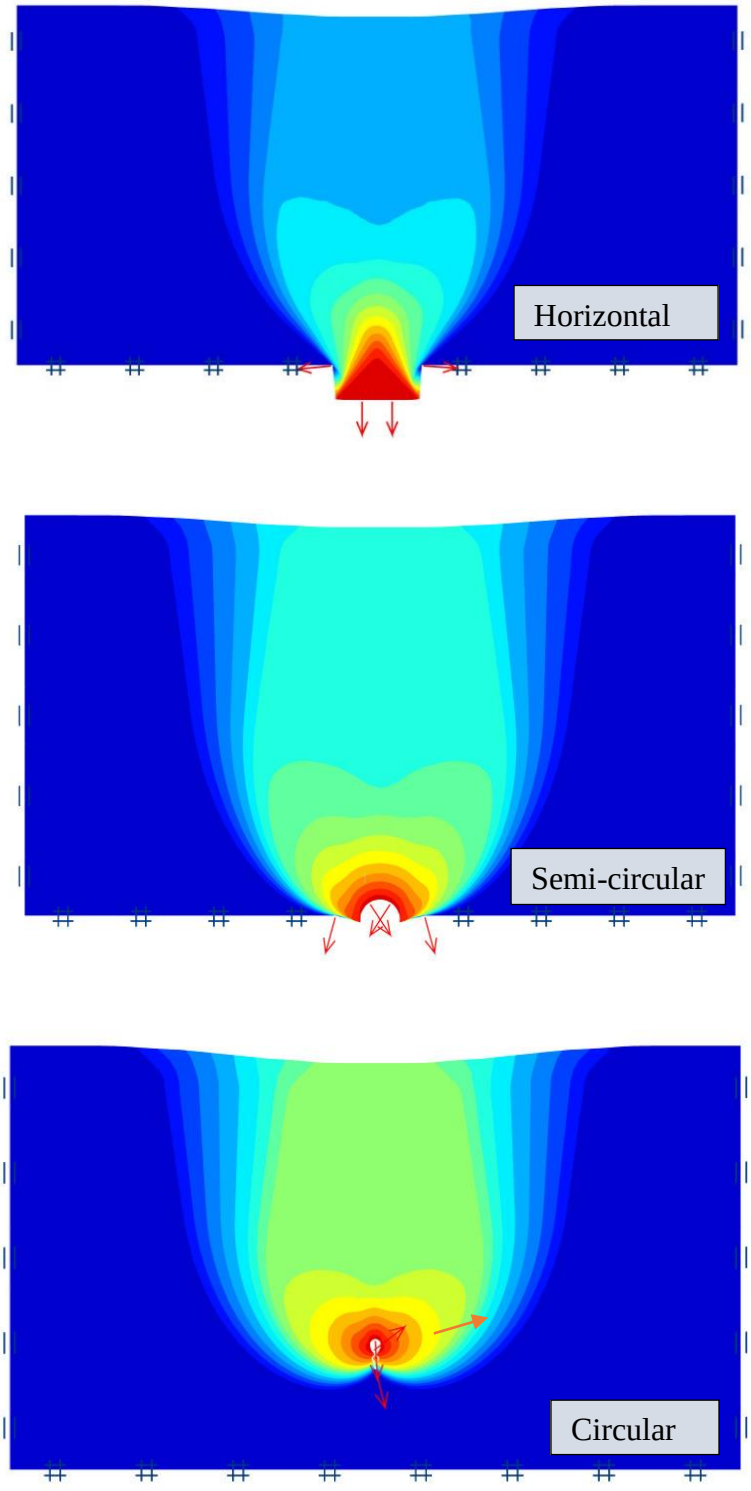

Figure 4.16. Absolute velocity (|u|) plots of three cavity shapes (*SR*=1, *C/W*=4)

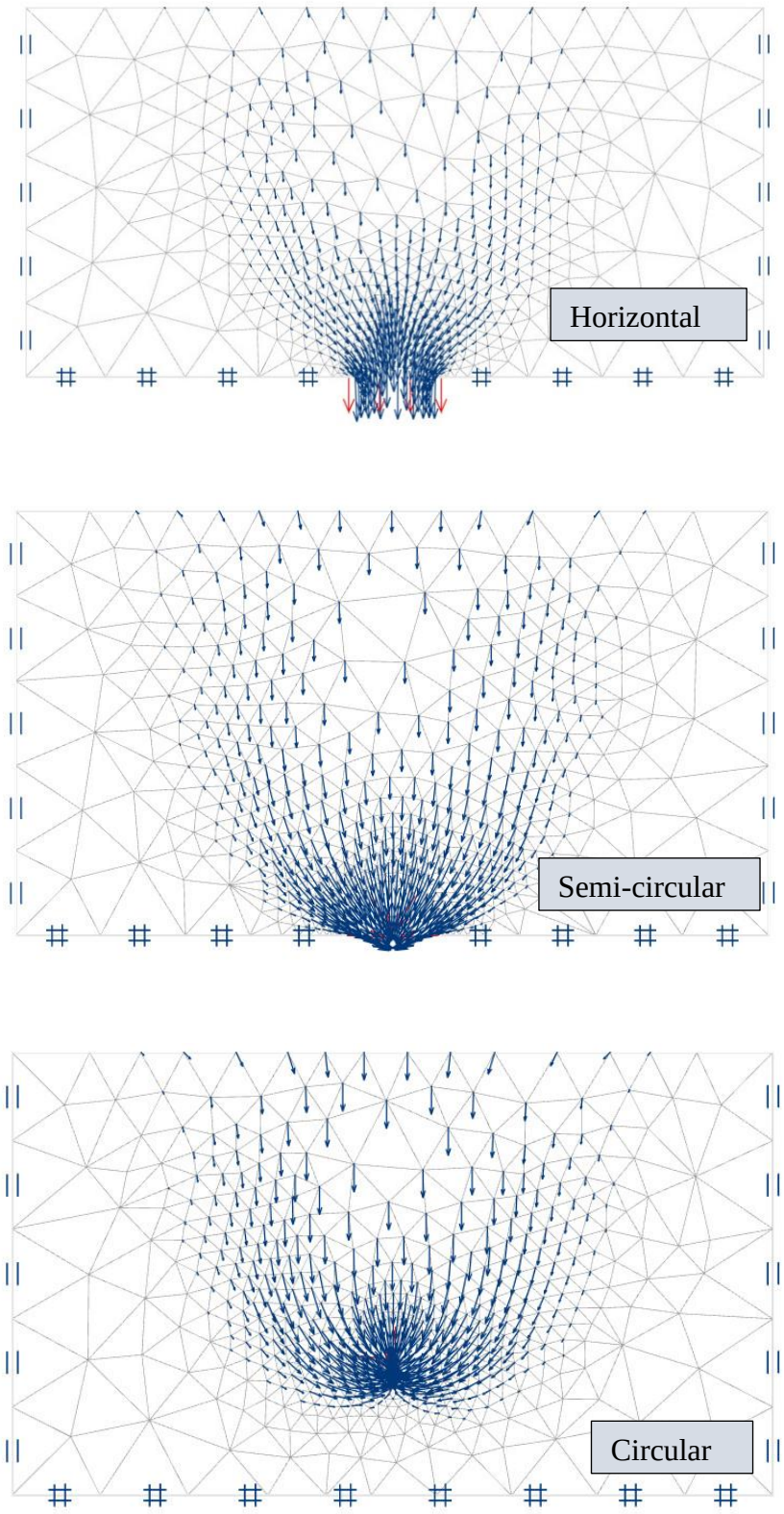

Figure 4.17. Velocity vector (v) plots of three cavity shapes (*SR*=1, *C/W*=4)

4.3.4. Comparison with published results

A comparison of *PR* values with other published results is shown in Figure 4.18. The comparison is for a horizontal trapdoor. Data used to plot Figure 4.18 is shown in Table 4.4 The analytical bounding solutions of Davis (1968) and Gunn (1980) have been significantly improved, whilst the linear programming technique in Sloan et al. (1990) agrees with the present results by some 10% gap differences. The recent results published by Shiau and Hassan (2020) are very close to those in the present study.

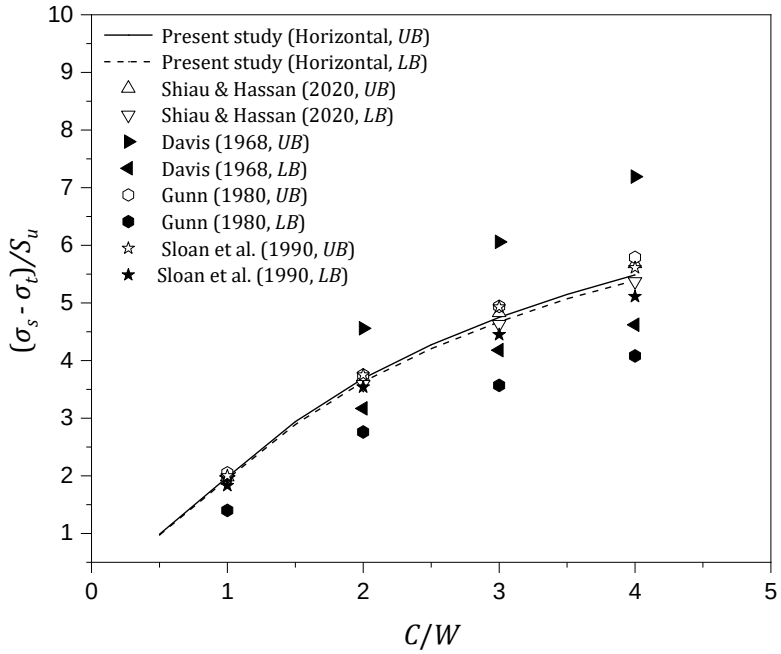

Figure 4.18. Comparison with published literature (horizontal openings)

Figure 4.19 compares *PR* values of circular trapdoors with other published results. Wilson et al. (2011) adopted the pressure ratio approach to present the stability of the circular tunnel. Whereas Shiau and Al-Asadi (2021) studied the tunnel blowout and collapse stability using the critical stability number of (Broms and Bennermark 1967).

Table 4.4. Comparison with existing literature (Horizontal opening)

C/*W*	Present Study		Shiau & Hassan (2020)		Davis (1968)		Gunn (1980)		Sloan et al. (1990)	
	LB	*UB*	*LB*	*UB*	*LB*	*UB*	*LB*	*UB*	*LB*	*UB*
0.5	0.97	0.99	----	----	----	----	----	----	----	----
1.0	1.95	1.98	1.94	1.98	2.00	2.00	1.40	2.05	1.83	2.00
1.5	2.89	2.94	----	----	----	----	----	----	----	----
2.0	3.63	3.69	3.59	3.71	3.17	4.56	2.76	3.75	3.54	3.75
2.5	4.21	4.28	----	----	----	----	----	----	----	----
3.0	4.67	4.75	4.63	4.83	4.18	6.06	3.57	4.94	4.45	4.93
3.5	5.07	5.15	----	----	----	----	----	----	----	----
4.0	5.39	5.49	5.37	5.68	4.62	7.19	4.08	5.79	5.11	5.61

To make this comparison possible, it is necessary to use the results of the pressure ratio component. This is because Broms and Bennermark's stability number would be reduced to the pressure ratio, *PR*, when the component ($\gamma H/S_u$) is equals to zero. The comparison in Figure 4.19 shows an excellent agreement between the current study and those published by (Wilson et al. 2011 and Shiau & Al-Asadi 2021). The data used to plot Figure 4.19 is shown in Table 4.5.

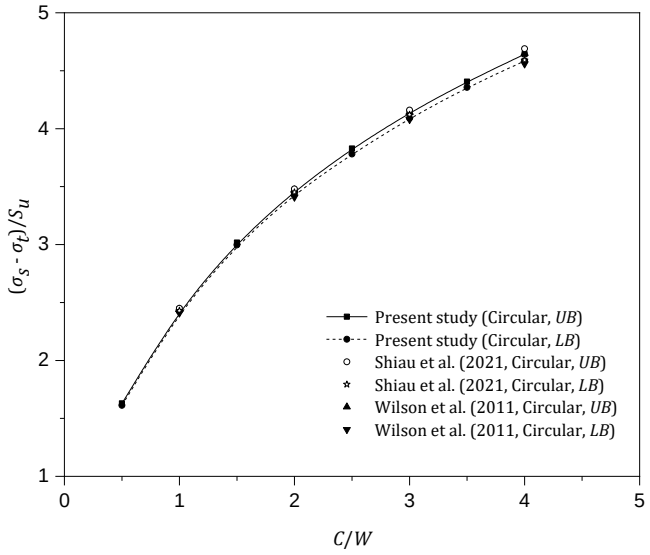

Figure 4.19. Comparison with existing literature (Circular opening)

Table 4.5. Comparison with existing literature (Circular opening)

C/W	Present Study		Shiau & Al-Asadi (2021)		Wilson et al. (2011)	
	LB	*UB*	*LB*	*UB*	*LB*	*UB*
0.5	1.63	1.61	----	----	----	----
1.0	2.44	2.42	2.41	2.44	2.43	2.45
1.5	3.02	3.00	----	----	----	----
2.0	3.46	3.44	3.41	3.47	3.45	3.48
2.5	3.83	3.78	----	----	----	----
3.0	4.14	4.09	4.08	4.14	4.12	4.16
3.5	4.41	4.36	----	----	----	----
4.0	4.64	4.59	4.56	4.65	4.59	4.69

4.3.5. Effect of $\gamma W/S_u$ on the original stability number (N_c)

Although the current stability study is based on the use of a pressure ratio approach, it is, however, interesting to present the effects of ($\gamma W/S_u$) on the original stability number (N_c) of Broms and Bennermark (1967), which was assumed as a function of depth ratio only (see equation 4.1). It is noted that the accuracy of (N_c) results from this equation depends on how the depth (*H)* is defined for the various geometries.

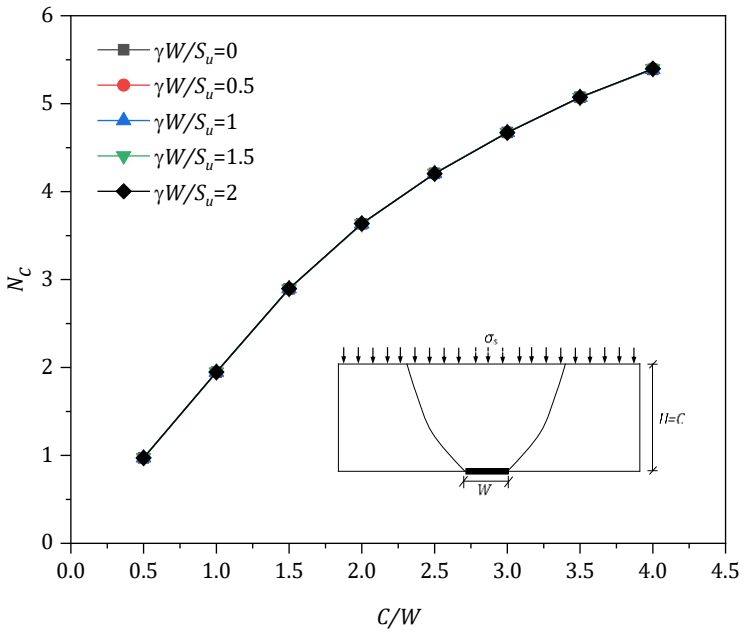

Figure 4.20. Effect of ($\gamma W/S_u$) on N_c (*LB*, horizontal opening)

For the horizontal trapdoor, Figure 4.20 presents the relationship between (N_c) and (C/W) for the range of strength ratios, SR =0 - 2. From the results, we can conclude that (N_c) is a function of (C/W) only and it is independent of the strength ratio (SR, $\gamma W/S_u$). Noting that W is equal to zero in the case of horizontal trapdoor, therefore ($H = C+W/2$) reduce to ($H = C$).

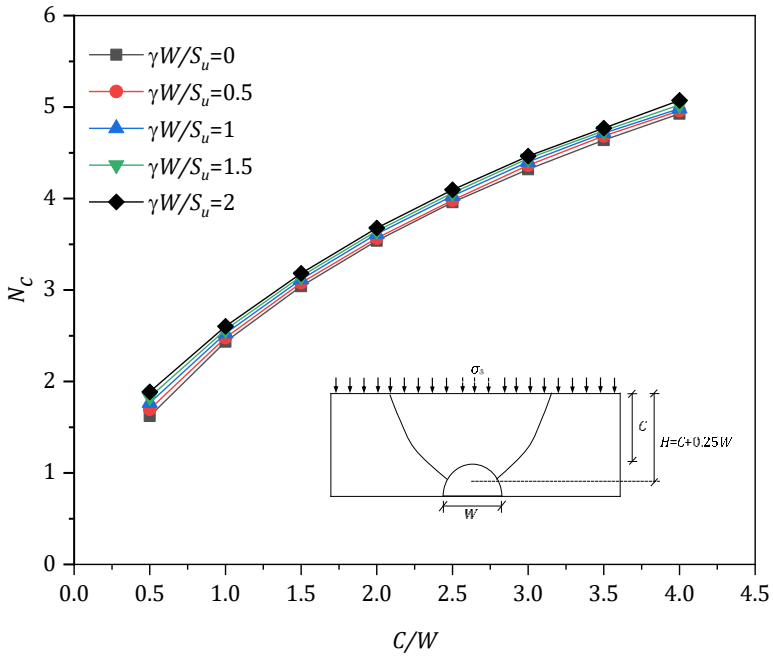

Figure 4.21. Effect of ($\gamma W/S_u$) on N_c (LB, semi-circular opening)

For the semi-circular trapdoor in Figure 4.21, the (N_c) values for all SR are very close and are of acceptable accuracy when H is defined as ($H= C + 0.25\ W$). It can be concluded that the original stability number can still be used in design practices, subjected with the modification of H definition to as ($H= C + 0.25\ W$).

Using (H) as ($H= C+ 0.5W$) for the circular trapdoor, variations of the critical stability number (N_c) with (C/W) are plotted in Figure 4.22 for various strength ratios (SR, $\gamma W/S_u$). "0.5" is the original coefficient that was used by many researchers for tunnel problems. From the presented results, it can be concluded that the effect of ($\gamma W/S_u$) on (N_c) cannot be simply ignored, especially for the shallow cases. By adjusting the coefficient to "0.25", another plot using (H) as ($H= C+0.25W$) is presented in Figure 4.23. From the numerical results, we can conclude that the effect of ($\gamma W/S_u$) on (N_c) is small and it can be ignored in practice.

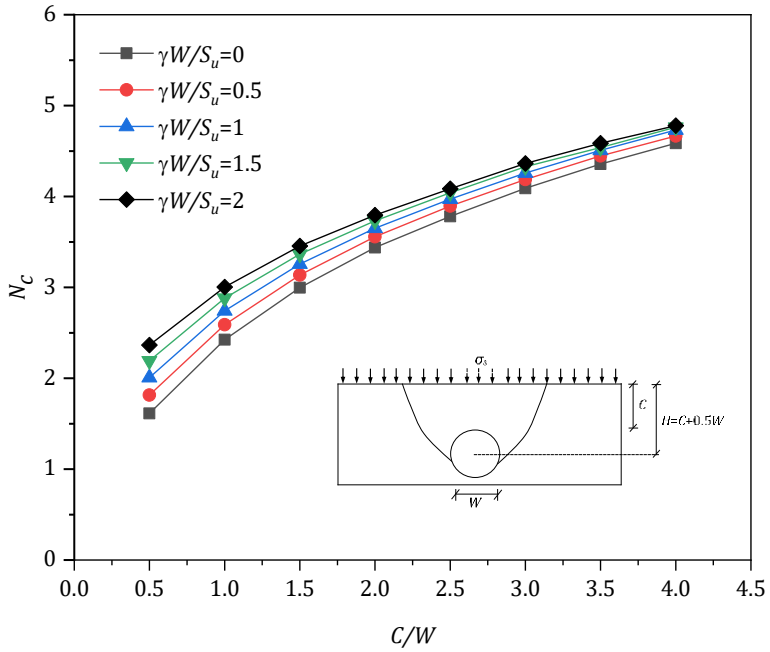

Figure 4.22. Effect of ($\gamma W/S_u$) on N_c (*LB*, circular opening) when (H= C+0. 5W)

It is therefore recommended that (H= C+0.25W) be used in the equation for the circular trapdoor, instead of the original (H= C+0. 5W).

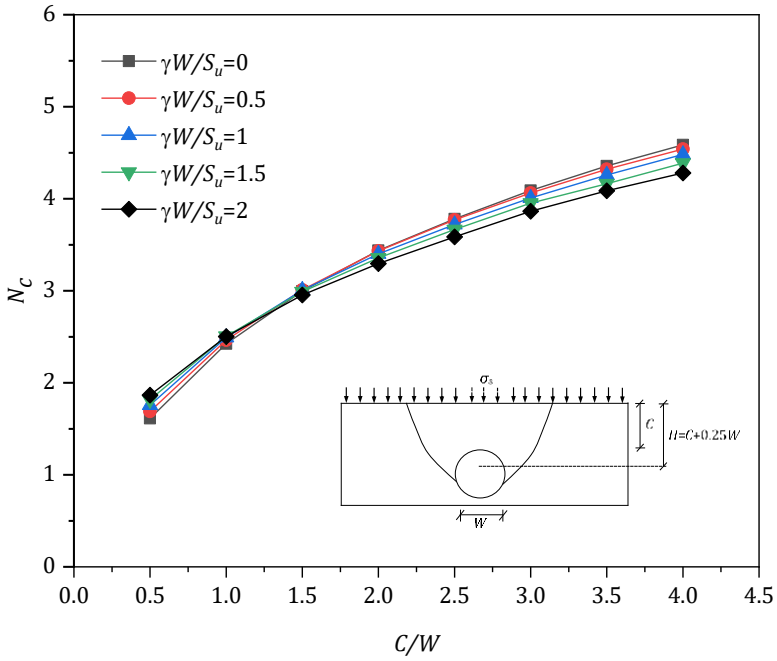

Figure 4.23. Effect of ($\gamma W/S_u$) on N_c (*LB*, circular opening) when (H= C+0.25W)

4.4. THE EXAMPLE

This section demonstrates the practical use of the numerical results produced in this Chapter. Design charts for the collapse stability of three idealised cavity shapes (i.e., horizontal, semi-circular, and circular openings) are considered in the example, as shown in Figure 25 (a-c). In the example, the material properties are given as the soil unit weight γ=18 kN/m^3 and the undrained shear strength of soil (S_u = 25 kPa). The design surcharge pressure is given as (σ_s = 50 kPa), whilst water mains pressure is assumed as (σ_t = 0). The example is studied for the following three stages of cavity development, and the corresponding factors of safety are determined.

Preliminary stage (Figure 4.24)

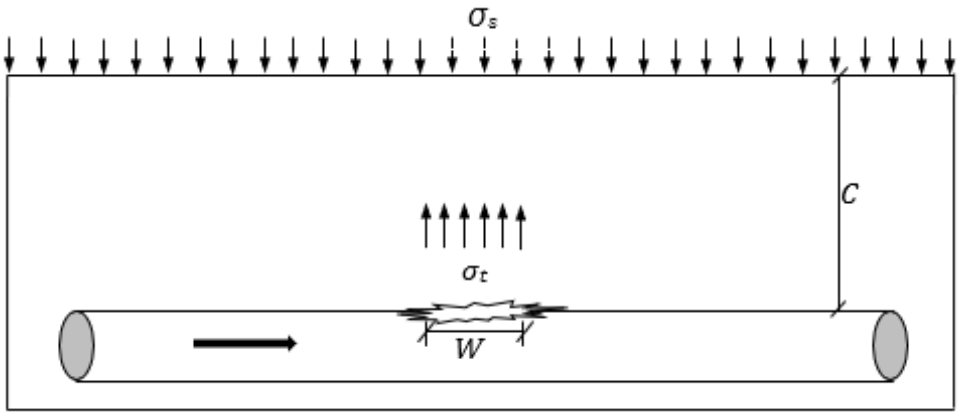

Figure 4.24. Initial stage of collapse stability

1. Given the cover depth C= 0.75m and the opening width W =0.5 m, C/W = 1.5.
2. The SR is calculated as: $\gamma W/S_u$ = (18 x 0.5)/25= 0.36.
3. Using Figure 4.4, the critical pressure ratio PR = (σ_s - σ_t)/S_u = 2.4.
4. Given S_u=25 kPa and σ_t =0 (to simulate zero water pressure), the limiting σ_s is calculated as σ_s = 60 kPa. Hypothetically, the "applied" surcharge pressure should not be greater than 60 kPa, or a collapse failure occurs.
5. The design surcharge pressure is given as 50 kPa, hence a collapse failure will not occur. The corresponding factor of safety (FoS) = 60/50 = 1.20

Secondary stage (Figure 4.25)

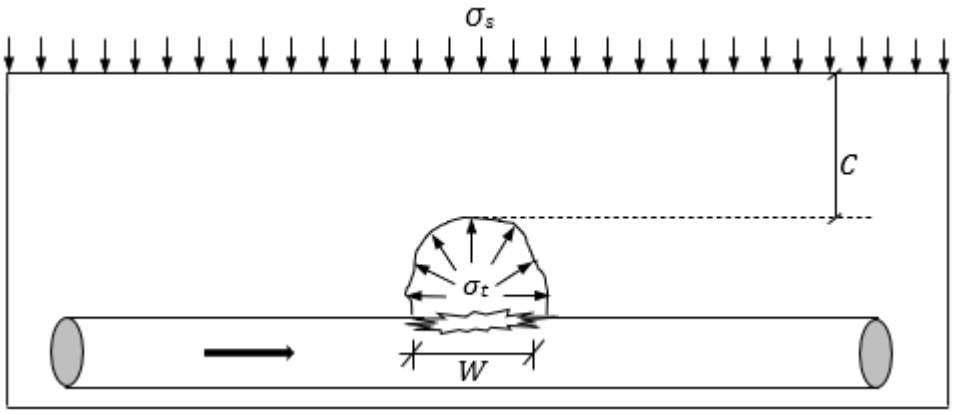

Figure 4.25. Intermediate stage of collapse stability

1. Given the cover depth C= 0.5m and the opening width W =0.5 m, C/W = 1.
2. The SR is calculated as: $\gamma W/S_u$ = (18 x 0.5)/25= 0.36.
3. Using Figure 4.6, the critical pressure ratio PR = (σ_s - σ_t)/S_u = 2.1.
4. Given S_u=25 kPa and σ_t =0 (to simulate zero water pressure), the limiting σ_s is calculated as σ_s = 52.5 kPa. It is expected that the "applied" surcharge pressure should not be greater than 52.5 kPa, or a collapse failure occurs.
5. The design surcharge pressure is given as 50 kPa, hence a collapse failure will not occur. The corresponding factor of safety (FoS) = 52.5/50 = 1.05

Final stage as in (Figure 4.26)

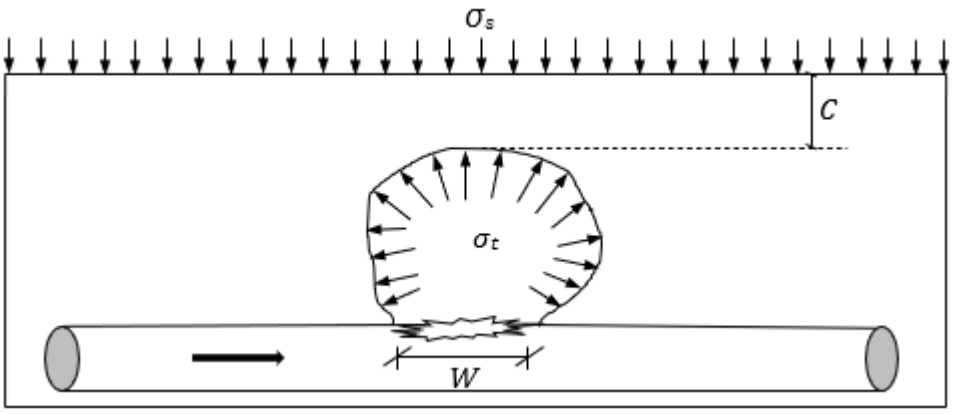

Figure 4.26. Final stage of collapse stability

1. Given the cover depth C= 0.4m and the opening width W =0.5 m, C/W = 0.8.
2. The SR is calculated as: $\gamma W/S_u$ = (18 x 0.5)/25= 0.36.
3. Using Figure 4.8, the critical pressure ratio $PR = (\sigma_s - \sigma_t)/S_u$ = 1.9.
4. Given S_u=25 kPa and σ_t =0 (to simulate zero water pressure), the limiting σ_s is calculated as σ_s = 47.5 kPa. To prevent a collapse failure, the "applied" surcharge pressure should not be greater than 47.5 kPa.
5. The design surcharge pressure is given as 50 kPa, hence a collapse failure will occur. The corresponding factor of safety (FoS) = 47.5/50 = 0.95, which is less than unity.

It can be demonstrated from the above examples that the cover depth decreases as the cavity size changes. Also, note that the corresponding FoS also decreases as the cavity shape changes. This finding is consistent with what happens in road-related sinkhole incidences.

4.5 CONCLUSIONS

In this study, we investigated the ground stability under pipe leakage-related sinkholes. Three idealised cavity shapes were chosen to represent the process of internal soil erosion. A set of numerical studies were carried out using the advanced finite element limit analysis of upper and lower bound theorems. The numerical models were found to be well suited to the proposed problem and the aim was to assess the stability performance of soils under the three cavity shapes. Numerical results were compared with published literature, stability charts and tables were developed for the three cavity shapes, and ground surface failure extents were studied using velocity contour plots. An example outlining the procedure in the practical use of charts was developed for practical uses. Noting that the cover depth decreases as the cavity size changes and that the corresponding FoS also decreases as the cavity shape changes. It is recommended that the current work can be extended to three-dimensional analysis as well as for realistic layered road pavement.

CHAPTER 5 PIPELINE BURST-RELATED BLOWOUT STABILITY

5.1. INTRODUCTION

Sinkhole incidents have increased rapidly in recent decades due to water main breaks. Although numerous researchers have recently conducted investigations in sinkhole phenomena, most of the studies are related to natural sinkhole formation, underground cavity detection, and collapse analysis. Very few studies can be found concerning the blowout stability of soils due to defective pipelines under high water main pressures, in spite of the frequent media news about the water main bursts which enlighten the relevance of the problem. This Chapter aims to study the soil's blowout stability above a damaged water main pipeline in three idealized stages of internal soil erosion, i.e., horizontal, semi-circular, and circular cavities using the latest finite element limit analysis technique. Dimensionless design parameters are used throughout the Chapter to present rigorous bounding solutions that can be used directly by designers to evaluate the blowout stability of soils above defective pipelines. Design charts and tables are presented to cover a wide range of design parameters, and a practical example is introduced to illustrate their use in practice.

5.2. PROBLEM LAYOUT

The problem definition with a typical adaptive mesh for the horizontal trapdoor (C/W = 2) is shown in Figure 5.1. For the semi-circular and circular trapdoors, they are presented in Figures 5.2 and 5.3, respectively. The horizontal trapdoor in Figure 5.1 has a width (W) and a cover (C). The face of the trapdoor is subjected to a normal blowout pressure (σ_t) that is positive when in compression, while the ground surface is subjected to a positive compressive surcharge (σ_s). Soils above the trapdoor are considered as a rigid-perfectly plastic Tresca material of a unit weight (γ) and a constant undrained shear strength (S_u).

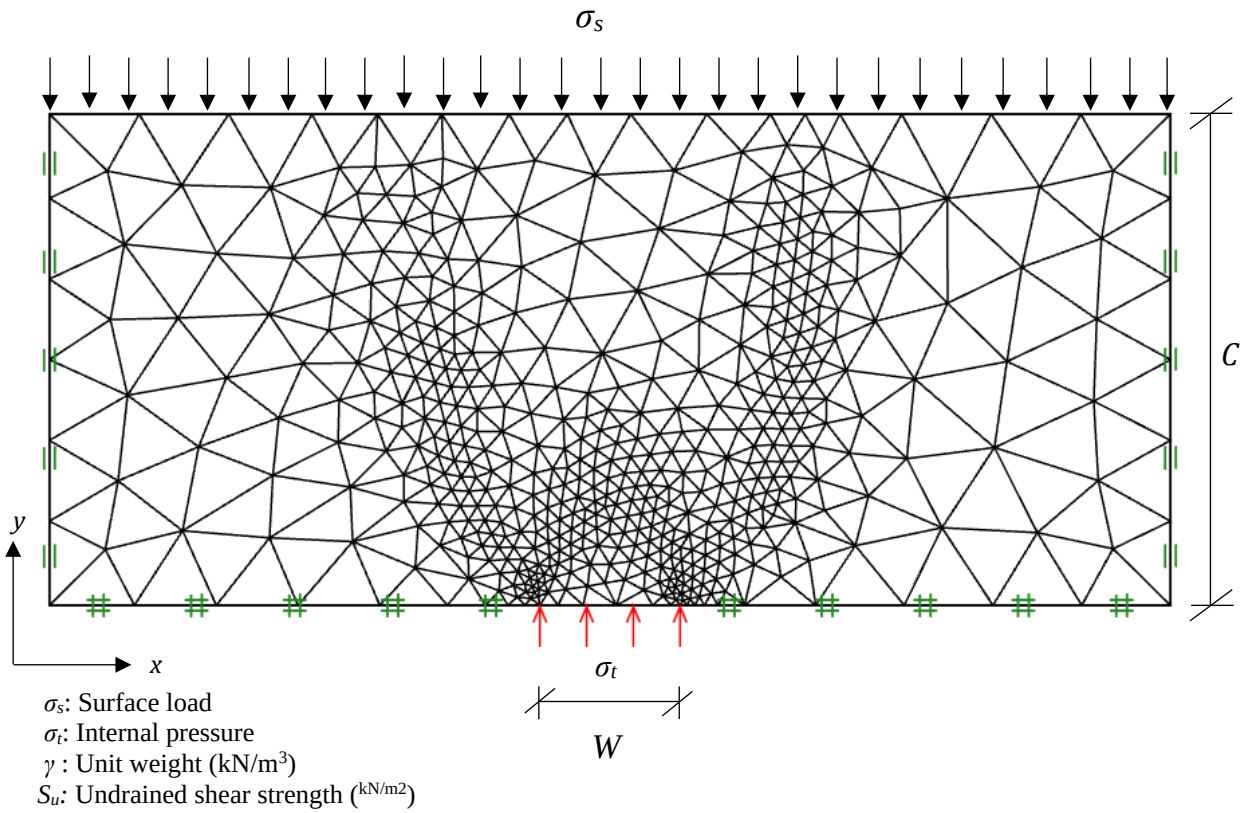

Figure 5.1. Problem definition (stage one, horizontal opening)

The numerical models are created carefully to make sure that the domain is sufficiently large, and the results are not affected by the boundaries. Both the vertical sides are restrained in the x-direction and the bottom of the domain is clamped in both x and y directions whereas the top side is kept as a free moving surface. The same boundary conditions are applied to the other two trapdoor shapes. In this study, numerical solutions are obtained using upper and lower bound theorems. The kinematically admissible velocity field can be demonstrated by the solution to the upper bound optimisation problem and it gives a rigorous upper bound stability solution, while the solution to the lower bound optimisation determines a statically admissible stress field and it gives a rigorous lower bound stability solution. The technique is robust as both the upper bound (*UB*) and lower bound (*LB*) projections are presented together to estimate gap error. More details of the finite element formulations of upper and lower bound theorems with the mathematical programming can be found in (Sloan 2013).

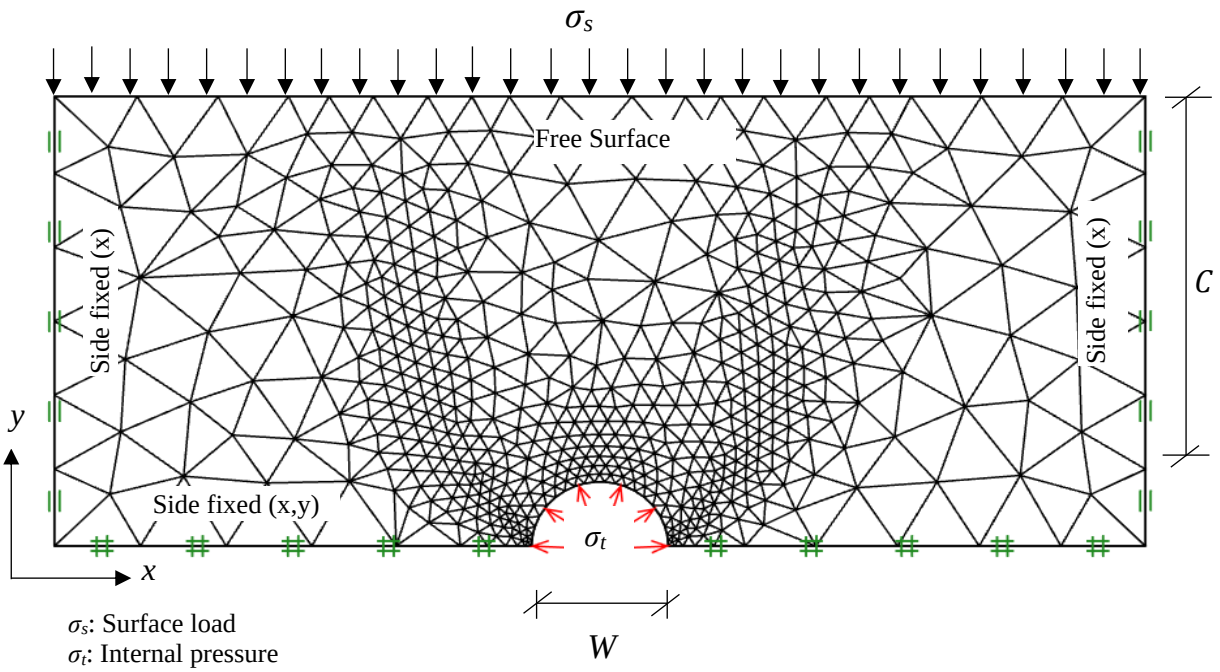

σ_s: Surface load
σ_t: Internal pressure
γ : Unit weight (kN/m^3)
S_u: Undrained shear strength (kN/m^2)

Figure 5.2. Problem definition (stage two, semi-circular opening)

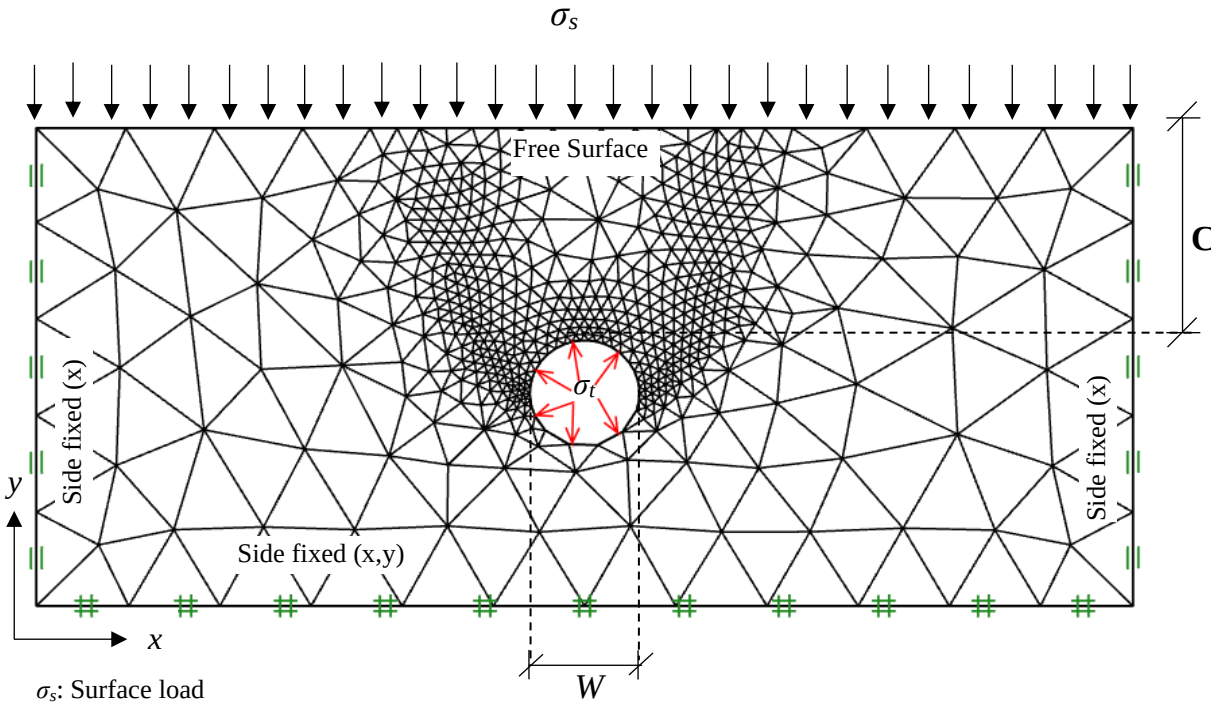

σ_s: Surface load
σ_t: Internal pressure
γ: Unit weight (kN/m^3)
S_u: Undrained shear strength (kN/m^2)

Figure 5.3. Problem definition (stage three, circular opening)

Typical *FELA* meshes used in this study are shown in Figures 5.1, 5.2, and 5.3 for the horizontal, semi-circular, and circular trapdoors, respectively. For all the studies, three iterations of adaptive meshing were used, with the number of elements developing from 3000 to 5,000 (Optum CE, 2020).

The stability number (N) of Broms and Bennermark (1967) as a combination of the surcharge pressure(σ_s), overburden pressure (γH), supporting pressure (σ_t) is shown in equation (1)

$$N = \frac{\sigma_s + \gamma H - \sigma_t}{S_u} \tag{5.1}$$

Davis et al. (1980) removed the overburden pressure (γH) component from equation (5.1) and the stability number reduces to a pressure ratio (σ_s - σ_t)/S_u that is a function of strength ratio ($\gamma W/S_u$) and depth ratio (C/W).

$$PR = \frac{\sigma_s - \sigma_t}{S_u} = f\left(\frac{C}{W}, \frac{\gamma W}{S_u}\right) \tag{5.2}$$

This analysis follows Davis's approach to present numerical results using equation (5.2). For all three trapdoors, a series of depth ratios (C/W = 0.5-4) and shear strength ratio ((SR = $\gamma W/S_u$ = 0-2) are studied for blowout scenarios to determine the lower and upper bound limits of the pressure ratio (PR). By substituting the obtained critical "blowout" pressure (σ_t) and the program input parameters (C, W, σ_s, γ, and S_u) into equation (5.2), the critical pressure ratio (PR) can be calculated.

5.3. RESULTS AND DISCUSSION

5.3.1. Stability results - pressure ratio

Blowout stability results of soils above a defective pipeline under three different internal cavity shapes are summarized in Figuress 5.4 –5.9 and Tables 5.1-5.3. These Figures plot the pressure ratio $\{PR = (\sigma_s - \sigma_t)/S_u\}$ versus the depth ratio (DR, C/W= 0.5 to 4.0) for various values of the strength ratio (SR, $\gamma W/S_u$ = 0 - 2). Note that, due to the PR definition, a negative value of $\{PR = (\sigma_s - \sigma_t)/S_u\}$ means that the compressive normal supporting pressure (σ_t) is greater than the compressive surcharge pressure (σ_s). It is therefore not surprising to see the negative PR values being presented throughout the Chapter for the current blowout study.

For the horizontal opening as in Figure 5.4, PR decreases as DR increases for all values of SR. As discussed before in the PR definition, the decrease in PR means an increase in the compressive normal blowout pressure (σ_t). The larger the SR value, the heavier the system is, and therefore it requires a larger (σ_t) to cause blowout failure. In general, the upper bound (UB) value is found to be greater than that of the lower bound (LB) value for each pressure ratio PR value, and an exact solution can always be closely found in between the limits of the UB and LB.

A design chart for evaluating the blowout stability of a horizontal opening is presented in Figure 5.5, where the x-axis represents the depth ratio (DR, C/W) and the y-axis represents the strength ratio (SR, $\gamma W/S_u$).

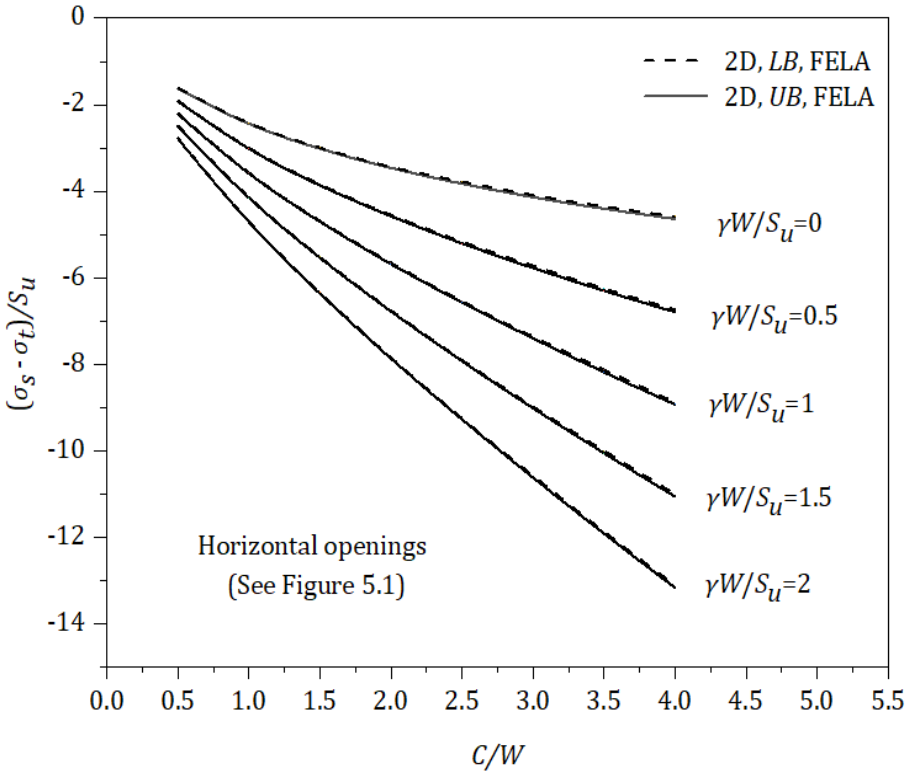

Figure 5.4. ($\sigma_s - \sigma_t / S_u$) vs ($C/W$) for horizontal openings

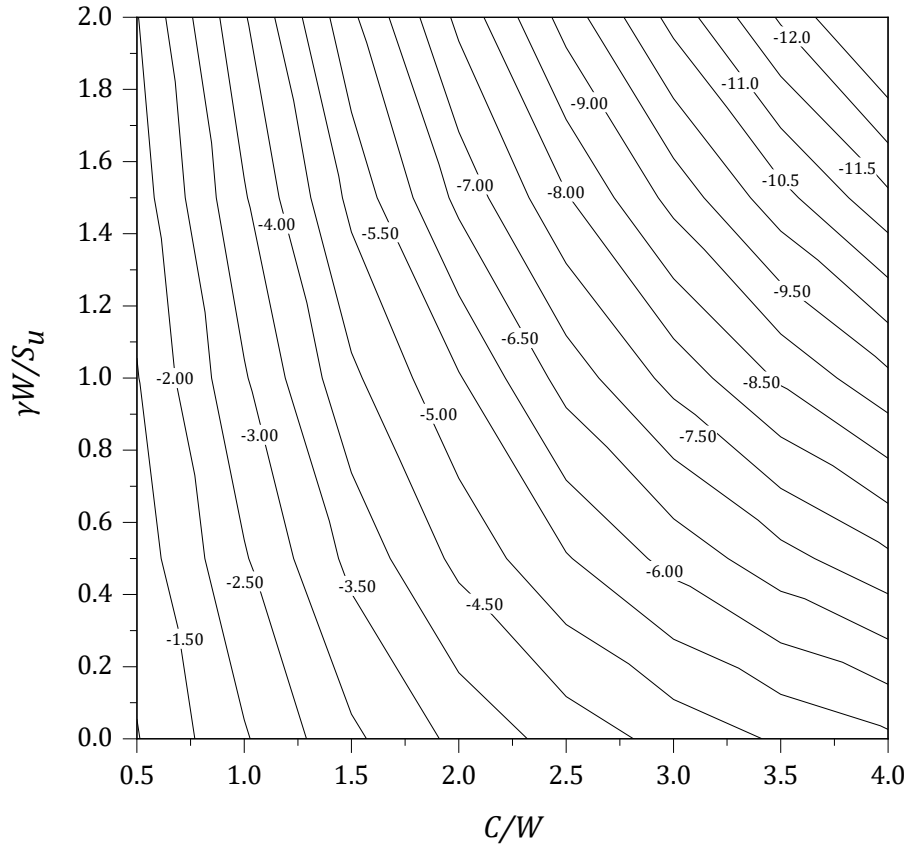

Figure 5.5. A blowout design chart to obtain *PR* (horizontal openings)

The contour values in the Figure 5.5 represent the pressure ratio *PR*, which are all in negatives in blowout cases. The data used to plot the Figure 5.5 is also shown in Table 5.1. One needs to input the chosen design values of *DR* and *SR* to determine the critical *PR* value, and thus the critical blowout pressure (σ_t). Similarly, the same observations are made for the semi-circular opening. The results are presented in Figures 5.6 and 5.7 as well as in Table 5.2. For the full circular opening, numerical results are shown in Figures 5.8, 5.9, and Table 5.3. The comprehensive results presented in Figures 5.4-5.9 and Tables 5.1-5.3 can be used to determine critical blowout pressures (σ_t) for various cavity shapes.

Table 5.1. Data used for plotting Figures 5.4 and 5.5 (horizontal openings)

C/W	$\gamma W/S_u$									
	0		0.5		1.0		1.5		2	
	LB	*UB*	*LB*	*UB*	*LB*	*UB*	*LB*	*UB*	*LB*	*UB*
0.50	-0.97	-0.99	-1.22	-1.24	-1.47	-1.49	-1.72	-1.74	-1.97	-1.99
1.0	-1.95	-1.98	-2.45	-2.48	-2.95	-2.98	-3.45	-3.48	-3.95	-3.98
1.5	-2.90	-2.94	-3.64	-3.69	-4.39	-4.44	-5.14	-5.19	-5.90	-5.94
2.0	-3.63	-3.69	-4.63	-4.69	-5.60	-5.69	-6.64	-6.69	-7.63	-7.69
2.5	-4.21	-4.27	-5.46	-5.52	-6.71	-6.78	-7.96	-8.03	-9.21	-9.28
3.0	-4.67	-4.75	-6.17	-6.25	-7.67	-7.75	-9.17	-9.25	-10.68	-10.75
3.5	-5.07	-5.15	-6.82	-6.90	-8.57	-8.65	-10.32	-10.40	-12.07	-12.15
4.0	-5.40	-5.49	-7.39	-7.49	-9.39	-9.49	-11.39	-11.49	-13.40	-13.49

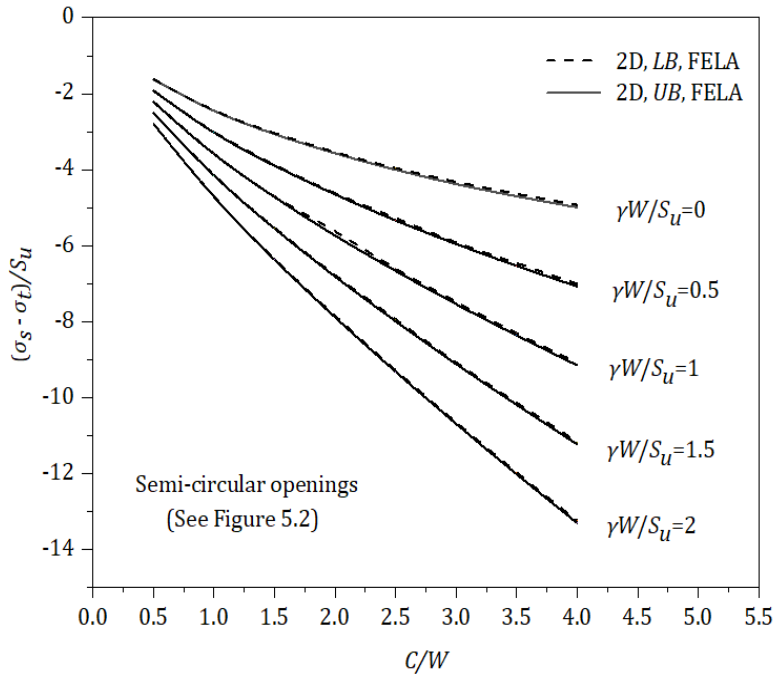

Figure 5.6. ($\sigma_s - \sigma_t / S_u$) vs ($C/W$) for semi-circular openings

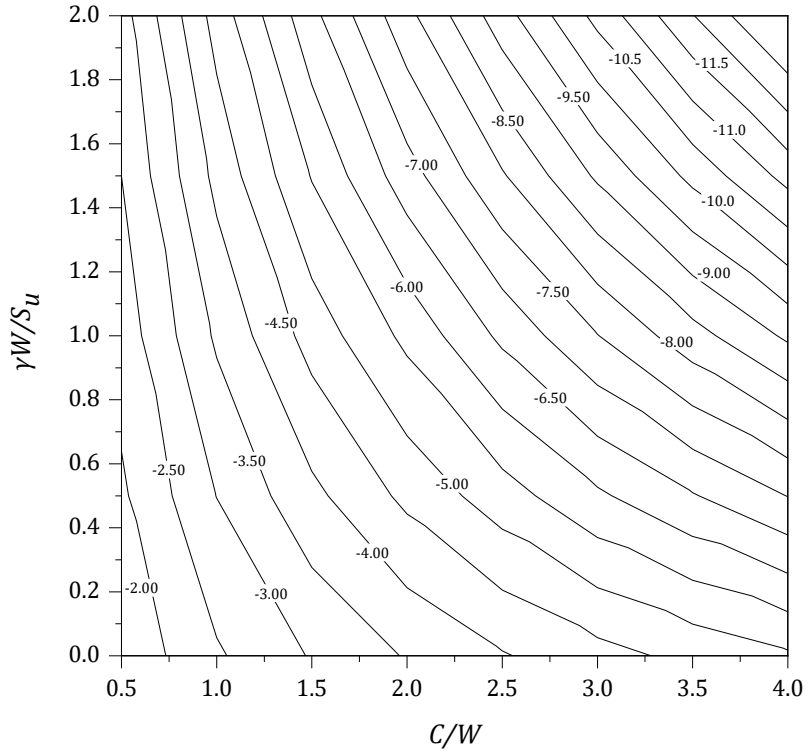

Figure 5.7. Blowout design chart to obtain *PR* (semi-circular openings)

Table 5.2. Data used for plotting Figures 5.6 and 5.7 (semi-circular openings)

C/W	$\gamma W/S_u$									
	0		0.5		1.0		1.5		2	
	LB	*UB*	*LB*	*UB*	*LB*	*UB*	*LB*	*UB*	*LB*	*UB*
0.5	-1.62	-1.63	-1.92	-1.93	-2.21	-2.22	-2.50	-2.51	-2.79	-2.80
1.0	-2.44	-2.45	-3.01	-3.02	-3.58	-3.59	-4.14	-4.16	-4.71	-4.72
1.5	-3.04	-3.06	-3.87	-3.90	-4.70	-4.73	-5.53	-5.55	-6.36	-6.38
2.0	-3.54	-3.57	-4.62	-4.65	-5.63	-5.74	-6.78	-6.82	-7.85	-7.89
2.5	-3.96	-4.00	-5.28	-5.34	-6.61	-6.67	-7.95	-8.00	-9.29	-9.33
3.0	-4.32	-4.38	-5.92	-5.96	-7.49	-7.54	-9.08	-9.12	-10.65	-10.70
3.5	-4.64	-4.71	-6.46	-6.54	-8.31	-8.37	-10.14	-10.20	-11.98	-12.02
4.0	-4.93	-5.00	-7.01	-7.08	-9.09	-9.16	-11.17	-11.23	-13.25	-13.31

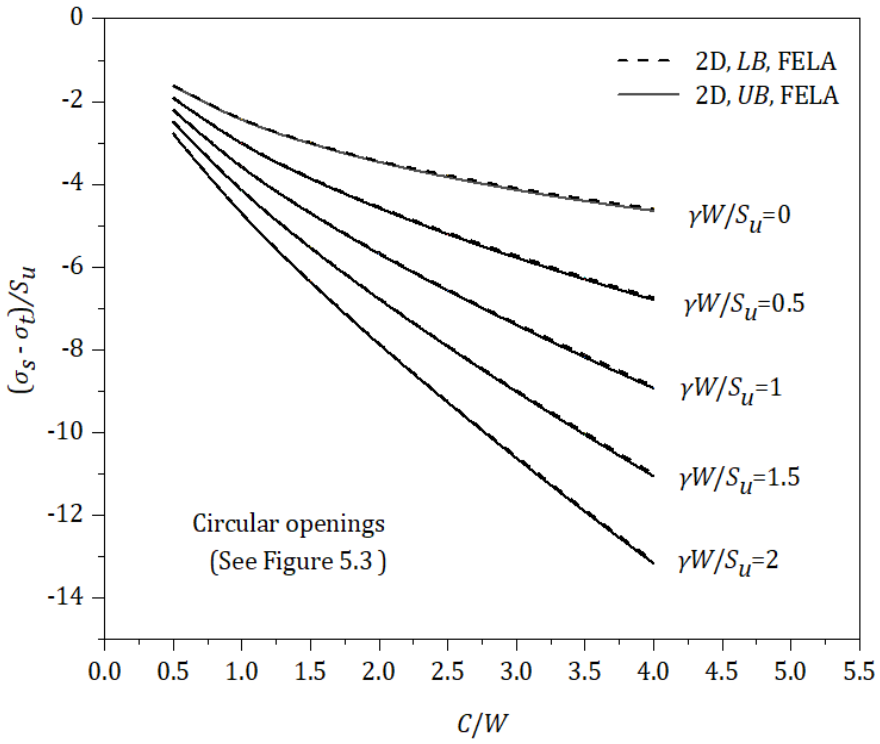

Figure 5.8. (σ_s - σ_t /S_u) vs (C/W) for circular openings

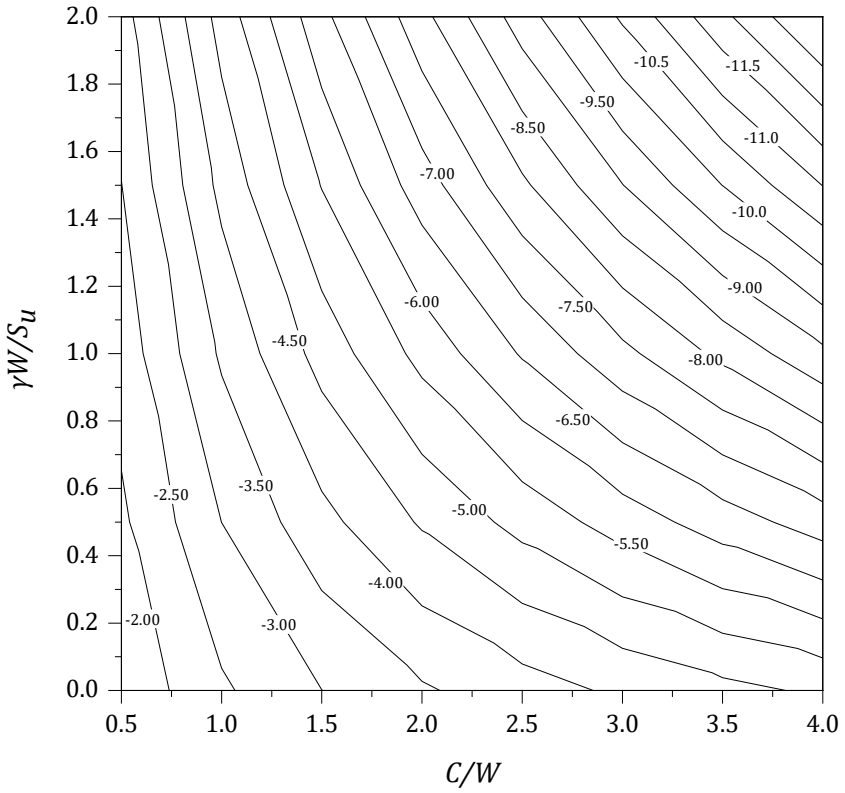

Figure 5.9. A blowout design chart to obtain *PR* (circular openings)

Table 5.3. Data used for plotting Figures 5.8 and 5.9 (circular openings)

C/W	$\gamma W/S_u$									
	0		0.5		1.0		1.5		2	
	LB	*UB*	*LB*	*UB*	*LB*	*UB*	*LB*	*UB*	*LB*	*UB*
0.50	-1.61	-1.63	-1.91	-1.93	-2.20	-2.22	-2.49	-2.51	-2.78	-2.80
1.0	-2.42	-2.44	-3.00	-3.02	-3.57	-3.59	-4.14	-4.16	-4.70	-4.72
1.5	-3.00	-3.02	-3.85	-3.87	-4.69	-4.71	-5.52	-5.54	-6.35	-6.37
2.0	-3.44	-3.46	-4.56	-4.58	-5.66	-5.69	-6.76	-6.78	-7.85	-7.87
2.5	-3.78	-3.83	-5.17	-5.21	-6.55	-6.58	-7.91	-7.93	-9.26	-9.28
3.0	-4.09	-4.14	-5.73	-5.78	-7.37	-7.40	-8.99	-9.02	-10.58	-10.62
3.5	-4.36	-4.41	-6.25	-6.30	-8.13	-8.19	-10.01	-10.06	-11.88	-11.92
4.0	-4.59	-4.64	-6.74	-6.80	-8.89	-8.94	-11.01	-11.06	-13.13	-13.18

5.3.2. Failure extent and soil arching

Contour plots of the absolute velocity fields of the three cavity shapes (horizontal, semi-circular, and circular) under blowout failures are presented in Figures 5.10-5.12 respectively. These plots are for a strength ratio ($\gamma W/S_u = 2$) and various depth ratios (C/W= 1 to 4). For the shallow horizontal openings (C/W=1.0) as in Figure 5.10, a more chimney type of blowout failure mechanism is observed.

The ground surface failure extent, which is practical information in the field, increases as the depth ratio C/W increases. It is interesting to note the uniform velocity within the triangular zone above the openings, indicating a rigid block movement under elastic deformation. Contour plots of the blowout velocity field for the semi-circular and circular openings are presented in Figures 5.11 and 5.12 respectively.

Noting that the overall pattern of blowout failure mechanism is somehow similar to the horizontal openings (Figure 5.10). Nevertheless, the elastic triangular zone is, however, not clearly displayed in Figures 5.11 and 5.12. Although the plots are not presented to scale, it can be clearly seen that the circular openings produce a larger surface failure extent than the semi-circular ones.

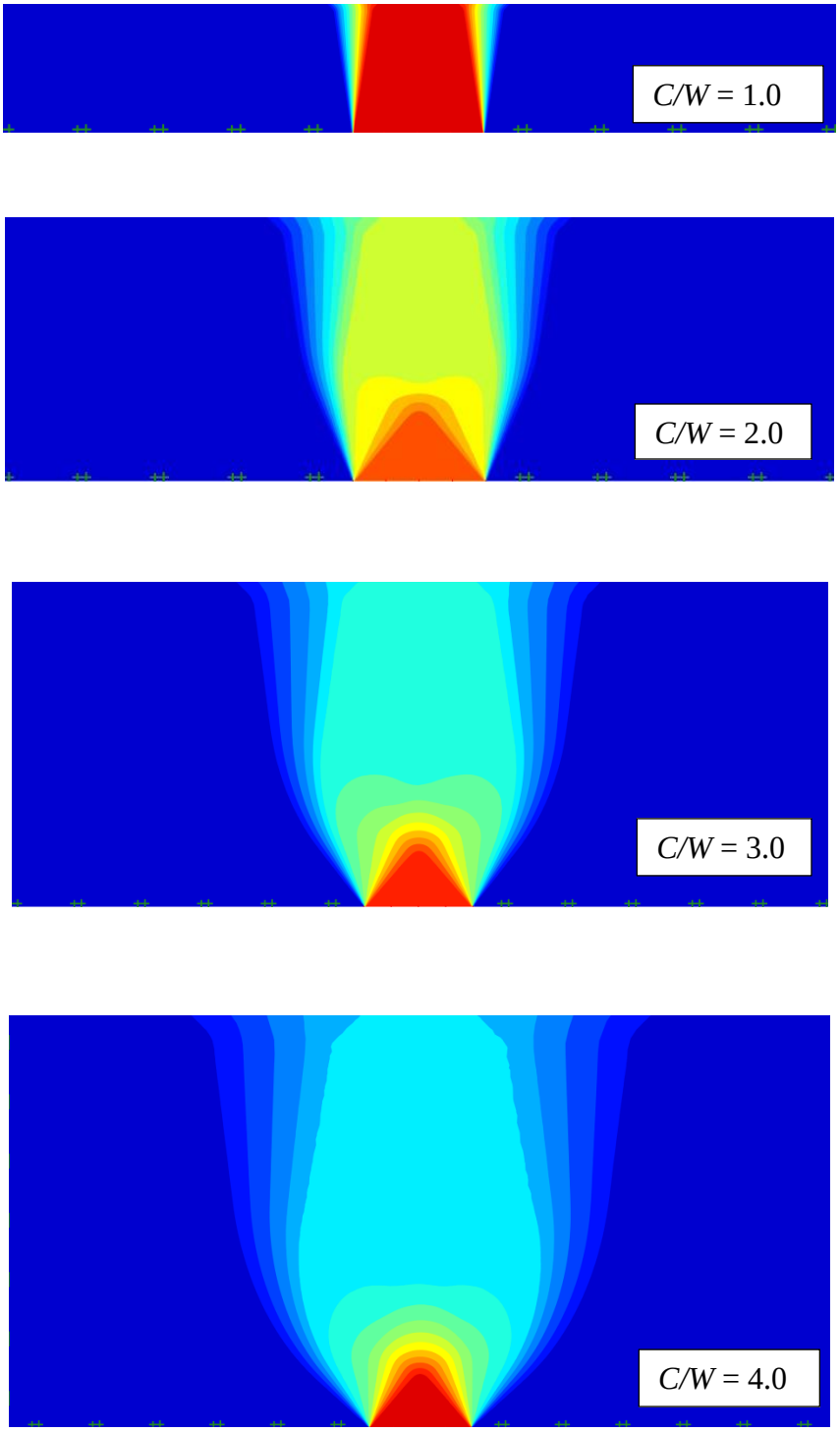

Figure 5.10. Contour plots of absolute velocity for horizontal openings ($\gamma W/S_u$ = 2.0)

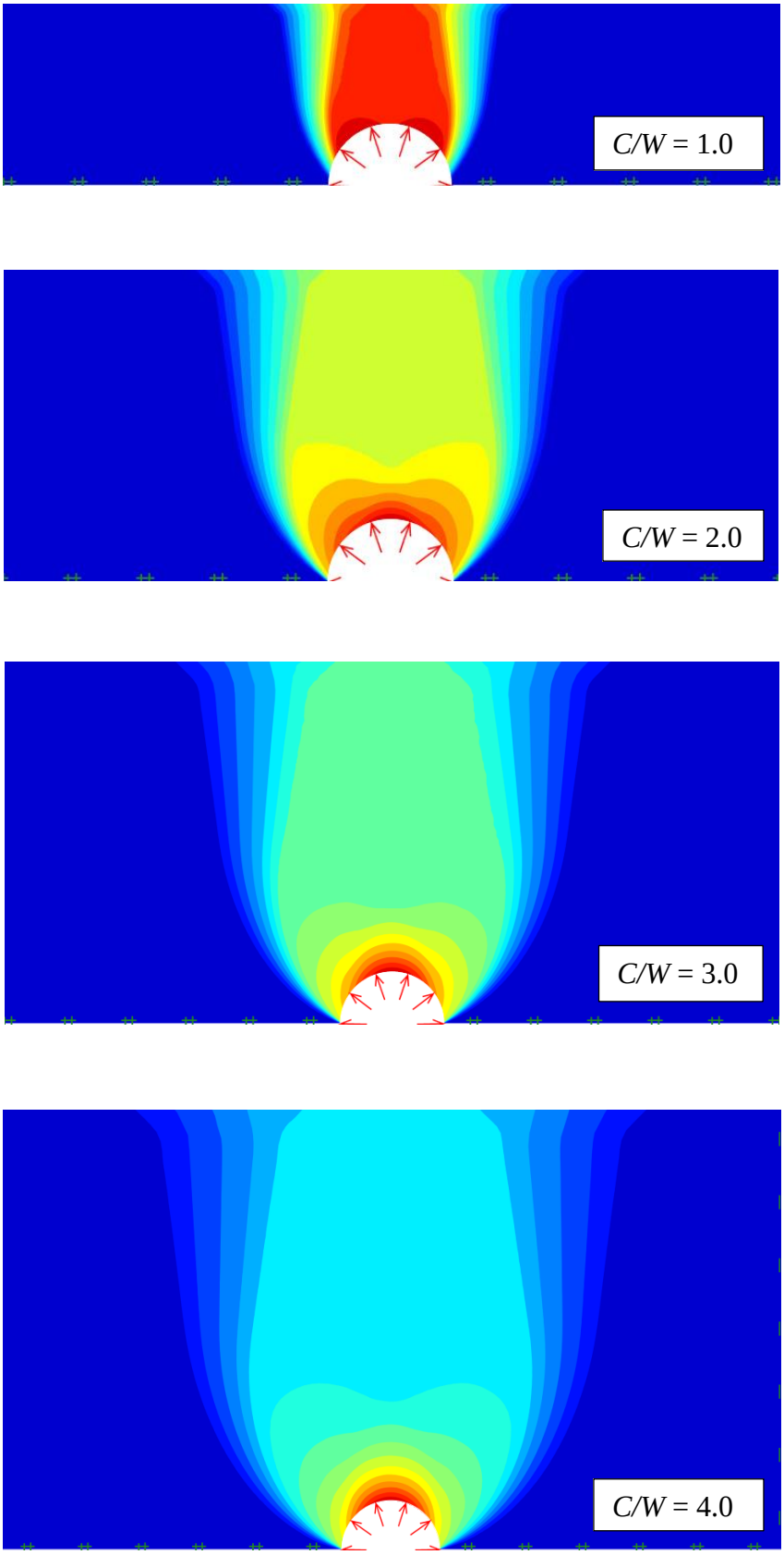

Figure 5.11. Contour plots of absolute velocity for semi-circular openings ($\gamma W/S_u$ = 2.0)

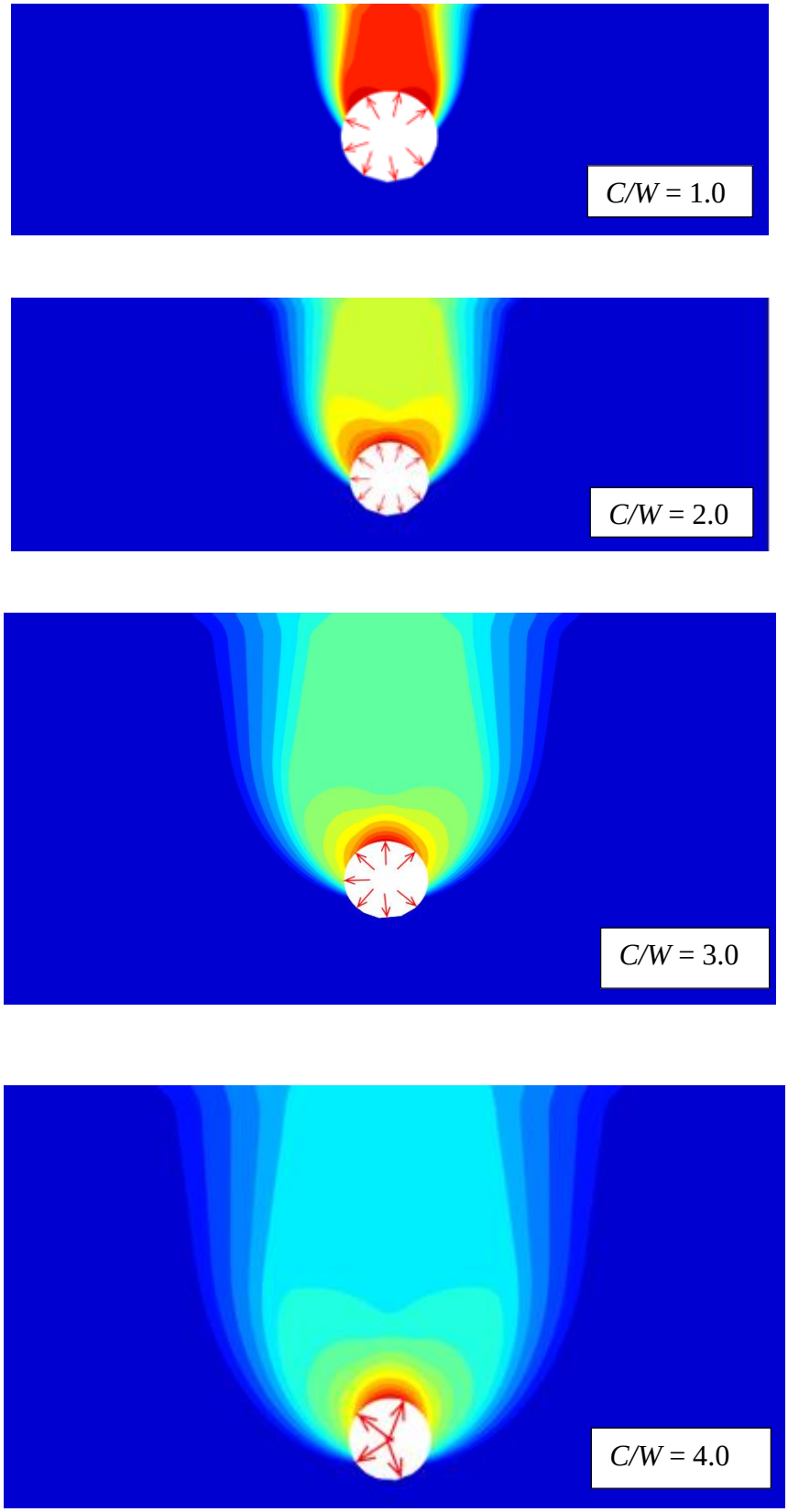

Figure 5.12. Contour plots of absolute velocity for circular openings ($\gamma W/S_u$ = 2.0)

5.3.3. Comparison of results

Figure 5.13 shows a stability comparison of the three cavity shapes i.e. the horizontal, semi-circular, and circular openings. The Figure 5.13 plots the pressure ratio $(\sigma_s - \sigma_t)/S_u$ versus the depth ratio (C/W) for the three cavity shapes. The chosen strength ratios for the plot are $\gamma W/S_u$ = 0, 1, and 2.

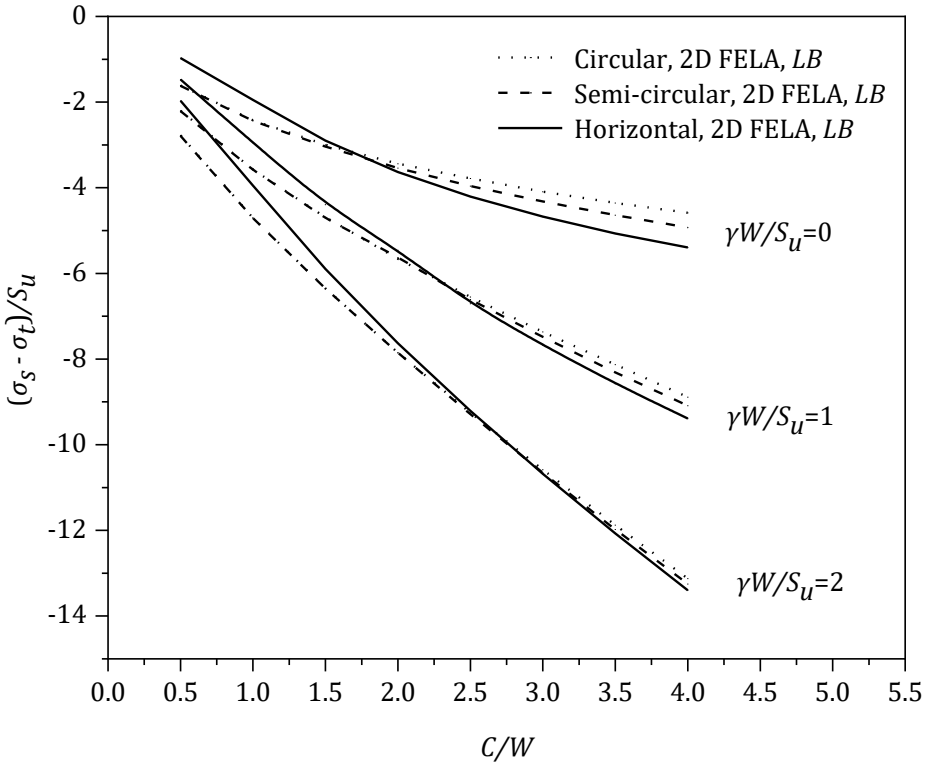

Figure 5.13. Comparison of three cavity shapes

For the weightless case ($\gamma W/S_u$ = 0), the three curves intersect at C/W = 1.75, giving two distinct responses in numerical results. For C/W > 1.75, the circular opening produces the lowest |PR| values of the three cavity shapes, whilst it has the largest |PR| values when C/W < 1.75. On the other hand, it is interesting to note that, for shallow cases such as C/W < 1.75, |PR| values are the same for both semi-circular and circular openings. This can be explained and further be justified from Figures 5.11 and 5.12, where the slip line initiates from a point above the centre of the circular openings.

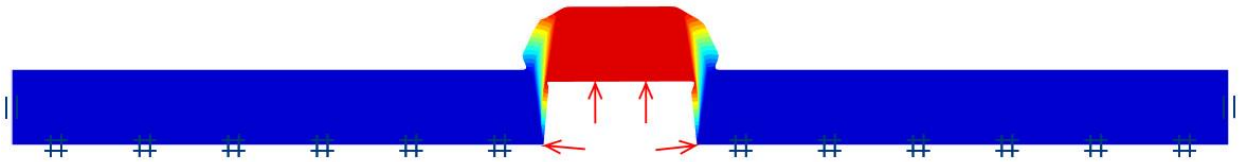

(a). Horizontal openings

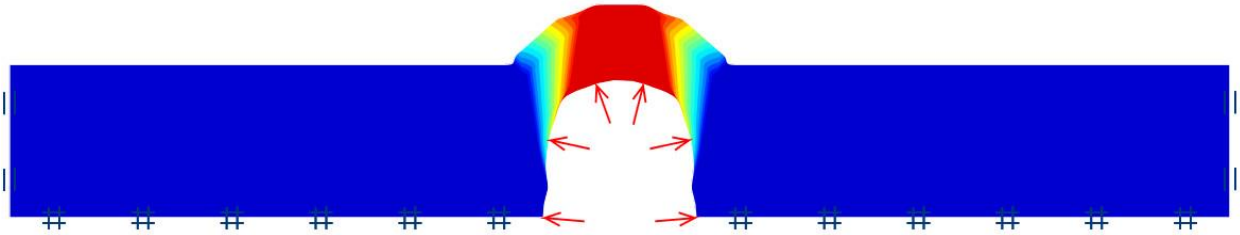

(b). Semi-circular openings

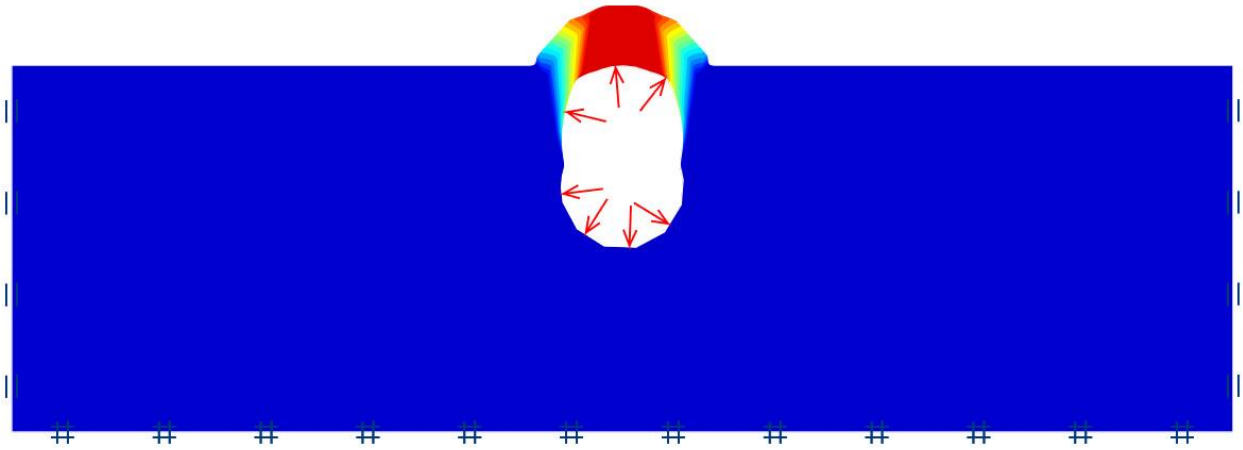

(c). Circular openings

Figure 5.14. Contour plots of absolute velocity and deformed shapes

($\gamma W/S_u$ = 2.0, C/W=0.5)

In addition, Figure 5.14 compares velocity fields of the three cavity shapes for a shallow case C/W = 0.5. Though they are not plotted to the same scale, it is not difficult to see that both semi-circular and circular openings have the same failure mechanism, as such, their $|PR|$ values are the same. The same observation applies to the cases with $\gamma W/S_u$ = 1 and 2 in Figure 5.13, where the intersection points are at C/W = 2.25 and 2.75, respectively.

It was noted that very few studies are available for a direct comparison of blowout stability. Nevertheless, Figure 5.15 shows a comparison between the present study and the tunnel blowout stability in Shiau and Al-Asadi (2021). To compare their critical stability number (N_c) with the current pressure ratio (PR), it is necessary to assume the soil unit weight to be zero ($\gamma = 0$). As seen in Figure 5.15, the comparison shows a good agreement between Shiau and Al-Asadi (2021) and the present study.

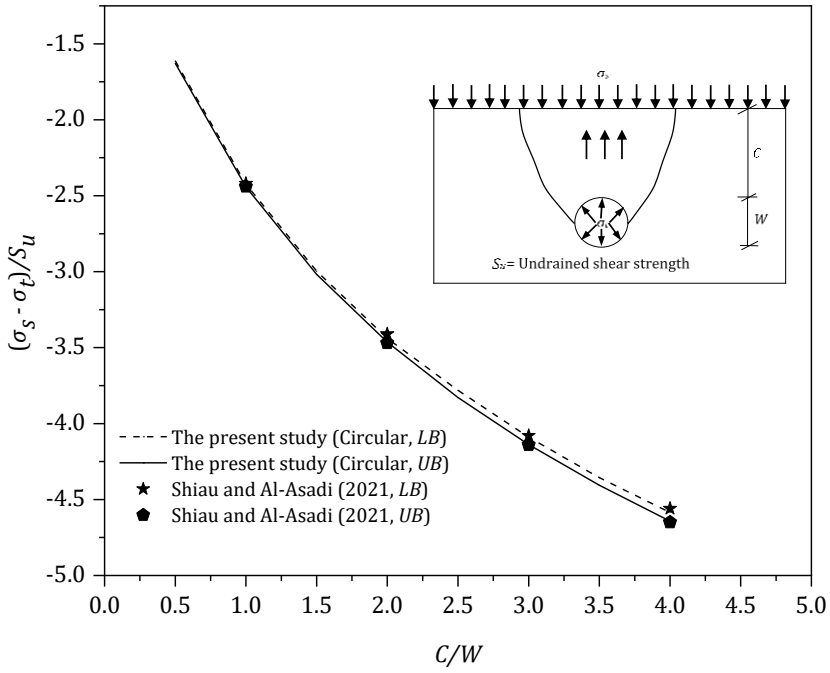

Figure 5.15. Comparison with published results (Circular openings)

5.4 EXAMPLES

Practical uses of the theoretical findings in the Chapter are best explained using examples. Figure 5.16, 5.17 & 5.18 shows a pipeline burst problem for the three stages of internal cavity shapes i.e., the horizontal, semi-circular, and circular openings. The material properties considered are: γ = 18 kN/m^3 and S_u = 80 kPa. Assuming that the average water main pressure is 300 kPa. With the surcharge σ_s = 0, the problem is analysed for the following three stages of development.

Initial stage (Figure 5.16)

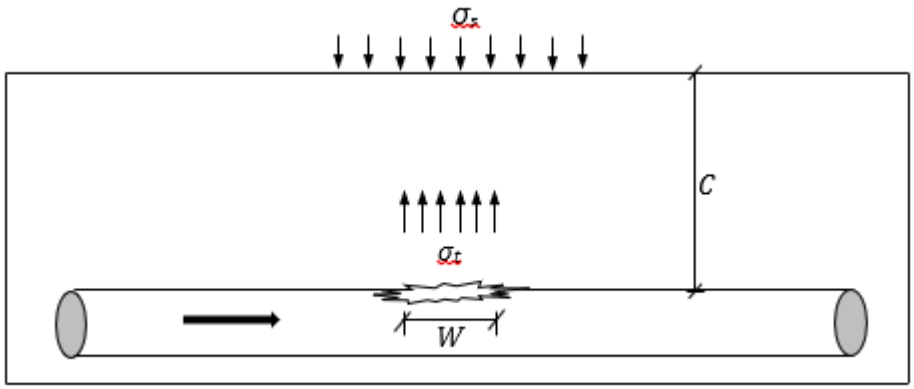

Figure 5.16. Initial stage of blowout stability

1. Given the cover depth C = 0.6 m and the cavity width W= 0.2 m, C/W = 3.
2. The strength ratio is calculated as $SR = \gamma W/S_u$ = (18 x 0.20)/80 = 0.05.
3. Using Figure 5.5, a critical pressure ratio is obtained $PR = (\sigma_s - \sigma_t)/S_u$ = - 4.75.
4. Since σ_s = 0 and S_u = 80 kPa, the critical σ_t is calculated as σ_t = 380 kPa. Theoretically, the water main pressure should not be greater than 380 kPa, or a blowout failure occurs.
5. The average water main pressure given in the example is 300 kPa, hence a blowout failure will not occur.
6. The corresponding factor of safety (FoS) = 380/300 = 1.17

Intermediate stage (Figure 5.17)

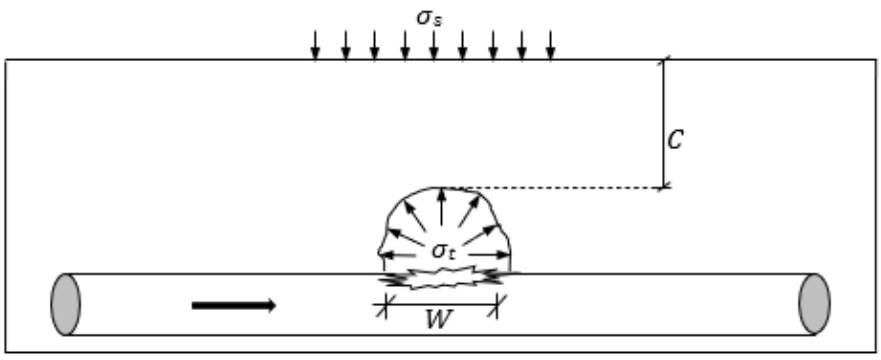

Figure 5.17. Intermediate stage of blowout stability

1. Given a new cover depth C=0.5 m and the cavity width W= 0.2 m, C/W= 2.5. The strength ratio $SR = \gamma W/S_u$ = (18 x 0.20)/ 80 = 0.05.
2. Using Figure 5.7, a critical pressure ratio is obtained $PR = (\sigma_s - \sigma_t)/S_u$ = - 4.
3. Since σ_s =0 and S_u = 80 kPa, the critical σ_t is calculated as σ_t = 320 kPa. It is expected that the water main pressure should not be greater than 320 kPa, or a blowout failure occurs.
4. The average water main pressure given in the problem is 300 kPa, hence a blowout failure will not occur. The corresponding factor of safety (FoS) = 320/300 = 1.07.

Final stage (Figure 5.18)

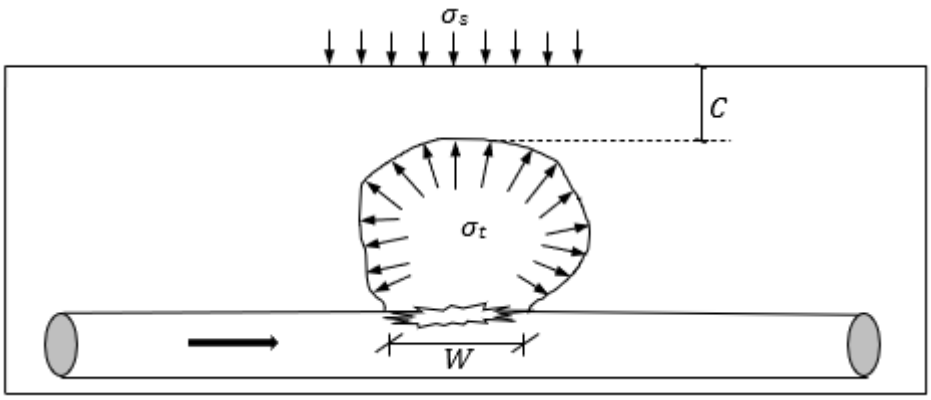

Figure 5.18. Final stage of blowout stability

1. Given a cover depth C=0.4 m and the cavity width W= 0.2 m, C/W = 2. The strength ratio is calculated as $SR = \gamma W/S_u$ = (18 x 0.20)/ 80 = 0.05.
2. Using Figure 5.9, a critical pressure ratio is obtained $PR = (\sigma_s - \sigma_t)/S_u$ = -3.50. Since σ_s =0 and S_u = 80 kPa, the critical σ_t is calculated as σ_t = 280 kPa.

3. The average water main pressure given in the problem is 300 kPa, which is greater than 280 kPa, hence a blowout failure will occur. The corresponding factor of safety (*FoS*) = 280/300 = 0.93.

From the above examples, one can see that *FoS* decreases as the cavity shape changes (so as the cover depth decreases). This is compatible with what is normally observed in the field. Should the water main pressure reduce to zero, it becomes a collapse problem with an existing cavity (downwards movement).

5.5 CONCLUSIONS

This Chapter investigated the blowout stability of soils above burst water pipes. Three different stages of soil erosion-related cavity shapes were considered in the study, namely, the horizontal, semi-circular, and circular openings. Broadly speaking, soils with horizontal openings provide better resistance to blowout stability than semi-circular and circular ones. In addition to this, the extent of surface failure increases with the increase in depth ratio irrespective of the trapdoor's shape. Comprehensive design charts and tables were produced for practical uses with examples. Future work recommendations may include a full three-dimensional study as well as using layered materials for a road pavement structure.

CHAPTER 6 CONCLUSIONS

This thesis studied the stability of underground cavities due to the water leakage from the sewer and water mains. Three progressive opening shapes considered were horizontal, semi-circular, and circular trapdoors. The finite element limit analysis (*FELA*) was utilised to explore the two-dimensional stability of different shapes. Davis's (1980) pressure ratio approach which derived from Broms and Bennermark's (1968) stability number equation was used to investigate two-dimensional (2*D*) problems. Stability results were presented in dimensionless forms for design purposes. Moreover, the velocity plots were used to determine the overall failure mechanism and the surface failure extent. The results throughout this study showed a good agreement with those published and those obtained by finite element limit analysis. Practical examples are also provided to demonstrate the use of design charts and tables by practical designers.

6.1. KEY CONCLUSION OF CHAPTER 4

In this Chapter, the ground collapse stability under pipe leakage-related sinkholes was investigated. Three idealised cavity shapes of horizontal, semi-circular, and circular were chosen to represent the process of internal soil erosion. A set of numerical studies were carried out using the advanced finite element limit analysis of upper and lower bound theorems. The key findings of the analysis are as follows:

- The horizontal trapdoor provided better resistance than the "curved" trapdoors and the circular trapdoor shown minimal support as cover depth decreased as the cavity size change and corresponding *FoS* also decreased.
- The horizontal trapdoor represented the least failure extent thus greater resistance compared to the "curved" trapdoors. A deep-seated failure mechanism is demonstrated throughout the deep cases in the circular opening.

- Original stability number (N_c) depended only on the depth (H) and the new value for the depth is defined as ($H= C$), for a horizontal trapdoor and ($H= C + 0.25\ W$) for both semi-circular and circular trapdoors.
- The dimensionless design charts and tables are useful for practicing engineers. Examples have also been given to illustrate the usefulness of such charts.

6.2. KEY CONCLUSION OF CHAPTER 5

The following main conclusions were drawn based on blowout stability above a damaged water main pipeline in three idealized stages of internal soil erosion, i.e., horizontal, semi-circular, and circular cavities using the latest finite element limit analysis technique. Dimensionless design parameters are used throughout the Chapter to present rigorous bounding solutions that can be used directly by designers to evaluate the blowout stability of soils above defective pipelines.

- Horizontal openings provide better resistance to blowout stability than semi-circular and circular ones as the circular openings produced a larger surface failure extent than the semi-circular ones.
- Failure extent increased with an increase in depth ratio irrespective of the trapdoor's shape.
- Numerical results were used to produce design charts and tables to cover a wide range of design parameters, and a practical example is introduced to illustrate their use in practice.

6.3. RECOMMENDATION

Underground studies are complicated as the complexity in defining parameters and their nature and this is very relevant to the water/sewer line leakage induced sinkhole problems, where the physical properties of the materials, the geological condition such as type of soil, and variation of properties such as homogeneity and load from surrounding structures such as utility building foundations varies place to place. Sinkhole failure above the water/sewer main could happen anywhere and anytime without warning. Therefore, a parametric study of the trapdoor is important and useful in the evaluation of the stability and ground surface failure extent. Based on the current investigation of trapdoor stability, some important points have been identified for future study.

- To simulate a more realistic situation, further studies need to be carried out to investigate the failure mechanism in increasing soil strength in homogeneous and layered soils.
- Full three-dimensional study as well as using layered materials for a realistic layered road pavement structure.
- Study on the early invention of water pipe leakage induced sinkholes using the thermal far-infrared camera mounted drone.
- Analysis on tracing shallow cavities above the water and sewer main using the microchip.
- Road-related sinkhole backfilling techniques and materials.

7.0. BIBLIOGRAPHY

Abdulla, WA & Goodings, DJ 1996, 'Modeling of sinkholes in weakly cemented sand', *Journal of Geotechnical Engineering*, vol. 122, no. 12, pp. 998-1005.

Al-Halbouni D, Holohan EP, Taheri A, Schöpfer MP, Emam S, Dahm T (2018) Geomechanical modelling of sinkhole development using distinct elements: model verification for a single void space and application to the Dead Sea area. Solid Earth 9(6):1341–1373.

Al-Halbouni D, Holohan EP, Taheri A, Watson RA, Polom U, Schöpfer MPJ, Emam S, Dahm T (2019) Distinct element geomechanical modelling of the formation of sinkhole clusters within large-scale karstic depressions. Solid Earth 10(4):1219–1241.

Ali, H & Choi, J-h 2020, 'Risk Prediction of Sinkhole Occurrence for Different Subsurface Soil Profiles due to Leakage from Underground Sewer and Water Pipelines', *Sustainability*, vol. 12, no. 1, p. 310.

Ali, H & Choi, J-h 2019, 'A review of underground pipeline leakage and sinkhole monitoring methods based on wireless sensor networking', *Sustainability*, vol. 11, no. 15, p. 4007.

Alsaydalani, M.O.A., and Clayton, C.R.I. 2014, 'Internal Fluidization in Granular Soils', *Journal of Geotechnical and Geoenvironmental Engineering* 140(3): 04013024. doi: doi:10.1061/(ASCE)GT.1943-5606.0001039.

Anderheggen, E & Knöpfel, H 1972, 'Finite element limit analysis using linear programming', *International Journal of Solids and Structures*, vol. 8, no. 12, pp. 1413-31.

Anon, (2019). *Sinkhole Nearly Swallows Car In Bushwick, Brooklyn*. [online] Available at: https://newyork.cbslocal.com/2019/08/01/crews-work-to-remove - car -from-sinkhole-in-brooklyn/ [Accessed 16 Jun. 2021].

Arai, K & Tagyo, K 1985, 'Limit analysis of geotechnical problems by applying lower-bound theorem', *Soils and Foundations*, vol. 25, no. 4, pp. 37-48.

Atkinson, J.H. and Potts, D.M., 1977, 'Stability of a shallow circular tunnel in cohesionless soil', *Geotechnique*, *27*(2), pp.203-215.

Augarde, CE, Lyamin, AV & Sloan, SW 2003, 'Prediction of undrained sinkhole collapse', *Journal of Geotechnical and Geoenvironmental Engineering*, vol. 129, no. 3, pp. 197-205.

avax.news. (2007). *Sinkholes*. [online] Available at: http://avax.news/pictures/60272 [Accessed 8 Jul. 2021].

Bae, Y, Shin, S, Won, J & Lee, D 2016, 'The road subsidence conditions, and safety improvement plans in Seoul', *The Seoul Institute*, pp. 1-60.

Baek, J, Yoon, J-S, Lee, C-M & Choi, Y 2018, 'A case study on detection of subsurface cavities of urban roads using ground-coupled GPR', *2018 17th International Conference on Ground Penetrating Radar (GPR)*, IEEE, pp. 1-4.

Basudhar, P, Valsangkar, A & Madhav, M 1979, 'Optimal lower bound of passive earth pressure using finite elements and non-linear programming', International Journal for Numerical and Analytical Methods in Geomechanics, vol. 3, no. 4, pp. 367-79.

Belytschko, T & Hodge, PG 1970, 'Plane stress limit analysis by finite elements', *Journal of the Engineering Mechanics Division*, vol. 96, no. 6, pp. 931-44.

Berger, S. (2015). *Massive Brooklyn Sinkhole Disrupts New York's Sunset Park Neighborh--ood [PHOTO]*. [online] International Business Times. Available at: https://www. ibtimes. com/massive-brooklyn-sinkhole-disrupts-new-yorks-sunset-park-neighborhood-photo 2038729 [Accessed 6 Jul. 2021].

Bhattacharya, P & Dutta, P 2020, ‘Stability of rectangular tunnel in Hoek–Brown rocks under steady-state groundwater flow’, *Géotechnique Letters*, vol. 10, no. 4, pp. 524–534.

Bhattacharya, P & Kumar, J 2016, ‘Uplift Capacity of Anchors in Layered Sand Using Finite-Element Limit Analysis: Formulation and Results’, *International Journal of Geomechanics*, vol. 16, no. 3, p. 04015078.

Bhattacharya, P & Sahoo, S 2020, ‘Pullout Resistance of Buried Pipeline in Cohesionless Soil Nearby Sloping Ground’, *Journal of Pipeline Systems Engineering and Practice*, vol. 11, no. 2, p. 04020008.

Biron, A & Charleux, G 1972, 'Limit analysis of axisymmetric pressure vessel intersections of arbitrary shape', *International Journal of Mechanical Sciences*, vol. 14, no. 1, pp. 25-41.

Bottero, A, Negre, R, Pastor, J & Turgeman, S 1980, 'Finite element method and limit analysis theory for soil mechanics problems', *Computer Methods in Applied Mechanics and Engineering*, vol. 22, no. 1, pp. 131-49.

Broms, BB & Bennermark, H 1967, 'Stability of clay at vertical openings', *Journal of the Soil Mechanic and Foundations Division, Proceedings of the American Society of Civil Engineers*, vol. 93, pp. 71- 94.

Burn, S., DeSilva, D., Eiswirth, M., Hunaidi, O., Speers, A. and Thornton, J., 1999. Pipe leakage–future challenges and solutions. *Pipes Wagga Wagga, Australia*.

Business Insider. (2017). *A 20-foot-long sinkhole ripped open a busy Manhattan street*. [online] Available at: https://www.businessinsider.in/a-20-foot-long-sinkhole-ripped-open-a-busy-manhattan-street/articleshow/61731910.cms [Accessed 15 Jun. 2021].

Calligeros, D.M., Marissa (2015). *Sinkhole swallows three lanes on busy Caulfield Road*. [online] The Age. Available at: https://www.theage.com.au/ national/victoria/sinkhole-

swallows-three-road-lanes-on-busy-caulfield-road-20150929-gjwx4l.html [Accessed 14 Jun. 2021].

Capsoni, A & Corradi, L 1997, 'A finite element formulation of the rigid–plastic limit analysis problem', *International Journal for Numerical Methods in Engineering*, vol. 40, no. 11, pp. 2063-86.

Chang, L & Hanssen, RF 2014, 'Detection of cavity migration and sinkhole risk using radar interferometric time series', *Remote Sensing of Environment*, vol. 147, pp. 56-64.

Ciria, HS 2004, 'Computation of upper and lower bounds in limit analysis using second-order cone programming and mesh adaptivity', Massachusetts Institute of Technology.

Costa, YD, Zornberg, JG, Bueno, BS & Costa, CL 2009, 'Failure mechanisms in sand over a deep active trapdoor', *Journal of Geotechnical and Geoenvironmental Engineering*, vol. 135, no. 11, pp. 1741-53.

Craig, W 1990, 'Collapse of cohesive overburden following removal of support', *Canadian Geotechnical Journal*, vol. 27, no. 3, pp. 355-64.

Daily (2013). *"I thought they're not going to get me out in time": Pictured the school principal whose car was swallowed by a sinkhole*. [online] Mail Online. Available at: https://www.dailymail.co.uk/news/article-2357077/Pamela-Knox-school-principal-car-swallowed-10ft-deep-Ohio-sinkhole.htm [Accessed 9 Mar. 2021].

Davis, E, Gunn, M, Mair, R & Seneviratine, H 1980, 'The stability of shallow tunnels and underground openings in cohesive material', *Geotechnique*, vol. 30, no. 4, pp. 397-416.

Davis E, (1968) Theories of plasticity and the failure of soil masses. In *Soil Mechanics Selected Topics* (Lee IK (ed.)), Butterworths, London, UK, pp.341 -380.

Detman, G. (2017). *California Highway Patrol names giant sinkhole "Steve."* [online] KUTV. Available at: https://kutv.com/news/offbeat/california-highway-patrol-names-giant-sinkhole-steve [Accessed 3 Apr. 2021].

Drucker, D.C. and Prager, W.,1952, 'Soil mechanics and plastic analysis or limit design', *Quarterly of applied mathematics*, *10*(2), pp.157-165.

Drumm, EC, Aktürk, Ö, Akgün, H & Tutluoğlu, L 2009, 'Stability charts for the collapse of residual soil in karst', *Journal of Geotechnical and Geoenvironmental Engineering*, vol. 135, no. 7, pp. 925-31.

Dutta, P & Bhattacharya, P 2019, 'Stability of rectangular tunnel in cohesionless soils', *International Journal of Geotechnical Engineering*, pp. 1–7.

Fairbridge, R.W., 1968.The Encyclopaedia of Geomorphology. In: Reinhold (Ed.), (New York,1295 pp.).

Fletcher, R & Reeves, CM 1964, 'Function minimization by conjugate gradients', *The computer journal*, vol. 7, no. 2, pp. 149-54.

Fortin, M & Glowinski, R 1983, Augmented Lagrangian methods: applications to the numerical solution of boundary-value problems, Elsevier.

Foster, B. (2017). *"I thought it was going to disappear": Ute falls into "sinkhole" in Perth's north*. [online] WAtoday. Available at: https://www.watoday.com.au/national/ western-australia/utility-falls-into-sinkhole-in-perths-north-20170630-gx1sx5.html.

FOX 5 San Diego. (2020). *Ruptured water pipe creates sinkhole in street*. [online] Available at: https://fox5sandiego.com/news/water-main-break-causes-sinkhole/ [Accessed 18 Mar. 2021].

Ghulam, A, Basim, K & Al-Baidhani, J 2018, 'Evaluation of the Effect of Leak Size of Defective Sewer Pipes on Soil Erosion', *Journal of Engineering and Applied Sciences*, vol. 13, pp. 10708-12.

Griffin, S & Pippett, T 2002, 'Ground penetrating radar', *Geophysical and Remote Sensing Methods for Regolith Exploration*, vol. 144, pp. 80-9.

Griffiths, D & Lane, P 1999, 'Slope stability analysis by finite elements', *Geotechnique*, vol. 49, no. 3, pp. 387-403.

Guarino, PM, Santo, A, Forte, G, De Falco, M & Niceforo, DMA 2018, 'Analysis of a database for anthropogenic sinkhole triggering and zonation in the Naples hinterland (Southern Italy)', *Natural Hazards*, vol. 91, no. 1, pp. 173-92.

Gunn M 1980, 'Limit analysis of undrained stability problems using a very small computer', *Proceedings of the Symposium on Computer Applications to Geotechnical Problems in Highway Engineering*, Cambridge, UK, pp. 5–30.

Guo, S, Shao, Y, Zhang, T, Zhu, DZ & Zhang, Y 2013, 'Physical modeling on sand erosion around defective sewer pipes under the influence of groundwater', *Journal of Hydraulic Engineering*, vol. 139, no. 12, pp. 1247-57.

Hadjmeliani, M 2015, 'Degradation of sewage pipe caused Sinkhole: A real case study in a main Road', *Congrès français de mécanique*, AFM, Association Française de Mécanique.

Herald, T.K.

(2016). *105 potential sinkholes in Seoul*. [online] www.koreaherald.com. Available at: http://www.koreaherald.com/view.php?ud=20160420000970. [Accessed 10 June. 2021]

Hit Network. (2017). *Massive Sinkhole Causes Road Closures in Sydney*. [online] Available at: https://www.hit.com.au/story/massive-sinkhole-causes-road-closures-in-sydney-15496 [Accessed 21 Mar. 2021].

Hodge, PG & Belytschko, T 1968, 'Numerical methods for the limit analysis of plates'.

HuffPost UK. (2016). *Woman Attempts to Drive Over Puddle, Ends Up in Sinkhole*. [online] Available at: https://www.huffingtonpost.co.uk/2016/02/22/ nottinghamshire-sinkhole-swallows-car_n_9288296.html [Accessed 18 Mar. 2021].

Huh, H & Yang, WH 1991, 'A general algorithm for limit solutions of plane stress problems', Int. J. Solids Struct. 28, No. 6, 727–738.

Indiketiya, S, Jegatheesan, P, Rajeev, P & Kuwano, R 2019, 'The influence of pipe embedment material on sinkhole formation due to erosion around defective sewers', *Transportation Geotechnics*, vol. 19, pp. 110-25.

Indiketiya, S, Jegatheesan, P & Rajeev, P 2017, 'Evaluation of defective sewer pipe–induced internal erosion and associated ground deformation using laboratory model test', *Canadian Geotechnical Journal*, vol. 54, no. 8, pp. 1184-95.

Jacobsz, S 2016, 'Trapdoor experiments studying cavity propagation', *Proceedings of the first Southern African Geotechnical Conference*, pp. 159-65.

Jiang, GL 1995, 'Non-linear finite element formulation of kinematic limit analysis', *International Journal for Numerical Methods in Engineering*, vol. 38, no. 16, pp. 2775-807.

Jiang, G-L 1994, 'Regularized method in limit analysis', *Journal of engineering mechanics*, vol. 120, no. 6, pp. 1179-97.

Jones, CE & Blom, RG 2014, 'Bayou Corne, Louisiana, sinkhole: Precursory deformation measured by radar interferometry', *Geology*, vol. 42, no. 2, pp. 111-4.

Kang, J-M & Lee, I-H 2015, 'IoT (Internet of Things)-based underground risk assessment system surrounding water pipes in Korea'.

Kang, M.S., Kim, N., Lee, J.J. and An, Y.K., 2020, 'Deep learning-based automated underground cavity detection using three-dimensional ground penetrating radar', *Structural Health Monitoring*, *19*(1), pp.173-185.

Karoui, T, Jeong, S-Y, Jeong, Y-H & Kim, D-S 2018, 'Experimental study of ground subsidence mechanism caused by sewer pipe cracks', *Applied Sciences*, vol. 8, no. 5, p. 679.

Kavlie, D & Moe, J 1971, 'Automated design of frame structures', *Journal of the Structural Division*, vol. 97, no. 1, pp. 33-62.

Keawsawasvong, S, 2021, 'Limit analysis solutions for spherical cavities in sandy soils under overloading', *Innovative Infrastructure Solutions* vol. 6, art. no. 33.

Keawsawasvong, S, Likitlersuang, S, 2020, 'Undrained stability of active trapdoors in two-layered clays', *Underground Space*. DOI: 10.1016/j.undsp.2020.07.002

Keawsawasvong, S, Ukritchon, B, 2021, 'Undrained stability of plane strain active trapdoors in anisotropic and non-homogeneous clays', *Tunnelling and Underground Space Technology*, vol. 107, art. no. 103628.

Keawsawasvong, S, Ukritchon, B, 2019, 'Undrained stability of a spherical cavity in cohesive soils using finite element limit analysis', *Journal of Rock Mechanics and Geotechnical Engineering*, vol. 11, no. 6, 1274-85.

Keawsawasvong, S & Ukritchon, B 2017, 'Undrained stability of an active planar trapdoor in non-homogeneous clays with a linear increase of strength with depth', *Computers and Geotechnics*, vol. 81, pp. 284-93.

KGTV. (2017). *Uber car falls into a sinkhole on Olde Hwy 80*. [online] Available at: https://www.10news.com/news/water-main-break-sinkhole-reported-on-olde-highway-80-in-lakeside [Accessed 6 Apr. 2021].

Kim, K, Kim, J, Kwak, T-Y & Chung, C-K 2018, 'Logistic regression model for sinkhole susceptibility due to damaged sewer pipes', *Natural Hazards*, vol. 93, no. 2, pp. 765-85.

Kim, Y, Kim, J-B, Kim, D & Han, J-G 2017, 'Experimental study on generating mechanism of the ground subsidence of due to damaged waters supply pipe', *Journal of the Korean Geosynthetics Society*, vol. 16, no. 2, pp. 139-48.

Klar, A, Osman, AS & Bolton, M 2007, '2*D* and 3*D* upper bound solutions for tunnel excavation using 'elastic'flow fields', *International Journal for Numerical and Analytical Methods in Geomechanics*, vol. 31, no. 12, pp. 1367-74.

Koutsabeloulis, N.C. and Griffiths, D.V., 1989, 'Numerical modelling of the trap door problem', *Geotechnique*, *39*(1), pp.77-89.

Krabbenhøft, K, Lyamin, AV & Sloan, SW 2008, 'Three-dimensional Mohr-Coulomb limit analysis using semidefinite programming', *Communications in Numerical Methods in Engineering*, vol. 24, no. 11, pp. 1107-19.

Krabbenhøft, K, Lyamin, AV & Sloan, SW 2007, 'Formulation and solution of some plasticity problems as conic programs', *International Journal of Solids and Structures*, vol. 44, no. 5, pp. 1533-49.

Krabbenhøft, K, Lyamin, AV, Hjiaj, M & Sloan, SW 2005, 'A new discontinuous upper bound limit analysis formulation', *International Journal for Numerical Methods in Engineering*, vol. 63, no. 7, pp. 1069-88.

Krabbenhoft, K & Damkilde, L 2003, 'A general non-linear optimization algorithm for lower bound limit analysis', *International Journal for Numerical Methods in Engineering*, vol. 56, no. 2, pp. 165-84.

Kuwano, R., Hiorii, T., Kohashi, H., and Yamauchi, K. 2006, 'Defects of sewer pipes causing cave-ins' in the road', *5th International Symposium on New Technologies for Urban safety of mega cities in Asia (USMCA),* Phuket, Thailand.

Kwak, P.J., Park, S.H., Choi, C.H., Lee, H.D., Kang, J.M. and Lee, I.H., 2015,' IoT (Internet of Things)-based underground risk assessment system surrounding water pipes in Korea',*International Journal of Control and Automation*, *8*(11), pp.183-190.

Leca, E & Dormieux, L 1990, 'Upper and lower bound solutions for the face stability of shallow circular tunnels in frictional material', *Geotechnique*, vol. 40, no. 4, pp. 581-606.

Lei, M, Gao, Y, Jiang, X & Hu, Y 2005, 'Experimental study of physical models for sinkhole collapse in Wuhan, China', in *Sinkholes and the Engineering and Environmental Impacts of Karst*, pp. 91-102.

Levy, M. (2017). *"Sinkhole" opens outside Point Piper mansion near Malcolm Turnbull's house after a deluge*. [online] The Sydney Morning Herald. Available at: https://www.smh.com.au/national/nsw/large-sinkhole-opens-outside-point-piper-mansion-after-deluge-20170208-gu7v3v.html [Accessed 14 Jun. 2021].

Liu, Y, Cen, Z & Xu, B 1995, 'A numerical method for plastic limit analysis of 3-D structures', *International Journal of Solids and Structures*, vol. 32, no. 12, pp. 1645- 58.

Lyamin, AV & Sloan, SW 2002a, 'Upper bound limit analysis using linear finite elements and non-linear programming', *International Journal for Numerical and Analytical Methods in Geomechanics*, vol. 26, no. 2, pp. 181-216.

Lyamin, AV & Sloan, SW 2002b, 'Lower bound limit analysis using non-linear programming', *International Journal for Numerical Methods in Engineering*, vol. 55, no. 5, pp. 573-611.

Lyamin, AV 1999, 'Three-dimensional lower bound limit analysis using nonlinear programming', University of Newcastle.

Lysmer, J 1970, 'Limit analysis of plane problems in soil mechanics', *Journal of the Soil Mechanics and Foundations Division*, vol. 96, no. 4, pp. 1311-34.

Maier, G, Zavelani-Rossi, A & Benedetti, D 1972, 'A finite element approach to optimal design of plastic structures in plane stress', *International Journal for Numerical Methods in Engineering*, vol. 4, no. 4, pp. 455-73.

Mair, R.J., 1979, 'Centrifugal Modelling of Tunnel Construction in SoftClay', *Ph.D. Thesis, Cambridge University Engineering Department*, UK.

Makrodimopoulos, A & Martin, C 2006, 'Lower bound limit analysis of cohesive frictional materials using second-order cone programming', *International Journal for Numerical Methods in Engineering*, vol. 66, no. 4, pp. 604-34.

Martin, CM, 2009, 'Undrained collapse of a shallow plane-strain trapdoor', *Géotechnique*, vol. 59, no. 10, pp. 855–63.

Matsui, T & San, K-C 1992, 'Finite element slope stability analysis by shear strength reduction technique', *Soils and Foundations*, vol. 32, no. 1, pp. 59-70.

Michalowski, RL 2002, 'Stability charts for uniform slopes', *Journal of Geotechnical and Geoenvironmental Engineering*, vol. 128, no. 4, pp. 351-5.

McKinnon Broadcasting, 2020, *Water main break causes sinkhole in Southcrest* -[online] Available at: https://www.kusi.com/water-main-break-causes-sinkhole-in-southcrest/ [Accessed 22 Jul. 2021].

Meng, Y, Dai, J, Jia, L, Lei, M & Ji, F 2013, 'Typical methods for forecasting karst collapse in China'.

Merifield, R, Sloan, S & Yu, H 2001, 'Stability of plate anchors in undrained clay', *Geotechnique*, vol. 51, no. 2, pp. 141-53.

Merifield, RS, Lyamin, A & Sloan, S 2006, 'Three-dimensional lower-bound solutions for the stability of plate anchors in the sand', *Geotechnique*, vol. 56, no. 2, pp. 123-32.

Mimicnews (2020). *Melbourne sinkhole forces closure of busy CBD street*. [online] Mimicnews. Available at: https://mimicnews.com/melbourne-sinkhole-forces-closure-of-busy-cbd-street [Accessed 14 Jun. 2021].

Morrison, S. (2017). *A huge sinkhole opens up and swallows a car in a major US city*. [online] www.standard.co.uk. Available at: https://www.standard.co.uk/news/world/huge-sinkhole-opens-up-and-swallows-car-in-missouri-city-a3576811.html [Accessed 2 Mar. 2021].

Mühlhaus, H.B., 1985, 'Lower bound solutions for circular tunnels in two and three dimensions', *Rock Mechanics and Rock Engineering*, *18*(1), pp.37-52.

Naylor, D 1982, 'Finite elements and slope stability', *in Numerical methods in geomechanics, Springer*, pp. 229-44

NBC 7 San Diego. (2020). *Sinkhole Closes Roads, Impacts School Pick-ups in Southcrest*. [online] Available at: https://www.nbcsandiego.com/news/local/sinkhole-closes-roads-in-southcrest/2247903/ [Accessed 6 Apr. 2021].

News, T.B.E. (2021). *Wellington's water woes turn into daily disasters, council is under pressure*. [online] The Bharat Express-News. Available at: https://www. the Bharat express news.com/wellingtons-water-woes-turn-into-daily-disasters-council-under-pressure/ [Accessed 24 Feb. 2021].

NewsComAu. (2021). *Pipe bursts in Sydney street before sinkhole open*. [online] Available at: https://www.news.com.au/national/nsw-act/news/sinkhole-opens-up-on-newport-nsw-road-after-water-pipe-bursts/news-story/ 1068cc414cd5da051d5453a88ecf4ef5/[Accessed 24 Feb. 2021].

NewsComAu. (2016). *Burst water main along Park St, Carlton North causes flash flooding, sinkhole fears*. [online] Available at: https://www.news.com.au/national/ victoria/burst-water-main-along-park-st-carlton-north-causes-flash-flooding-sinkhole-fears/news-story/ 0718e282ea6b4c625e8f6a8098137935 [Accessed 8 Apr. 2021].

Nguyen, HS, Trapletti, M & Ransart, D 1978, 'Quasi-lower bounds and upper bounds for the buckling pressure of shells of revolution by the finite element method and by nonlinear programming', *International Journal of Non-Linear Mechanics*, vol. 13, no. 2, pp. 79-102.

Nof, RN, Baer, G, Ziv, A, Raz, E, Atzori, S & Salvi, S 2013, 'Sinkhole precursors along the Dead Sea, Israel, revealed by SAR interferometry', *Geology*, vol. 41, no. 9, pp. 1019-22.

OptumCE 2020, *OptumG2. Copenhagen, Denmark: Optum Computational Engineering. See https://optumce.com/.*

Oren, G & Stroh, N 2012, 'Antileaks: A device for detection and discontinuation of leakages in domestic water supply systems', *European Journal for Young Scientist and Engineers*, vol. 1, pp. 10-3.

Osman, AS 2010, 'Stability of unlined twin tunnels in undrained clay', *Tunnelling and Underground Space Technology*, vol. 25, no. 3, pp. 290-6.

Osman, AS, Mair, RJ & Bolton, MD 2006, 'On the kinematics of 2*D* tunnel collapse in undrained clay', *Géotechnique.*, vol. 56, no. 9, pp. 585-95.

Otago Daily Times Online News. (2009). *Lucky escape as fire truck falls into a sinkhole*. [online] Available at: https://www.odt.co.nz/news/world/lucky-escape-fire-truck-falls-sinkhole [Accessed 15 Jun. 2021].

Pastor, J 1978, 'Analyse limit determination numerique de solutions statistique completes, Application au talus vertical', *J. de Mechanique Appliquee*, vol. 2, pp. 16796.

Pastor, J. and Turgeman, S., 1982, 'Limit analysis in axisymmetrical problems: numerical determination of complete statical solutions', *International Journal of Mechanical Sciences*, *24*(2), pp.95-117.

Paulam (2016). *The sheriff's deputy dies after the car plunges into a massive sinkhole in Texas*. [online] The Straits Times. Available at: https://www.straitstimes.com/world/united-states/ sheriffs-deputy-dies-after-car-plunges-into-massive-sinkhole [Accessed19 Jun. 2021].

Plaxis, B.V. 2011, PLAXIS 2D Finite element software, https://www.plaxis.com Point, H 2017, 'Umpherston Sinkhole', viewed 4th July 2018,

Powell, MJ 1964, 'An efficient method for finding the minimum of a function of several variables without calculating derivatives', *The computer journal*, vol. 7, no. 2, pp. 155-62.

Press, A. (2017). *The Latest: Truck removed, but no word on the cause of the sinkhole*. [online] Daily Herald. Available at: https://www.dailyherald.com/article /20170505/news /305059905 [Accessed 18 Mar. 2021].

Rajeev, P, Kodikara, J, Chiu, WK & Kuen, T 2013, 'Distributed optical fiber sensors and their applications in pipeline monitoring', *Key Engineering Materials*, Trans Tech Publ, pp. 424-34.

Renuka, I & Kuwano, R 2011, 'Formation and evaluation of loosened ground above a cavity by laboratory model tests with uniform sand', *Proc. of 13th International Summer Symposium, Uji, Japan*, pp. 211-4.

Rogers, C.J., 1986. *Sewer Deterioration Studies: The Background to the Structural Assessment Procedure in the Sewerage Rehabilitation Manual*. London: Water Research Centre.

Rosdi, MAHM, Othman, AN, Abdul, MAMZZ & Yusoff, ZM 2017, 'Sinkhole susceptibility hazard zones using gis and analytical hierarchical process (AHP): A case study of kuala lumpur and ampang jaya', *International Archives of the Photogrammetry, Remote Sensing & Spatial Information Sciences*, vol. 42.

Sahoo, JP & Khuntia, S 2018, 'Lower bound solutions for uplift capacity of strip anchors adjacent to sloping ground in clay', *Marine Georesources & Geotechnology*, vol. 36, no. 4, pp. 405-16.

Seeman, M. (2018). *Water main break leads to gushing water on Green Valley Parkway in Henderson*. [online] KSNV. Available at: https://news3lv.com/news/local/water-main-break-leads-to-gushing-water-on-green-valley-parkway-in-henderson [Accessed 15 Jun. 2021].

Shiau, J., Keawsawasvong, S., Chudal, B., Mahalingasivam, K. and Seehavong, S., 2021. Sinkhole stability in elliptical cavity under collapse and blowout conditions. *Geosciences*, *11*(10), p.421.

Shiau, J & Al-Asadi, F 2021, 'Revisiting Circular Tunnel Stability Using Broms and Bennermarks' Original Stability Number', *International Journal of Geomechanics*, vol. 21, no. 5, p. 06021009.

Shiau, J & Al-Asadi, F 2020a, 'Three-Dimensional Analysis of Circular Tunnel Headings Using Broms and Bennermark's Original Stability Number', *International Journal of Geomechanics*, vol. 20, no. 7, p. 06020015.

Shiau, J & Al-Asadi, F 2020b, 'Determination of critical tunnel heading pressures using stability factors', *Computers and Geotechnics*, vol. 119, p. 103345.

Shiau, J & Al-Asadi, F 2020c, 'Two-dimensional tunnel heading stability factors Fc, Fs and Fr'., *Tunnelling and Underground Space Technology*, Vol. 97. https://doi.org/ 10.1016/ j.tust.2020.103293.

Shiau, J & Al-Asadi, F 2020d, 'Stability analysis of twin circular tunnels using shear strength reduction method, *Géotechnique Letters*, 10(2), Institution of Civil Engineers. https://doi.org/10.1680/jgele.19.00003.

Shiau, J & Al-Asadi, F 2020e, 'Three-dimensional heading stability of twin circular tunnels', *Geotechnical and Geological engineering*, vol. 38, no. 3, pp. 2973-88.

Shiau, J & Al-Asadi, F 2018, 'Revisiting Broms and Bennermarks' original stability number for tunnel headings', *Géotechnique Letters*, vol. 8, no. 4, pp. 310-5.

Shiau, JS, Augarde, CE, Lyamin, AV & Sloan, SW 2008, 'Finite element limit analysis of passive earth resistance in cohesionless soils', *Soils and Foundations*, vol. 48, no. 6, pp. 843-50.

Shiau, J., Chudal, B., Mahalingasivam, K., and Keawsawasvong, S., 2021, 'Pipeline burst-related ground stability in blowout condition', *Transportation Geotechnics*, 29, p.100587.

Shiau, J & Hassan, MM 2021, 'Numerical modelling of three-dimensional sinkhole stability using finite different method', *Innovative Infrastructure Solutions*, vol. 6, no. 4, pp. 1-9.

Shiau, J & Hassan, MM 2021, ‘Numerical Investigation of Undrained Trapdoors in Three Dimensions’, *International Journal of Geosynthetics and Ground Engineering*, vol.7, no. 2.

Shiau, J & Hassan, MM 2020, 'Undrained stability of active and passive trapdoors', *Geotechnical Research*, vol. 7, no. 1, pp. 40-8.

Shiau, J., Keawsawasvong, S., Lee, J.S. and Hassan, M.M., 2022, 'Three-dimensional circular trapdoor stability', *Transportation Infrastructure Geotechnology*, *9*(2), pp.173-184.

Shiau, J & Al-Asadi, F 2021, 'Twin tunnels stability factors Fc, Fs and Fγ', *Geotechnical and Geological engineering*, vol. 39, no. 1, pp. 335-45.

Shiau, J, Lee, J-S & Al-Asadi, F 2021, 'Three-dimensional stability analysis of active and passive trapdoors', *Tunnelling and Underground Space Technology*, vol. 107, p. 103635.

Shiau, JS, Lyamin, AV & Sloan, SW 2003, ‘Bearing capacity of a sand layer on clay by finite element limit analysis’, *Canadian Geotechnical Journal*, vol. 40, no. 5, pp. 900-15.

Shiau, J, Lamb, B & Sams, M 2016, ‘The use of sinkhole models in advanced geotechnical engineering teaching’, *International Journal of Geomate*, vol. 10, no. 2, pp. 1718-24.

Shiau, J, Sams, M & Lamb, B 2016, ‘Introducing advanced topics in geotechnical engineering teaching–Tunnel modelling’, *International Journal of Geomate*, vol. 10, no. 1, pp. 1698-705.

Sloan, S 2013, 'Geotechnical stability analysis', *Geotechnique*, vol. 63, no. 7, pp. 531-71.

Sloan, S & Assadi, A 1994, 'Undrained stability of a plane strain heading', *Canadian Geotechnical Journal*, vol. 31, no. 3, pp. 443-50.

Sloan, S & Assadi, A 1992, 'Stability of shallow tunnels in the soft ground', *Predictive soil mechanics: Proceedings of the Wroth Memorial Symposium held at St Catherine's College, Oxford, 27-29 July 1992*, Thomas Telford Publishing, pp. 644-63.

Sloan, S & Assadi, A,1991, 'Undrained stability of a square tunnel in a soil whose strength increases linearly with depth', *Computers and Geotechnics*, vol. 12, no. 4, pp. 321-46.

Sloan, SW, Assadi, A, & Purushothaman, N, 1990, 'Undrained stability of a trapdoor', *Géotechnique*, vol. 40, no. 1, 45–62.

Sloan, SW 1989, 'Upper bound limit analysis using finite elements and linear programming', *International Journal for Numerical and Analytical Methods in Geomechanics*, vol. 13, no. 3, pp. 263-82.

Sloan, SW 1988a, 'A steepest edge active set algorithm for solving sparse linear programming problems', *International Journal for Numerical Methods in Engineering*, vol. 26, no. 12, pp. 2671-85.

Sloan, SW 1988b, 'Lower bound limit analysis using finite elements and linear programming', *International Journal for Numerical and Analytical Methods in Geomechanics*, vol. 12, no. 1, pp. 61-77.

Sloan, SW & Kleeman, PW 1995, 'Upper bound limit analysis using discontinuous velocity fields', *Computer Methods in Applied Mechanics and Engineering*, vol. 127, no. 1-4, pp. 293-314.

staff/zoe-schlanger (2010). *Photo: Giant Sinkhole Cuts Off Water in the Bronx*. [online] Gothamist. Available at: https://gothamist.com/news/photo-giant-sinkhole-cuts-off-water-in-bronx [Accessed 6 Apr. 2021].

Suchowerska, AM, Merifield, RS, Carter, JP & Clausen, J 2012, 'Prediction of underground cavity roof collapse using the Hoek–Brown failure criterion', *Computers and Geotechnics*, vol. 44, pp. 93-103.

Sutton, C. (2014). *Firetruck out of huge sinkhole but road "still unstable."* [online] Mail Online. Available at: https://www.dailymail.co.uk/news/article-2626687/Fire-truck-falls-sinkhole-three-families-evacuated-road-implodes-Sydneys-northern-beaches.html [Accessed 14 Jun. 2021].

Szathmary, Z. (2017). *Sinkhole swallows truck weighing 55,000 pounds*. [online] Mail Online. Available at: https://www.dailymail.co.uk/news/article-4132428/ Sinkhole-swallows-truck-weighing-55-000-pounds.html [Accessed 19 Jun. 2021].

Tang, Y., Chan, D.H. and Zhu, D.Z., 2017, 'A coupled discrete element model for the simulation of soil and water flow through an orifice', *International Journal for Numerical and Analytical Methods in Geomechanics*, *41*(14), pp.1477-1493.

Taylor, A., (2013) *Sinkholes: When the Earth Opens Up - The Atlantic*. [online] www.theatlantic.com.Available at: https://www.theatlantic.com/photo /2013/07/ sinkholes-when-the-earth-opens-up/100552/ [Accessed 24 Mar. 2021].

Terzaghi, K 1936, 'Stress distribution in dry and in saturated sand above a yielding trap-door'.

The Guardian. (2015). *Sinkhole opens on busy Manchester road*. [online] Available at: https://www.theguardian.com/uk-news/2015/aug/14/sinkhole-manchester-road-mancunian-way-rain [Accessed 18 Mar. 2021].

The Guardian. (2015). *Sinkhole opens on busy Manchester road for the second time in two months*. [online] Available at: https://www.theguardian.com/uk-news/2015/sep/15/ sinkhole-mancunian-way-road-manchester-city-juventus [Accessed 19 Jun. 2021].

The News Minute. (2019). *Another sinkhole in Chennai's busy Madhya Kailash.* [online] Available at: https://www.thenewsminute.com/article/another-sinkhole-chennai-s-busy-madhya-kailash-103527 [Accessed 18 Mar. 2021].

Tohda, J., and Hachiya, M. 2005, 'Response and design of buried pipelines subjected to differential ground settlement', *In Proceedings of 16th International Conference on Soil Mechanics and Geotechnical Engineering*. pp. 1659-1662.

toronto.citynews.ca., (2018) *Car swallowed by sinkhole in North York - CityNews Toronto*. [online] Available at: https://toronto.citynews.ca/ 2018/10/16/north-york-sinkhole/ [Accessed 15 Jun. 2021].

Ukritchon, B & Keawsawasvong, S 2017, 'Design equations for undrained stability of opening in underground walls', *Tunnelling and Underground Space Technology*, vol. 70, pp. 214-20.

Ukritchon, B, Yoang, S, Keawsawasvong, S, 2019, 'Three-dimensional stability analysis of the collapse pressure on flexible pavements over rectangular trapdoors', *Transportation Geotechnics* vol. 21, art. no. 100277.

Ukritchon, B., Whittle, A.J. and Sloan, S.W., 1998, 'Undrained limit analyses for combined loading of strip footings on clay', *Journal of Geotechnical and Geoenvironmental Engineering*, *124*(3), pp.265-276.

Van Schoor, M 2002, 'Detection of sinkholes using 2*D* electrical resistivity imaging', *Journal of Applied Geophysics*, vol. 50, no. 4, pp. 393-9.

Wang, L, Leshchinsky, B, Evans, TM, Xie, Y, 2017, 'Active and passive arching stress in $c - \phi$ soils: A sensitivity study using computational limit analysis', *Computers and Geotechnics*, vol. 84, pp. 47–5.

Wijaya, H, Rajeev, P & Gad, E 2019, 'Effect of seismic and soil parameter uncertainties on seismic damage of buried segmented pipeline', *Transportation Geotechnics*, vol. 21, p. 100274.

Wilson, DW, Abbo, AJ, Sloan, SW & Lyamin, AV 2011, 'Undrained stability of a circular tunnel where the shear strength increases linearly with depth', *Canadian Geotechnical Journal*, vol. 48, no. 9, pp. 1328-42.

www.abc.net.au. (2014). *Sinkhole swallows cars as burst main floods Port Melbourne street*. [online] Available at: https://www.abc.net.au/news/2014-12-16/sinkhole-swallows-cars-as-burst-main-floods-port-melbourne-st/5969446 [Accessed 14 Jun. 2021].

www.abc.net.au. (2020). *Moment Perth sinkhole swallows front half of car caught on camera*. [online] Available at: https://www.abc.net.au/news/2020-07-10/caught-on-video-sinkhole-swallows-part-of-car-in-perth/12442252.

www.abc.net.au. (2020). *Sinkhole opens on a busy intersection near major Gold Coast shopping center*. [online] Available at: https://www.abc.net.au/news/2020-12-09/queensland-sinkhole-pacific-fair-gold-coast-traffic-congestion/12964500 [Accessed 9 Mar. 2021].

www.abc.net.au. (2020). *"The damage has been done": Sinkhole opens up in Sydney as heavy rain drenches NSW*. [online] Available at: https://www.abc.net.au/news/2020-07-28/nsw-weather-south-coast-residents-warned-to-brace-for-flooding/12498018 [Accessed 9 Mar. 2021].

www.abc.net.au. (2015). *Three-lane road collapse in Melbourne's south-east*. [online] Available at: https://www.abc.net.au/news/2015-09-29/road-closed-in-melbournes-south-east-after-sinkhole/6812780 [Accessed 17 Mar. 2021].

www.abc.net.au. (2016). *Sinkhole swallow car in Newcastle*. [online] Available at: https://www.abc.net.au/news/2016-11-17/sinkhole-swallows-car-in-newcastle/8032840 [Accessed 9 Mar. 2021].

www.abc.net.au. (2016). *Sinkhole opens up on street in China swallowing up passersby*. [online] Available at: https://www.abc.net.au/news/2016-08-03/sinkhole-opens-up-on-street-in-china-swallowing-up-passersby/7688044 [Accessed 9 Mar. 2021].

www.abc.net.au. (2017). *Father, son killed after driving into sinkhole on Mexican highway*. [online] Available at: https://www.abc.net.au/news/2017-07-13/mexico-city-father-son-killed-after-driving-into-sinkhole/8704372. [Accessed 18 July 2022].

www.goldcoastbulletin.com.au. (2014). *Sinkhole warning of more to come*. [online] Available at: https://www.goldcoastbulletin.com.au/news/gold-coast/50yearold-water-pipes-midlife-crisis-blamed-for-10m-sinkhole-at-broadbeach-but-authorities-warn-it-could-be-just-the-start/news-story/41f5071473d1745944cb07e183080399/[Accessed 14 June 2021].

www.ntnews.com.au. (2017). *Swear there was not a hole here before ...* [online] Available at: https://www.ntnews.com.au/news/national/car-falls-into-sink-hole-created-by-burst-water-main-at-pratt-ave-pooraka/news-story/18255abd0ac1d909db7984fa73ffb835 [Accessed 9 Mar. 2021].

www.9news.com.au. (2019). *Sydney bus gets stuck in a sinkhole caused by burst water main*. [online]Availableat: https://www.9news.com.au/national/caringbah-burst-watermain-bus-falls-in-sinkhole-sydney-news/aef48cec-4082-43f9-8b5c-4794b41893e0 [Accessed 17 Mar. 2021].

www.yahoo.com. (2017) *Cost to fix Michigan sinkhole estimated at more than $78M*. [online] Available at: https://news.yahoo.com/cost-fix-michigan-sinkhole-estimated-more-78m-201012803.html [Accessed 18 Jun. 2021].

Yamamoto, K, Lyamin, AV, Wilson, DW, Sloan, SW & Abbo, AJ 2011, 'Stability of a circular tunnel in cohesive-frictional soil subjected to surcharge loading', *Computers and Geotechnics*, vol. 38, no. 4, pp. 504-14.

Yokota, T., Fukatani, W., and Miyamoto, T.: The present situation of the road cave-in sinkholes caused by sewer systems, 95 pp., 2012.

Yu, H, Salgado, R, Sloan, S & Kim, J 1998, 'Limit analysis versus limit equilibrium for slope stability', *Journal of Geotechnical and Geoenvironmental Engineering*, vol. 124, no. 1, pp. 1-11.

Zeinkiewicz, O, Humpheson, C & Lewis, R 1975, 'Associated and non-associated visco-plasticity in soils mechanics', *Journal of Geotechnique*, vol. 25, no. 5, pp. 671- 89.

Zhang, F, Gao, YF, Wu, YX & Zhang, N 2018, 'Upper-bound solutions for face stability of circular tunnels in undrained clays', *Geotechnique*, vol. 68, no. 1, pp. 76-85.

Zheng, Y-R, Zhao, S-Y, Kong, W-X & Deng, C-J 2005, 'Geotechnical engineering limit analysis using finite element method', *Yantu Lixue(Rock Soil Mech.)*, vol. 26, no. 1, pp. 163-8.

Zouain, N, Herskovits, J, Borges, LA & Feijóo, RA 1993, 'An iterative algorithm for limit analysis with nonlinear yield functions', *International Journal of Solids and Structures*, vol. 30, no. 10, pp. 1397-417.

13newsnow.com. (2019). *Car gets trapped in sinkhole that opens up in Bay View area of Norfolk*. [online] Available at: https://www.13newsnow.com/ article/news/local/car-gets-trapped-in-sinkhole-that-opens-up-in-bay-view-area-of-norfolk/291-8ba9b456-e315-46b3-8804-86b1955b6d8c [Accessed 15 Jun. 2021].